

# **PHYSICO-CHEMICAL CHARACTERIZATION OF BOLAAMPHIPHILE AGGREGATES:**

## **THE INFLUENCE OF CHAIN AND HEADGROUP STRUCTURE ON SELF-ASSEMBLY**

### **Dissertation**

zur Erlangung des akademischen Grades  
doctor rerum naturalium (Dr. rer. nat.)

vorgelegt der

Naturwissenschaftlichen Fakultät II - Chemie, Physik und Mathematik  
der Martin-Luther-Universität Halle-Wittenberg

von Frau Dipl. Chem. Gesche Graf

geb. am 02. August 1982 in Kiel

Gutachter:

1. Prof. Dr. A. Blume (Halle (Saale))
2. Prof. Dr. H. Heerklotz (Toronto)

Halle (Saale), im September 2011

verteidigt am 12.12.2011

# Contents

<b>1</b>	<b>Introduction .....</b>	<b>1</b>
1.1	Self-Assembly of Symmetrical Single-Chain Bolaamphiphiles .....	3
1.2	Aim.....	6
<b>2</b>	<b>Experimental Part .....</b>	<b>7</b>
2.1	Materials.....	7
2.2	Methods.....	7
2.2.1	Sample Preparation.....	7
2.2.2	Differential Scanning Calorimetry (DSC).....	8
2.2.3	Isothermal Titration Calorimetry (ITC) .....	9
2.2.4	Fourier Transform-Infrared Spectroscopy (FT-IR).....	9
2.2.5	UV/Vis Spectroscopy .....	10
2.2.6	Dynamic Light Scattering (DLS) .....	12
2.2.7	Small Angle Neutron Scattering (SANS).....	13
2.2.8	(cryo-) Transmission Electron Microscopy (TEM).....	14
2.2.9	Oscillatory Rheology.....	15
<b>3</b>	<b>Results and Discussion .....</b>	<b>21</b>
3.1	pH- and Salt-Dependent Aggregation Behavior of Me <sub>2</sub> PE-C32-Me <sub>2</sub> PE .....	22
3.1.1	pH-Dependent Aggregation Behavior of Me <sub>2</sub> PE-C32-Me <sub>2</sub> PE .....	23
3.1.2	Salt-Dependent Aggregation Behavior at pH 11.....	26
3.1.3	Rheology of Me <sub>2</sub> PE-C32-Me <sub>2</sub> PE Suspensions .....	31
3.1.4	Rheology of PC-C32-PC Suspensions .....	39
3.1.5	Conclusions .....	41
3.2	Aggregation Behavior of Asymmetrical Single-Chain Bolaamphiphiles with Two Different Headgroups .....	43
3.2.1	Aggregation Behavior of DMAPPC-C32-POH in Aqueous Suspension.....	44
3.2.1.1	Mixing Behavior with Symmetrical Bolaamphiphiles.....	55
3.2.1.1.1	Miscibility with PC-C32-PC in Water .....	55
3.2.1.1.2	Miscibility with Me <sub>2</sub> PE-C32-Me <sub>2</sub> PE in Acetate Buffer at pH 5 .....	56
3.2.2	Aggregation Behavior of DMAPPC-C32-OH in Aqueous Suspension.....	58

3.2.3	Conclusions .....	60
3.3	Aggregation Behavior of Bolaamphiphiles Containing Thioether Groups in the Spacer Chain .....	61
3.3.1	Aggregation Behavior of PC-C32SS-PC and Me <sub>2</sub> PE-C32SS-Me <sub>2</sub> PE in Aqueous Suspension.....	61
3.3.1.1	Mixing Behavior of PC-C32SS-PC and Me <sub>2</sub> PE-C32SS-Me <sub>2</sub> PE with Bolaamphiphiles with Non-Modified Alkyl Chains .....	71
3.3.1.1.1	Miscibility of PC-C32SS-PC with PC-C32-PC .....	71
3.3.1.1.2	Miscibility of Me <sub>2</sub> PE-C32SS-Me <sub>2</sub> PE with Me <sub>2</sub> PE-C32-Me <sub>2</sub> PE .....	77
3.3.2	Conclusions .....	81
3.4	Aggregation Behavior of Bolaamphiphiles Containing Polymerizable Diacetylene Groups in the Spacer Chain.....	82
3.4.1	Aggregation Behavior of Diacetylene-Modified Bolaamphiphiles.....	83
3.4.1.1	Diacetylene-Modified Bolaamphiphiles with PC Headgroups.....	84
3.4.1.2	Diacetylene-Modified Bolaamphiphiles with Me <sub>2</sub> PE Headgroups .....	86
3.4.2	Polymerization of Diacetylene-Modified Bolaamphiphiles.....	89
3.4.2.1	Polymerization of Diacetylene-Modified Bolaamphiphiles with PC Headgroups .....	91
3.4.2.2	Polymerization of Diacetylene-Modified Bolaamphiphiles with Me <sub>2</sub> PE Headgroups .....	98
3.4.3	Conclusions .....	102
3.5	Interaction of Bolaamphiphiles with Gold Nanoparticles.....	104
3.5.1	Interaction of PC-C32SS-PC and Me <sub>2</sub> PE-C32SS-Me <sub>2</sub> PE Fibers with Gold Nanoparticles.....	104
3.5.2	Interaction of DMAPP-PC-C32-POH Fibers with Gold Nanoparticles .....	110
3.5.3	Conclusions .....	112
<b>4</b>	<b>Conclusions .....</b>	<b>113</b>
<b>5</b>	<b>References .....</b>	<b>117</b>

## List of abbreviations

### Methods

(cryo-) TEM	(cryo-) Transmission Electron Microscopy
DLS	Dynamic Light Scattering
DSC	Differential Scanning Calorimetry
FT-IR	Fourier Transform-Infrared Spectroscopy
ITC	Isothermal Titration Calorimetry
SANS	Small Angle Neutron Scattering
UV/Vis	UV/Visible Spectroscopy

### Substances

AuNP	gold nanoparticle
DMAPPC	dimethylaminopropylphosphocholine
DMAPPC-C32-OH	32-hydroxydotriacontane-1-yl- $\{2-[N-(3\text{-dimethylaminopropyl})-N,N\text{-dimethylammonio}]ethylphosphate\}$
DMAPPC-C32-POH	32- $\{[hydroxy(2\text{-hydroxyethoxy})phosphinyl]oxy\}$ dotriacontane-1-yl- $\{2-[N-(3\text{-dimethylaminopropyl})-N,N\text{-dimethylammonio}]ethylphosphate\}$
Me <sub>2</sub> PE	dimethylphosphoethanolamine
Me <sub>2</sub> PE-C32-Me <sub>2</sub> PE	dotriacontane-1,32-diyl-bis[2-(dimethylammonio)-ethylphosphate]
Me <sub>2</sub> PE-C32SS-Me <sub>2</sub> PE	12,21-dithiadotriacontane-1,32-diyl-bis[2-(dimethylammonio)-ethylphosphate]
Me <sub>2</sub> PE-C32diAc-Me <sub>2</sub> PE	dotriacontane-15,17-diin-1,32-diyl-bis[2-(dimethylammonio)-ethylphosphate]
Me <sub>2</sub> PE-C34diAc-Me <sub>2</sub> PE	tetatriacontane-16,18-diin-1,34-diyl-bis[2-(dimethylammonio)-ethylphosphate]
Me <sub>2</sub> PE-C36diAc-Me <sub>2</sub> PE	hexatriacontane-17,19-diin-1,36-diyl-bis[2-(dimethylammonio)-ethylphosphate]
NP	nanoparticle

PC	phosphocholine
PC-C32-PC	dotriacontane-1,32-diyl-bis[2-(trimethylammonio)-ethylphosphate]
PC-C32SS-PC	12,21-dithiadotriacontane-1,32-diyl-bis[2-(trimethylammonio)-ethylphosphate]
PC-C32diAc-PC	dotriacontane-15,17-diin-1,32-diyl-bis[2-(trimethylammonio)-ethylphosphate]
PC-C34diAc-PC	tetracontane-16,18-diin-1,34-diyl-bis[2-(trimethylammonio)-ethylphosphate]
PC-C36diAc-PC	hexatriacontane-17,19-diin-1,36-diyl-bis[2-(trimethylammonio)ethylphosphate]
PMMA	poly(methylmethacrylate)
POH	hydroxyethylphosphate

### Symbols

A	area
$C_p$	apparent molar heat capacity
CPK model	calotte model (R. Corey, L. Pauling, W. Koltun)
d	diameter
F	force
$G'$	storage modulus
$G''$	loss modulus
h	height
$\Delta H$	reaction enthalpy
$k_B$	Boltzmann constant
$p(r)$	pair distance distribution function
$pK_a^{app}$	negative common logarithm of the apparent acid dissociation constant K
Q	binding heat
q	scattering vector
R	molar ratio (ITC)
r	radius

$r_h$	hydrodynamic radius
$s$	deflection
$T$	temperature
$\tan \delta$	loss factor
$v$	velocity
$x$	molar ratio
$\gamma$	deformation
$\lambda$	wavelength
$\eta$	viscosity
$\tau$	shear stress
$\omega$	angular frequency
$\dot{\gamma}$	shear rate
$\tilde{\nu}$	wavenumber

## 1 Introduction

Bipolar amphiphiles (or bolaamphiphiles) are in the focus of an expanding area of research concerned with the self-assembly process and properties of these molecules, as well as the behavior and functionality of the resulting aggregates.<sup>[1-4]</sup> Bolaamphiphiles consist of a hydrophobic spacer chain and two hydrophilic headgroups attached to each end of the spacer. They occur naturally in archaebacteria, in which they increase the stability of the membrane against extreme living conditions such as high temperature, or high and low pH values.<sup>[5]</sup> This is due to the unique molecular structure of the bolaamphiphiles that adopt a membrane-spanning orientation inside the lipid membrane.<sup>[6-8]</sup> The chemical structures of bolaamphiphiles occurring in archaebacteria membranes are very complex as, e.g., the bolaamphiphile Caldarchaeol (Figure 1.1).<sup>[3, 9]</sup>

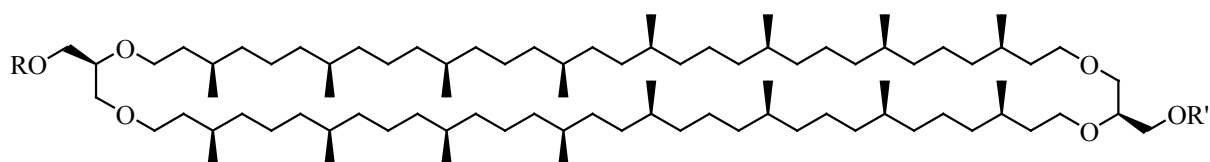


**Figure 1.1:** Chemical structure of the bolaamphiphile Caldarchaeol. R = H, sugar, or phosphate moieties and R' = H or polyol moieties.

The self-assembly of this kind of amphiphilic molecules depends on the properties and the structure of the two different parts, i.e., the hydrophobic spacer chain and the hydrophilic headgroups. A model for predicting the type of aggregates formed by monopolar amphiphiles is the critical packing parameter defined by Israelachvili.<sup>[10]</sup> It is calculated as the ratio of the volume of the hydrophobic chain and the length of the chain divided by the cross-section of the hydrophilic headgroup. The value of this ratio can be used to determine whether a specific system forms, e.g., micellar aggregates or planar membranes. A comparable effect can be observed for bipolar amphiphiles as the ratio between headgroup and spacer chain cross-section essentially affects the organization of the aggregates formed during the self-assembly process. However, due to the presence of two polar groups this shape concept cannot be used in the same simple way.

As the synthesis of bola molecules with a structure similar to the ones occurring naturally is very time-consuming, highly simplified bolaamphiphiles were synthesized showing the most important structural features of the natural ones. The diversity of chemical structures that can be used for the design of bolaamphiphiles induces a large variety of possible aggregate configurations.<sup>[11]</sup> Diverse areas of research have evolved, which are concerned with different aspects of the self-assembly behavior of bolaamphiphiles. On the one hand,

mimicking the behavior of naturally occurring bolaamphiphiles, the formation of monolayer membranes or the incorporation into lipid double layers is possible. This enables the development of mechanically and chemically stable membrane structures, which can be used in drug delivery systems.<sup>[11-12]</sup> Bolaamphiphiles designed for this purpose are characterized by headgroups and spacer chains with similar cross-sections.

On the other hand, a second field of research is the formation of lipid nanotubes (LNTs) by asymmetrical bolaamphiphiles.<sup>[13-14]</sup> In this case, the difference in the cross-section of the two headgroups causes either the formation of symmetrical monolayer lipid membranes (MLMs) with antiparallel orientation of the bolaamphiphiles or the formation of asymmetrical MLMs with parallel orientation of the single molecules.<sup>[15]</sup> LNTs can be used for the incorporation of guest molecules such as metal ions or polymers as the diameter of the hollow cylinders can be up to 1000 nm in size.<sup>[16]</sup>

An additional area of interest is the research on hydrogel forming bolaamphiphiles, as the self-assembly process of bolaamphiphiles can also lead to aggregates inducing gelation of aqueous suspensions. This is caused by the presence of a three-dimensional network of fibers. It is an interesting feature of this kind of hydrogels that the molecules first have to self-assemble into fiber-like aggregates that subsequently gel the solvent by interactions between the aggregates (e.g., hydrogen bonds, hydrophobic interaction, or simply entanglements).<sup>[2, 17-18]</sup> This is contrary to the formation of hydrogels out of polymers or biological macromolecules such as collagen. In this case, the fibers consist of covalently linked groups, e.g., amino acids.<sup>[19]</sup>

Several systems of different bolaamphiphiles containing lipid, sugar, or amino acid headgroups and different spacer chains lengths have been described.<sup>[20-23]</sup> Through this use of varying chemical structure it is possible to add stimuli-responsive groups to the hydrogelators and thus enable the formation of fibers and gels under different conditions of pH or salt concentration.

## 1.1 Self-Assembly of Symmetrical Single-Chain Bolaamphiphiles

The attempt to synthesize bolaamphiphiles with a structure similar to the ones occurring in archaeobacteria membranes led to the two symmetrical bolalipids PC-C32-PC and Me<sub>2</sub>PE-C32-Me<sub>2</sub>PE. The chemical structure of the two molecules is shown in Figure 1.2.

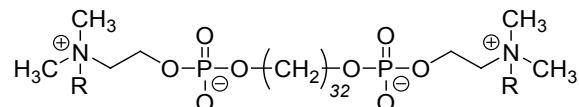


**Figure 1.2:** Chemical structure of the bolaamphiphiles PC-C32-PC with R = CH<sub>3</sub> and Me<sub>2</sub>PE-C32-Me<sub>2</sub>PE with R = H.

The structure of PC-C32-PC and Me<sub>2</sub>PE-C32-Me<sub>2</sub>PE is much simpler compared to naturally occurring bolaamphiphiles with their complex chemical composition. The spacer consists only of one alkyl chain without any methyl-branches instead of two spacer chains and is attached to the headgroups without the glycerol group present in natural bolalipids. The phosphocholine (PC) headgroup is common in phospholipids. In the dimethylphosphoethanolamine (Me<sub>2</sub>PE) headgroup one methyl moiety of the PC headgroup is replaced by a hydrogen atom to add the possibility of changing the charge and to form hydrogen bonds depending on the pH value.

The aggregation behavior of these molecules in aqueous suspension differs from the behavior usually found in suspensions of natural bolaamphiphiles. Instead of forming vesicles, the molecules self-assemble into nanofibers building transparent, homogenous gels (Figure 1.3A). The self-assembly and the properties of the nanofibers and the gel were examined with several complementary methods to gain detailed information on this process.<sup>[24-30]</sup>

The formation of fibers can be explained by the molecules tendency to reduce the contact of the hydrophobic alkyl chains with the water and to minimize the energy of the system by aggregation. However, there is a size conflict between the large headgroups and the alkyl chains, which have a considerably smaller cross-section. In a lamellar arrangement, as it would be needed for the formation of vesicular aggregates, van-der-Waals-interactions between the alkyl chains cannot be optimized as the distance between the chains is too large.

This results in the formation of the observed fiber structure with molecules that are aligned side by side and twisted relative to each other to enable closer contact of the alkyl chains and to gain enough space for the bulky headgroups. FT-IR measurements showed that the alkyl chains have a highly ordered all-*trans* conformation in this fiber structure.<sup>[25-26]</sup>

The assembly process was simulated by Monte Carlo simulations that visualize the formation of fibers with a helical superstructure (Figure 1.3B).<sup>[30-31]</sup>

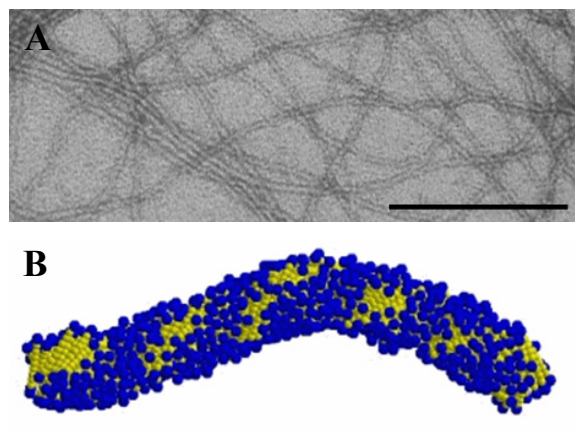


**Figure 1.3:** (A) TEM image of a PC-C32-PC suspension at 25 °C stained with uranyl acetate. The bar corresponds to 100 nm. (B) Coarse-grained off-lattice Monte Carlo simulation of the fiber structure.

Figure 1.3B shows that both, the hydrophobic alkyl chains (yellow spheres) and the hydrophilic headgroups (blue spheres), are exposed at the fiber surface and are in contact with water. It is notable that a chiral, helical structure arises from the self-assembly of achiral molecules. It can be expected that as many right-handed as left-handed helices are formed in suspension and, indeed, both arrangements could be found in AFM measurements with a suspension of the

molecule PC-C34-PC.<sup>[30]</sup> The helical pitch of the bolaamphiphile fiber is 8 nm.<sup>[30]</sup>

The noncovalent interactions inducing and stabilizing this structure are the van-der-Waals-interactions of the alkyl chains and the hydrophobic effect. In the case of PC-C32-PC no additional interaction takes place as the zwitterionic headgroups can form no further bonds. However, the Me<sub>2</sub>PE headgroup can form additional hydrogen bonds provided the headgroup is in its zwitterionic state. This depends on the pH value of the suspension and leads to the possibility of influencing the stability of the fiber structure (see Chapter 3.1) via changes in the pH value.

The aggregation of the bolaamphiphiles into fibers depends on temperature. The fibers of PC-C32-PC are stable up to 48.7 °C. Above this temperature they collapse into micellar aggregates (fibers to micelles I). This is accompanied by a decrease in the alkyl chain order as was shown by FT-IR measurements. Another transition, connected with a further increase in the alkyl chains disorder, occurs inside the micellar stability range at 73.0 °C (micelles I to micelles II).<sup>[25, 28]</sup> ESR measurements revealed that the *trans/gauche* isomerization, inducing the increasing amount of disorder, starts at the outer parts of the alkyl chains close to the headgroups.<sup>[32]</sup> In addition, the mobility of the headgroups increases with rising temperature as determined by <sup>31</sup>P-NMR.<sup>[27]</sup>

The aggregation behavior of Me<sub>2</sub>PE-C32-Me<sub>2</sub>PE in acetate buffer at pH 5 differs slightly from the behavior observed for PC-C32-PC in aqueous suspensions. The first transition in this

system is a transformation into a second stable fiber structure that shows increased disorder of the alkyl chain and mobility of the headgroups at 45.5 °C (fibers I to fibers II). At 69.5 °C these fibers dissolve into micelles (fibers II to micelles I), which show another transition at 83.4 °C as was also observed in PC-C32-PC suspensions (micelles I to micelles II).<sup>[26]</sup> The enhanced stability of the fiber structure in the case of Me<sub>2</sub>PE-C32-Me<sub>2</sub>PE originates from the ability to form hydrogen bonds between adjacent headgroups.

The suspensions of both bolaamphiphiles form transparent gels, which were shown to have viscoelastic properties in the stability range of the fiber structure at a concentration as low as 1 mg ml<sup>-1</sup> or 0.1 wt%.<sup>[24, 27]</sup> One molecule of the bolaamphiphile PC-C32-PC immobilizes 45,000 water molecules in a suspension of the concentration  $c = 1 \text{ mg ml}^{-1}$ .<sup>[24]</sup> The three-dimensional fiber network is stabilized via entanglements, hydrophobic interactions of the alkyl chains exposed at the surface, and, if possible, interactions between the headgroups. After the transformation to micellar aggregates with increasing temperature, the suspensions show viscous flow behavior (see Chapter 3.1.3).<sup>[27]</sup>

The miscibility of the bolaamphiphile PC-C32-PC with phospholipids was investigated in order to examine the possibility of incorporating these bolaamphiphiles into the double layer structure of the lipid vesicles. DSC measurements indicated that PC-C32-PC is not incorporated to a large extent into lipid vesicles preventing the application of these molecules as membrane stabilizers.<sup>[33]</sup> This immiscibility is caused by the large difference in the cross-sectional area of headgroups and spacer that do not fit into the lipid bilayer structure and might be overcome by structural changes in the alkyl chain or by reducing the size of the headgroup.

Several other factors influencing the aggregation behavior of single-chain bolaamphiphiles have been investigated so far. Longer alkyl chains, e.g., led to the formation of square lamellar aggregates in the case of Me<sub>2</sub>PE headgroups.<sup>[29]</sup> Shorter alkyl chains resulted in thermally destabilized fiber structures.<sup>[28]</sup> In addition, changes in the chemical structure of the spacer chains, such as the incorporation of hetero atoms (see Chapter 3.3),<sup>[34]</sup> phenyl groups, methyl branches, or diacetylene-modified chains (see Chapter 3.4)<sup>[35]</sup> were examined. Differently functionalized headgroups were also attached to the alkyl spacer chains of the single-chain bolaamphiphiles including lipoic acid<sup>[30]</sup> and amino moieties.<sup>[34, 36]</sup>

### 1.2 Aim

The well characterized aggregate structures that were found for aqueous suspensions of symmetrical single-chain bolaamphiphiles such as PC-C32-PC or Me<sub>2</sub>PE-C32-ME<sub>2</sub>PE raise the question, how the self-assembly of the bolalipids and the properties of the resulting aggregates may be influenced via changes of the chemical structure. Two different strategies were employed for this purpose that enable precise tailoring of the aggregates properties and, additionally, functionalization of the molecules for specific fields of applications.

The first approach was to control the aggregation behavior via modification of the hydrophilic headgroups. The main focus was laid on two different approaches:

- The headgroups of the symmetrical bolaamphiphile ME<sub>2</sub>PE-C32-ME<sub>2</sub>PE are protonated or deprotonated depending on the pH value of an aqueous suspension. Therefore, the pH- and salt-dependent aggregation behavior of this bolalipid was examined to determine how the aggregates can be tailored to show specific properties such as temperature stability or viscoelasticity.
- The self-assembly process of the asymmetrical bolaamphiphile DMAPPC-C32-POH in aqueous suspension was studied to determine whether the asymmetry of the molecule induces the formation of other aggregate forms. Furthermore, the interaction between the aggregates and gold nanoparticles was examined.

The second investigated approach was to change the chemical structure of the spacer chain.

Two different approaches were used:

- The aggregation process of bolaamphiphiles in aqueous suspension containing two thioether groups inside the spacer chains was examined. In addition, the use of the resulting aggregates as template for the binding and organization of gold nanoparticles was investigated.
- The influence of polymerizable diacetylene moieties in the middle of the spacer chain on the self-assembly of the bolaamphiphiles in aqueous suspension was determined. Polymerization of the resulting aggregates was initiated by irradiation with UV light to check whether the formation of thermostable aggregates can be achieved.

## 2 Experimental Part

### 2.1 Materials

All single-chain bolaamphiphiles were synthesized by S. Drescher and the group of Prof. B. Dobner of the department of biochemical pharmacy of the Institute of Pharmacy at the Martin-Luther-University Halle-Wittenberg.

Ultra-pure water was used from a Millipore Milli-Q A10 system (Millipore GmbH, Schwalbach, Germany).

Sodium chloride (NaCl), potassium chloride (KCl), magnesium chloride ( $MgCl_2$ ), calcium chloride ( $CaCl_2$ ), sodium hydroxide (NaOH), sodium acetate ( $Na(CH_3COO)$ ), and acetic acid ( $CH_3COOH$ ) were purchased from Carl Roth GmbH + Co. KG (Karlsruhe, Germany) or Merck KGaA (Darmstadt, Germany) and used without further purification.

Chloroform ( $CHCl_3$ ) and methanol ( $CH_3OH$ ) (HPLC grade) were purchased from Carl Roth GmbH + Co. KG (Karlsruhe, Germany).

Heavy water ( $D_2O$ ) was purchased from Isotec (Sigma-Aldrich, Inc., St. Louis, USA).

Low viscosity silicone oil (M20) for the rheological measurements was purchased from Carl Roth GmbH + Co. KG (Karlsruhe, Germany).

Uranyl acetate ( $UO_2(CH_3COO)_2$ ) for staining of the TEM samples was purchased from Sigma-Aldrich, Inc. (St. Louis, USA).

Citrate stabilized gold nanoparticles (AuNPs) with a diameter of  $d = 5$  nm and a concentration of  $c = 5 \cdot 10^{13}$  NP  $ml^{-1}$  were purchased from Plano GmbH (Wetzlar, Germany).

### 2.2 Methods

#### 2.2.1 Sample Preparation

To achieve a homogenous suspension of the bolaamphiphiles, the appropriate amount of bolaamphiphile was suspended in water or buffer, heated to 80 °C, and vortexed three times. When mixtures of bolaamphiphiles were examined, the substances were first dissolved in a mixture of chloroform and methanol ( $V/V = 2/1$ ) to achieve complete mixing of the components. Afterwards, the solvent was evaporated in a stream of nitrogen and the sample was stored in a vacuum chamber over night to ensure the removal of all traces of solvent. Finally, the dry bolaamphiphile mixture was suspended in water or buffer. All samples were stored at 4 °C until they were used in the single experiments.

### 2.2.2 Differential Scanning Calorimetry (DSC)

Differential Scanning Calorimetry (DSC) is a method used for the determination of transition temperatures and transition enthalpies. The calorimeter consists of two thermally isolated, separate cells that can be heated and cooled with a constant rate. The sample cell is filled with the sample solution and the reference cell with the pure solvent. During the measurement both cells are heated or cooled simultaneously and the temperature of sample and reference cell has to be kept equal. If an endothermic or exothermic transition of the aggregates inside the sample occurs, the sample cell has to be heated more or less compared to the reference cell to prevent temperature differences. The difference in the heating power applied to both cells is proportional to the difference of the heat capacities and serves as measuring signal.<sup>[19]</sup>

For the analysis of the measurements the apparent molar heat capacity  $C_p$  is calculated according to Equation 2.1.

$$C_p = \left( c_{p,W} \cdot \frac{V_L}{V_W} - \frac{\Delta}{m_L} \right) \cdot M_L \quad \text{Equation 2.1}$$

$c_{p,W}$  is the specific heat of water, and  $V_L$  and  $V_W$  the specific volume of lipid and water, respectively.  $m_L$  is the mass of the lipid in the sample cell,  $M_L$  the molecular weight of the lipid and  $\Delta$  the displacement of the measurements base line relative to the water/water or buffer/buffer base line. For the calculation of  $C_p$  a constant value of 0.95 was assumed for the term  $c_{p,W} \cdot \frac{V_L}{V_W}$ .<sup>[37]</sup>

The apparent molar heat capacity is displayed as a function of temperature. The maxima of the peaks of this function determine the main temperature of the corresponding transitions. The area under the peak, i.e., the integral of the apparent molar heat capacity, equals the transition enthalpy.<sup>[19]</sup>

#### Experimental procedure

DSC measurements were performed using a MicroCal VP-DSC (MicroCal Inc., Northampton, USA). The concentration of the bolalipids was 1 mg ml<sup>-1</sup> if not stated otherwise. As a reference, water or buffer were used. The suspension of the sample and the reference solvent were degassed in a vacuum chamber for 15 minutes prior to each measurement.

For the measurements with salts added to the suspension, a solution of the salt at the required concentration was used as reference. For these experiments the suspensions were degassed before adjusting the pH value with a 2.5 M NaOH solution (see Chapter 3.1).

Measurements were performed with heating and cooling rates of 60 and 20 °C h<sup>-1</sup> in the temperature range between 2 and 95 °C. Between the single scans an equilibration period of

10 minutes was inserted. At least three consecutive heating and cooling scans of each sample were recorded to check the reproducibility. The measurements were analyzed using the software Origin 8 (OriginLab).

### 2.2.3 Isothermal Titration Calorimetry (ITC)

Isothermal Titration Calorimetry (ITC) is a suitable method for determining interaction energies between a sample and a reactant. Small amounts of the reactant are injected into a sample cell using a syringe. Sample cell and an additional reference cell filled with the solvent are kept at a constant temperature. The heat, released or needed during each titration step in the sample cell, is measured by recording the differential power needed to keep the temperature difference between the two cells minimal. Integration of the differential power signal for the single injection peaks gives the reaction enthalpy  $Q$  that can be used to calculate equilibrium constants, molar binding enthalpies  $\Delta H$  or stoichiometric ratios.<sup>[38]</sup> The molar binding enthalpy  $\Delta H$  is determined as the difference between the maximal and minimal value of the reaction enthalpy. The binding constant can be estimated from the slope of the function of the reaction enthalpy against the concentration.

#### Experimental procedure

ITC experiments were made using a MicroCal VP-ITC (MicroCal Inc., Northampton, USA). Before starting the experiment the samples were degassed in a vacuum chamber for 15 minutes. A suspension of the bolaamphiphile ( $c = 0.3$  mM) was titrated into a gold nanoparticle (AuNP) solution (citrate stabilized AuNPs,  $d = 5$  nm, concentration of single NPs  $c = 8.3 \cdot 10^{-5}$  mM) at 25 °C. During the experiment 80 aliquots of 1  $\mu$ l were injected into the measuring cell. The reference cell was filled with water. Difficulties in cleaning of the ITC cells of the AuNPs only permitted few measurements.

The experimental data were analyzed using the software Origin 7 (OriginLab) for ITC as provided by MicroCal. The heat of dilution of the bolaamphiphile suspension was subtracted.

### 2.2.4 Fourier Transform-Infrared Spectroscopy (FT-IR)

Fourier Transform-Infrared Spectroscopy (FT-IR) is used for the determination of the structure of molecules or specific parts of molecules. Irradiation with infrared light ( $\lambda = \tilde{\nu}^{-1} = 800 - 10^6$  nm) excites oscillations (stretching or bending vibrations) of different functional groups in the sample molecules.<sup>[19]</sup> In this process, irradiation with a frequency specific to each functional group is absorbed. The Fourier Transform method enables the

measurement of the absorption spectrum for the whole wavelength region at the same time making the single measurements very fast.<sup>[39]</sup>

The exact position and intensity of IR bands is dependent on the conformation of the examined molecules and therefore dependent on factors such as temperature, concentration of the sample, and the solvent. The wavenumbers of the absorption peaks of the symmetric and asymmetric methylene stretching vibrational bands give information on the *trans/gauche* ratio of a methylene chain, i. e. the degree of order of in the chain.<sup>[40-42]</sup>

### Experimental procedure

FT-IR experiments were carried out with a Bruker Vector 22 Fourier transform spectrometer (Bruker Optik GmbH, Karlsruhe, Germany) operating at  $2\text{ cm}^{-1}$  resolution. The bolaamphiphiles were used at a concentration of  $50\text{ mg ml}^{-1}$  and were suspended in water or 300 mM acetate buffer at pH 5. Each sample was placed between  $\text{CaF}_2$  windows with a  $12\text{ }\mu\text{m}$  Teflon spacer and equilibrated for 2 h at  $5\text{ }^\circ\text{C}$  prior to the measurement. FT-IR spectra with 64 scans each were recorded in the temperature range from 5 to  $95\text{ }^\circ\text{C}$  with an equilibration time of 8 minutes at each temperature. The spectra of water or buffer were measured with an identical setup and were subtracted from the sample spectra using the OPUS software supplied by Bruker Optik GmbH.

### **2.2.5 UV/Vis Spectroscopy**

UV/Vis spectroscopy is based on the absorption of light in the region from 200 to 800 nm with a wavelength that is specific to the sample molecule and the functional moieties it contains such as aromatics, carbonyl groups, or olefins.<sup>[43]</sup> The absorption is determined from the intensity of the incident light before and after it passes through a cuvette with the sample solution. A reference spectrum is recorded to eliminate influences of the solvent and the empty cuvette.

The position of the absorption maximum contains information on the absorbing sample and can be influenced by concentration, temperature, changes in conformation, solvent, pH value, and ionic strength.<sup>[19]</sup>

### Surface Plasmon Resonance (SPR)

Nanoparticles (NP) are particles ranging from 2 to 100 nm in size and they exhibit properties that differ distinctly from the properties of solid state materials. Noble metal NPs show a special, very strong absorption band in the UV/Vis region that is referred to as the surface

plasmon band (SPB).<sup>[44]</sup> This absorption has been described by Gustav Mie in 1908 and is also called Mie resonance.<sup>[45]</sup>

The SPB arises from scattering of the incident light with a certain frequency range through interaction with the NPs. This can be explained with the collective resonance of the conduction electrons of the NPs.<sup>[44, 46]</sup> Shifting of the conduction electrons under the influence of the electric field of the incident light causes the formation of surface charges. This leads to the shifting of all the NPs electrons resulting in positive and negative surface charges. These surface charges form the relocating force that causes the electrons to perform an oscillating movement.<sup>[44]</sup>

Absorbance of light between 500 and 550 nm is observed in solutions of gold nanoparticles (AuNPs), depending on the diameter of the AuNPs, and resulting in the characteristic dark red color of the AuNP solutions. Changes in the distance between the AuNPs, e.g., through aggregation or linear orientation of the AuNPs, lead to a red shift to wavelengths above 600 nm and a broadening of the absorbance.<sup>[47-48]</sup> The maximum of the UV/Vis absorption spectrum therefore is a good indication for the distance between single AuNPs.

Position, form, and intensity of the surface plasmon band also depend strongly on factors such as the dielectric constant of the surrounding medium, the electronic interaction between NPs and stabilizing ligands, as well as size, shape, and monodispersity of the NPs.<sup>[44]</sup>

### Experimental procedure

UV/Vis absorption spectra of AuNPs were recorded with a Hewlett-Packard spectrophotometer HP 8453 (Hewlett-Packard GmbH, Waldbronn, Germany) at a resolution of 1 nm between 300 and 800 nm using PMMA cuvettes with a path length of 10 mm. Bolaamphiphile suspensions were mixed with an AuNP solution (citrate stabilized AuNPs,  $d = 5$  nm, concentration of single NPs  $c = 8.3 \cdot 10^{-5}$  mM) at the mixing ratios bolalipid to AuNP = 1000:1 or 100:1 and equilibrated at the temperature of the experiment for 15 minutes prior to each measurement. Pure AuNP solutions were diluted to the same concentration and used as a reference for the measurements.

Absorption spectra of the diacetylene containing bolaamphiphiles were recorded using a Cary 4000 spectrophotometer (Agilent Technologies Deutschland GmbH, Böblingen, Germany) with a resolution of 1 nm. The concentration of the bolaamphiphile was 1 or

5 mg ml<sup>-1</sup> in water or 10 mM acetate buffer at pH 5. The samples were equilibrated in quartz cuvettes (10 mm path length) for 15 minutes at the temperature of the experiment.

The bolaamphiphile suspensions were irradiated with an UV lamp (low-pressure Hg lamp,  $\lambda = 254$  nm,  $P = 15$  W) at a distance of 4.5 cm to achieve polymerization of the diacetylene units. The suspensions were not stirred during the irradiation process but carefully shaken by hand between intervals of irradiation before the UV/Vis spectra were recorded.

Previous polymerization experiments were carried out by M. Bastrop. An isolated box containing an ice water bath kept at 0 °C was used for cooling of the bolaamphiphile suspensions. Polymerization was achieved using irradiation with a low-pressure Hg-lamp (254 nm,  $P = 15$  W).<sup>[49]</sup> UV/Vis spectra were recorded using a Hewlett-Packard spectrophotometer HP 8453 (Hewlett-Packard GmbH, Waldbronn, Germany).

### 2.2.6 Dynamic Light Scattering (DLS)

Dynamic Light Scattering (DLS) can be utilized for determining the size of spherical colloidal particles. A sample is irradiated with a laser beam and the intensity of the scattered light is measured at a certain angle depending on the time of the experiment. The intensity shows a fluctuation that is connected with the diffusion of the particles in the sample solution. From this measurement the time autocorrelation function of the intensity fluctuations can be calculated.<sup>[19, 50]</sup> A fit of this function with the Stokes-Einstein relation

$$D = \frac{k_B \cdot T}{6 \cdot \pi \cdot \eta \cdot r_h} \quad \text{Equation 2.2}$$

enables the calculation of the hydrodynamic radius of the scattering particles in the sample.<sup>[19]</sup>  $D$  is the diffusion coefficient,  $\eta$  the viscosity,  $k_B$  the Boltzmann constant, and  $r_h$  the hydrodynamic radius. This relation, however, is only valid for spherical, non-interacting particles.

#### Experimental procedure

DLS experiments were carried out with an ALV-NIBS-HPPS particle sizer (ALV-Laser Vertriebsgesellschaft m.b.H., Langen, Germany). The device was equipped with a 3 mW HeNe laser with a wavelength of 632.8 nm and a scattering angle of 173° was used. All samples ( $c = 1$  mg ml<sup>-1</sup>) were filtered through a Nylon membrane filter of 0.45  $\mu$ m pore size at 80 °C into quartz cuvettes (path length 10 mm). Before starting the measurement, each sample was equilibrated for 30 minutes at the required temperature. Three individual

measurements were performed for each sample to test the reproducibility with one measurement consisting of 3 runs of 30 seconds each. The experimental data were analyzed with the aid of the ALV-correlator software taking into account the temperature correction of viscosity.

### 2.2.7 Small Angle Neutron Scattering (SANS)

Due to the small wavelength of neutrons, Small Angle Neutron Scattering (SANS) can be used to resolve atomic structures as neutrons are scattered by atomic nuclei. Neutrons for scattering experiments are obtained from nuclear fission and are slowed down to thermal neutrons ( $\lambda \approx 1.8 \text{ \AA}$ ) by moderators. A neutron beam with a narrow wavelength distribution is focused on a cuvette with a sample solution and the scattered neutrons are recorded with a two-dimensional, position sensitive detector (e.g., BaF<sub>3</sub>-detector). The position of the detector is varied to enable the measurement in a large region of the scattering vector  $q$ .<sup>[19, 51]</sup>

The intensity of the scattered neutrons  $\Sigma$  is recorded at an angle  $2\theta$  in the solid-angle element  $d\Omega$ . For analysis, the differential scattering intensities  $d\Sigma(q)/d\Omega$  are plotted as a function of the scattering vector  $q$ . A fit of this function with the Indirekt Fourier Transform Method (IFT, Glatter-Fit) needs only minor additional information on the possible aggregate structure (dimensions (e.g., spherelike or rodlike), maximal value of the diameter, cross-section diameter, and thickness, respectively) and gives a value for the radius of gyration of the aggregate structure.<sup>[27, 52-53]</sup>

The pair distance distribution function  $p(r)$  is the self-convolution of the scattering distribution within the aggregates and can be used to calculate further characteristic values such as the mass of the aggregates (spherical aggregates) or the mass per unit length of the aggregate (rodlike aggregates).<sup>[27-28]</sup> After calculating the scattering length of the sample molecules, further values such as the aggregation number or the radius of the aggregates can be determined. This procedure has been described in detail previously.<sup>[54]</sup>

#### Experimental procedure

SANS experiments were carried out with the SANS-1 instrument in the FRG 1 research center, Geesthacht, Germany.

The bolaamphiphiles were suspended in heavy water or in deuterated acetate buffer at pH 5 (10 mM) at a concentration of  $1 \text{ mg ml}^{-1}$  and the suspensions were filtered through a Nylon membrane filter of  $0.45 \text{ }\mu\text{m}$  pore size at  $80 \text{ }^\circ\text{C}$ . The samples were placed in a thermostated sample holder for isothermal conditions ( $\Delta T = 0.5 \text{ }^\circ\text{C}$ ) in quartz cuvettes with a

path length of 2 mm (suspensions of DMAPPC-C32-POH, PC-C36diAc-PC and Me<sub>2</sub>PE-C36diAc-Me<sub>2</sub>PE) or 5 mm (suspensions of PC-C32SS-PC and Me<sub>2</sub>PE-C32SS-Me<sub>2</sub>PE).

For polymerization the suspensions of PC-C36diAc-PC and Me<sub>2</sub>PE-C36diAc-Me<sub>2</sub>PE were irradiated in a cold room at 5 °C for 20 minutes with a UV lamp (low-pressure Hg lamp,  $\lambda = 254$  nm,  $P = 15$  W) at a distance of 4.5 cm. Four sample-to-detector distances were employed to cover the range of scattering vectors  $q$  from 0.05 to 2.5 nm<sup>-1</sup>. Transmission of the samples was approx. 70 % and the contribution of multiple scattering can be considered negligible. The raw scattering data were corrected for the background from the solvent, sample cell, and other sources using conventional procedures. Subsequently, the scattering data were fitted the Indirect Fourier Transform Method. A detailed description of this process was given by Meister et al.<sup>[27-28]</sup>

### 2.2.8 (cryo-) Transmission Electron Microscopy (TEM)

With the help of Transmission Electron Microscopy (TEM) high resolution images of samples can be recorded due to the small wavelength of the electron beam. To minimize scattering of electrons by gases the inside of the microscope is kept at high to ultra-high vacuum. A hot cathode emits electrons that are accelerated by an accelerating voltage of 60 kV to 200 kV. Electron lenses are then used to focus the beam onto the sample where the electrons are scattered or absorbed. In parts with high amounts of material many electrons are scattered or absorbed resulting in a lower intensity of the electron beam than in parts with small amounts of material. The image is shown on a fluorescent screen and can be recorded with a camera.<sup>[19]</sup>

Due to the strong interaction of the electron beam with the sample material only very thin samples of up to 0.1  $\mu\text{m}$  can be examined. These may be thin slices of the material or a sample suspended on a small grid. If the contrast of the pure sample is too low, a contrast medium can be added in the preparation process. Solutions of heavy metals (e.g.,  $\text{UO}_2(\text{CH}_3\text{COO})_2$  or  $\text{OsO}_4$ ) scatter and absorb electrons strongly and can be used for this purpose.<sup>[19]</sup>

A disadvantage of TEM is that only dried samples can be examined in a limited temperature region. Cryo-TEM enables the examination of solutions without prior drying as the samples are quickly cooled down from a specific temperature in the preparation process. This is achieved by rapid plunging of a grid supporting a thin film of the sample into liquid ethane preventing the crystallization of the solvent.<sup>[55]</sup>

### Experimental procedure

Transmission Electron Microscopy (TEM) images were recorded with a Zeiss EM 900 electron transmission microscope (Carl Zeiss NTS GmbH, Oberkochen, Germany). 5  $\mu\text{l}$  of the sample suspensions ( $c = 0.3 \text{ mg ml}^{-1} - 0.01 \text{ mg ml}^{-1}$ ) were spread on a copper grid coated with a Formvar film. After 1 minute the excess solution was blotted off with filter paper. The samples were stained with 1 % uranyl acetate solution (20  $\mu\text{l}$ ) which was again drained off after 1 minute. The samples were dried at 30 °C overnight.

For the samples prepared below ambient temperature the components were stored (24 h) and the samples prepared in a cold room below 5 °C. They were dried for 2 days at 5 °C and kept in an exsiccator at ambient temperature until the images were recorded.

For the samples prepared at 30 °C, the suspension and all utensils were kept in a drying oven at 30 °C for 1 hour. The preparation and drying of the TEM grid were carried out inside the drying oven, too.

The cryo-Transmission Electron Microscopy (cryo-TEM) images were recorded with a Zeiss 902A instrument (Carl Zeiss NTS GmbH, Oberkochen, Germany) in cooperation with G. Karlsson and Prof. M. Almgren (Department of Physical and Analytical Chemistry, Uppsala University, Sweden). The samples were prepared in a chamber with controlled temperature and humidity. A drop of the bolaamphiphile suspension ( $c = 1 \text{ mg ml}^{-1}$ ) was placed on a grid coated with a perforated polymer film. Excess solution was removed after 1 minute with filter paper. Vitrification of the remaining thin film was achieved by rapid plunging of the grid into liquid ethane, held just above the freezing point. The vitrified sample was kept below 108 K after this process and while recording the images.

### **2.2.9 Oscillatory Rheology**

Ideal viscous fluids can be described with Newton's law, whereas ideal elastic solids follow Hook's law. Most samples, however, combine viscous and elastic properties. They exhibit viscoelasticity. Viscoelastic properties can be examined using oscillatory rheology.

A suitable model for the theoretical description of oscillatory rheology is a variation of the model of sliding plates. The plates have the area  $A$  and the distance  $h$ . The moving plate is attached to a rotating wheel causing the plate to execute an oscillating movement with the force  $F$ , the deflection  $s$ , and the velocity  $v$ , while the lower plate remains immobile (Figure 2.1).

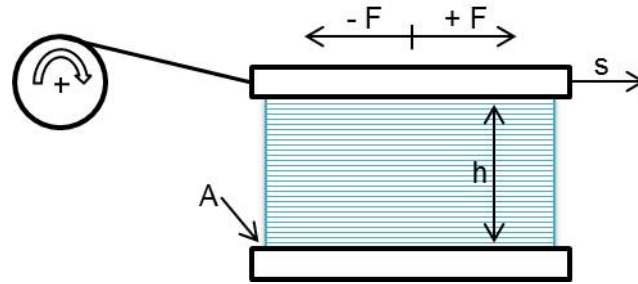


**Figure 2.1:** Sliding plates model for oscillatory rheological experiments.

Using the model of sliding plates the characteristic parameters shear stress  $\tau$ , deformation  $\gamma$ , and shear rate  $\dot{\gamma}$  can be defined.

$$\tau = \frac{F}{A} \quad \text{Equation 2.3}$$

$$\gamma = \frac{s}{h} \quad \text{Equation 2.4}$$

$$\dot{\gamma} = \frac{v}{h} \quad \text{Equation 2.5}$$

The oscillating movement of the upper plate can be described using the harmonic function in Equation 2.6.

$$\gamma(t) = \gamma_A \cdot \sin \omega t \quad \text{Equation 2.6}$$

$\gamma_A$  is the amplitude of the oscillation,  $\omega$  the angular frequency, and  $t$  the time of the measurement. The shear rate then performs an oscillation according to Equation 2.7.

$$\dot{\gamma}(t) = \frac{d\gamma}{dt} = \gamma_A \cdot \omega \cdot \cos \omega t \quad \text{Equation 2.7}$$

The resulting shear stress  $\tau$  depends on the movement of the upper plate and can, like the deformation  $\gamma$ , be described using a harmonic function.<sup>[56-57]</sup>

If an ideal elastic solid is examined between the sliding plates, the functions of shear stress  $\tau$  and deformation  $\gamma$  will be in phase. According to Hook's law, the force  $F$  is proportional to the deflection, meaning that the shear stress will be maximal if the deflection is maximal, i.e., the phase difference angle  $\delta$  will be zero ( $\delta = 0^\circ$ ).

In the case of ideal viscous samples the behavior is described by Newton's law leading to a dependence of the shear stress  $\tau$  on the shear rate  $\dot{\gamma}$ . For the oscillating movement of the upper plate, the shear rate is maximal if the deflection is minimal. This causes a shift of  $90^\circ$  for the shear stress with respect to the applied deformation ( $\delta = 90^\circ$ ).

If real, viscoelastic samples are examined, a phase difference between deformation and shear stress is detected. The phase difference angle  $\delta$  is found to be between  $0^\circ$  and  $90^\circ$ . This is caused by the different properties of the sample that contribute to the rheological response.

The contribution of the elastic properties is in phase and the contribution of the viscous properties is out of phase with the applied deformation.<sup>[56-57]</sup>

The phase difference angle  $\delta$  of the harmonic function of the deformation  $\gamma$  and the resulting harmonic function of the shear stress  $\tau$  are detected by the rheometer and used to calculate the two values  $G'$  and  $G''$  following Equation 2.8 and Equation 2.9.

$$G' = \frac{\tau_A}{\gamma_A} \cdot \cos \delta \quad \text{Equation 2.8}$$

$$G'' = \frac{\tau_A}{\gamma_A} \cdot \sin \delta \quad \text{Equation 2.9}$$

The storage modulus  $G'$  characterizes the elastic properties of a sample and the amount of stored deformation energy. The loss modulus  $G''$  characterizes the viscous properties of a sample and the amount of deformation energy lost by thermal dissipation or through structural changes of the sample. The loss factor  $\tan \delta$  is the ratio of  $G''$  and  $G'$ .

$$\tan \delta = \frac{G''}{G'} \quad \text{Equation 2.10}$$

For a sample in the gel state  $G'$  will be higher than  $G''$  and  $\tan \delta < 1$ . At the transition point from gel to sol state  $G'$  and  $G''$  have the same size and  $\tan \delta$  will be 1. Fluids are characterized by loss factors larger than 1.

It is important for the examination of the rheological properties of samples to prevent a break-down of the specific sample structure during the measurement. To ensure the stability of the sample structure, oscillatory rheological experiments are performed inside the linear viscoelastic (LVE) region. Inside this region no irreversible deformation of the structure occurs. The limit of this region is determined in an amplitude sweep and a frequency sweep experiment. For the amplitude sweep the amplitude of the harmonic function describing the deformation is increased during the experiment while keeping the angular frequency constant. During the frequency sweep, the amplitude is kept constant with increasing angular frequency. Storage and loss modulus are displayed as a function of the deformation and the angular frequency, respectively. The moduli remain independent on the deformation and the angular frequency up to a certain limit. Above this limit the structure of the sample is changed and may take a long time to reform. Therefore, values of the deformation and the angular frequency have to be chosen below this limit to ensure that measurements are performed inside the LVE region.

Experimental procedure

Oscillatory rheological measurements were carried out with an Anton Paar MCR301 rheometer (Anton Paar GmbH, Graz, Austria) controlled by the software RheoPlus supplied by Anton Paar. A cone-plate shear geometry (2°, 50 mm, gap size: 50 or 209  $\mu\text{m}$ ) with a thermostating unit and a thermostatted hood to improve temperature stability were used. The concentration of the bolaamphiphile suspensions was  $1 \text{ mg ml}^{-1}$  if not stated otherwise. The samples were left to equilibrate for 30 minutes prior to the measurements, which were performed in the temperature range from 2 to 80  $^{\circ}\text{C}$ . Temperature dependent measurements were performed with a heating and cooling rate of  $20 \text{ }^{\circ}\text{C h}^{-1}$ . Cone and gap were covered with small amounts of low viscosity silicone oil to prevent evaporation of water. Amplitude sweeps were carried out with a constant angular frequency of  $\omega = 1 \text{ rad s}^{-1}$  and for the frequency sweeps a deformation of  $\gamma = 1\%$  was utilized.

Experimental remarks

All samples were prepared at least one day prior to the measurements and were stored at 4  $^{\circ}\text{C}$  until they were examined. A systematic dependence of the storage and loss modulus or the loss factor on the age of the suspensions could not be found (Figure 2.2).

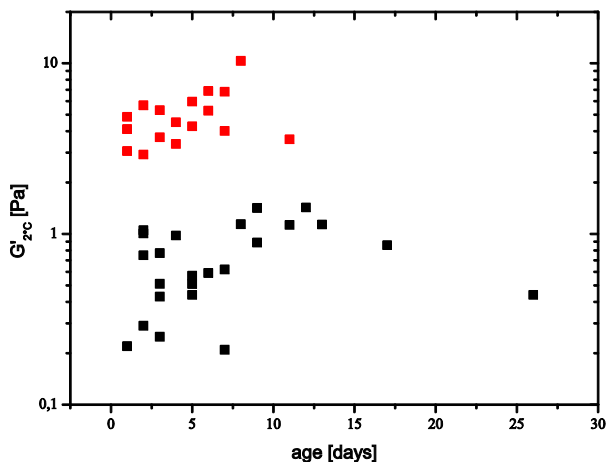


**Figure 2.2:** Dependence of the initial value of the storage modulus ( $G'$ ) of suspensions ( $c = 1 \text{ mg ml}^{-1}$ ) of PC-C32-PC in water (black) and Me<sub>2</sub>PE-C32-Me<sub>2</sub>PE in acetate buffer at pH 5 (red) at 2  $^{\circ}\text{C}$  on the age of the sample. Samples were equilibrated for 30 minutes at 2  $^{\circ}\text{C}$  before oscillatory rheological measurements with  $\gamma = 1\%$  and  $\omega = 1 \text{ rad s}^{-1}$  were performed.

The values in Figure 2.2 show that the storage moduli measured for the viscoelastic gels depend on the sample property and not on their age. Analysis of the data results in a mean value of  $G' = 0.76 \pm 0.35 \text{ Pa}$  for PC-C32-PC suspensions and a mean value of  $G' = 5.35 \pm 1.80 \text{ Pa}$  for Me<sub>2</sub>PE-C32-Me<sub>2</sub>PE suspensions at 2  $^{\circ}\text{C}$  at the concentration  $c = 1 \text{ mg ml}^{-1}$ . This shows that an exact reproduction of the values is difficult and depends on the samples preparation history.

Therefore, it is important to treat all samples in the same way to achieve reproducibility and to insert equilibration times prior to each measurement to diminish influences caused by the filling of the sample in the measuring gap.

The influence of the silicone oil used to prevent solvent evaporation on the values of the rheological measurements was examined previously showing no significant change with respect to the measured values.<sup>[49]</sup>

Temperature dependent measurements were carried out in the temperature range from 2 to 60 or 80 °C. Depending on the bolaamphiphile in the suspension, the aggregates were in different aggregation states at 60 or 80 °C (e.g., micelles I or II).<sup>[28]</sup> However, a systematic dependence of the gel reformation process on this aggregate structure could not be detected.

Frequency sweeps were performed in the angular frequency region from 0.05 to 500 rad s<sup>-1</sup>. The increase of storage and loss modulus at high angular frequencies can be ascribed to the influence of wall slip effects at the interface of the suspension with the surface of cone and plate<sup>[58]</sup> and the beginning of turbulent instead of laminar flow.<sup>[56]</sup>

A cone-plate shear geometry was used instead of a plate-plate shear geometry to achieve independence of the shear rate from the radius of the measuring system.<sup>[57]</sup>

### Measuring gap

Due to an exchange of the cone measuring system, experiments on the salt-dependent rheological properties of Me<sub>2</sub>PE-C32-Me<sub>2</sub>PE at pH 11 were carried out with a different size of the measuring gap between cone and plate. The gap increased from 50 μm to 209 μm after this exchange. However, an influence on the storage and loss moduli was only detected for measurements of the Me<sub>2</sub>PE-C32-Me<sub>2</sub>PE suspensions at pH 11 with NaCl and KCl. The values of the moduli were almost 10 times smaller in the experiments with the larger gap. Measurements with Me<sub>2</sub>PE-C32-Me<sub>2</sub>PE suspensions at pH 11 with CaCl<sub>2</sub> and MgCl<sub>2</sub> or in acetate buffer at pH 5 did not show a change depending on the size of the gap between cone and plate. This might be connected with the size of the aggregates present in the suspension. In suspensions of Me<sub>2</sub>PE-C32-Me<sub>2</sub>PE in acetate buffer at pH 5 the fibers can be up to several micrometers long<sup>[26]</sup> but at pH 11 the fibers can be considerably less stable and shorter (see Chapter 3.1.1). Salt added to the Me<sub>2</sub>PE-C32-Me<sub>2</sub>PE suspension at pH 11 enabled the formation of longer and more stable fiber segments.

It is important for rheological measurements to consider the size of the measuring gap with respect to the order of magnitude of the aggregates within the examined sample. Sample structures that are able to form gap-spanning structures can lead to an increase in the elastic behavior of the sample. Non-gap-spanning structures can, on the other hand, induce a more viscous behavior caused by “loose ends” in the space between cone and plate.<sup>[59-60]</sup>

In the case of very long fibers, the single fibers are probably aligned to some degree parallel to the surfaces of cone and plate and are entangled to form a viscoelastic structure. If the fibers are shorter, however, an orientation perpendicular to these surfaces is possible, which leads to gap-spanning fiber segments that cause an increase in the measured elasticity of the sample. In the suspensions of Me<sub>2</sub>PE-C32-Me<sub>2</sub>PE at pH 11 with NaCl and KCl some of the short fiber segments can span the gap distance of 50 μm and increase the elasticity but at a gap distance of 209 μm this behavior is not possible as the segments are either too short to span the distance or too long and therefore oriented parallel to the surface resulting in the observed decrease of the viscoelasticity of the samples with shorter and less stable fibers.

### 3 Results and Discussion

The aggregation behavior of single-chain bolaamphiphiles strongly depends on the ratio of the spatial requirements of headgroups and spacer chain. The possibility to vary the chemical structure of the headgroups enables a tuning of the aggregation behavior.

The charge and degree of protonation of the Me<sub>2</sub>PE headgroup of the bolaamphiphile Me<sub>2</sub>PE-C32-Me<sub>2</sub>PE depends on the pH value of the suspension. The properties of the aggregates and the suspensions were investigated before<sup>[26]</sup> and are here expanded by the dependence of the self-assembly process on pH value and salinity (see Chapter 3.1). In addition, an extensive rheological characterization of the gel was performed (see Chapter 3.1.3).

Asymmetry of the single-chain bolaamphiphiles is another way of influencing the aggregation behavior. The formation of several different aggregate structures was observed for systems of bolaamphiphiles such as, e.g., nanotubes or membranes.<sup>[15, 61]</sup> The self-assembly process of the asymmetrical bolaamphiphile DMAPP-PC32-POH in aqueous suspension is described in Chapter 3.2. The interaction of gold nanoparticles (AuNPs) with aggregates of the asymmetrical bolaamphiphile enables the one-dimensional orientation of AuNPs (see Chapter 3.5.2) as it was also described for nanofibers of PC-C32-PC.<sup>[30]</sup>

After extensive characterization of the aggregation behavior of the bolaamphiphiles PC-C32-PC and Me<sub>2</sub>PE-C32-Me<sub>2</sub>PE into fibers<sup>[24-29]</sup> the question arose, how tolerant the fiber structure is to differences induced to the chemical structure of the spacer chain.

This structural modification was realized via the incorporation of heteroatoms (e.g., oxygen or sulfur) into the structure of the spacer chain (see Chapter 3.3) and by adding diacetylene groups to the alkyl chain within the spacer (see Chapter 3.4). A related topic is the idea of utilizing these structural changes to attain functionality of the nanofibers for different purposes.

The possibility of achieving a one-dimensional orientation of AuNPs along the bolaamphiphile fibers was described before<sup>[30]</sup> and the use of sulfur containing bolaamphiphiles as building block of the nanofibers might improve the interaction between the fibers and the AuNPs (see Chapter 3.5.1 and Chapter 3.5.2).<sup>[62]</sup>

The possibility of forming thermostable nanofibers via polymerization of diacetylene containing bolaamphiphiles is described in Chapter 3.4.2. This procedure is also used for stabilization of films and membranes<sup>[63]</sup> and might prevent the temperature dependent break-up of the nanofibers into micelles.

### 3.1 pH- and Salt-Dependent Aggregation Behavior of Me<sub>2</sub>PE-C32-Me<sub>2</sub>PE

Gels formed by nanofibers or wormlike micelles in water are a field of research that has gained much interest due to the large variety of substances that can be utilized for different applications like optical components, tissue engineering, or drug release and delivery.<sup>[2, 17, 64-65]</sup> In the case of low molecular weight gelators it is easy to influence the gelling properties of the substances by changing parameters such as temperature, pH value, or salinity to achieve well-defined properties.<sup>[65-67]</sup>

The formation of fibers of Me<sub>2</sub>PE-C32-Me<sub>2</sub>PE depends on the pH value of the suspension. At neutral pH values the bolalipid has a zwitterionic headgroup (Figure 1.2). The  $pK_a^{\text{app}}$  values for the phosphate group and the dimethylammonium group were determined to be approximately 3.3 and 6.5, respectively.<sup>[26]</sup> Therefore, at high pH values the headgroup is deprotonated and the aggregation into fibers becomes unfavorable due to the repulsion between the negatively charged headgroups. However, SANS and TEM measurements still prove the presence of short fiber segments, but no gelation of the system can be observed.<sup>[26-27]</sup> This suggests that the charged headgroups mainly prevent the entanglements of the fibers stabilizing the gel structure.

The aggregates can be described as nanofibers, but they are more like an intermediate state between classical crystalline nanofibers and wormlike micelles of surfactants as they have properties similar to both systems.<sup>[18, 68]</sup> In contrast to classical crystalline fibers they form clear homogeneous gels that have quite high straining limits (see Chapter 3.1.3) and the SANS data show a slope of -1 in a plot of intensity  $I$  versus wave vector  $q$ .<sup>[27]</sup> This proves that they do not show Porod behavior implying molecular assemblies rather than crystalline fibers.<sup>[66, 68]</sup> On the other hand, disrupted gels of the symmetrical single-chain bolaamphiphiles take several hours to recover, a behavior which is uncommon in systems of wormlike surfactant gels.<sup>[68]</sup>

The aim of this study was to investigate how the aggregation behavior of Me<sub>2</sub>PE-C32-Me<sub>2</sub>PE can be influenced to obtain fibers and viscoelastic gels, tailoring the properties via changes of pH value and salt contents. Changing the pH value is a suitable way of adjusting the protonation of the headgroup and thus controlling the self-assembly process. In combination, the shielding of repulsive interaction between charged headgroups by means of additional salts is a promising method. This effect has already been examined with a bolalipid containing positively charged amino moieties in the headgroups.<sup>[36]</sup> The stabilizing effect of salts on different aggregates has often been described, e.g., for collagen fibers,<sup>[69]</sup> for the

rheological properties of mixtures of gellan gum and konjac glucomannan,<sup>[70]</sup> for interactions between phospholipids and calcium,<sup>[71]</sup> or for cationic wormlike micelles.<sup>[72]</sup>

### 3.1.1 pH-Dependent Aggregation Behavior of Me<sub>2</sub>PE-C32-Me<sub>2</sub>PE

#### DSC

To investigate the pH dependence of the aggregation behavior of Me<sub>2</sub>PE-C32-Me<sub>2</sub>PE and possible influences of buffer salts, a series of DSC measurements at different pH values were performed to analyze the changes in transition temperatures (Figure 3.1). In acetate buffer at pH 5, where the headgroup is zwitterionic, we can observe three transitions as reported before, with the first being a fiber-fiber transition (45 °C), the second a fiber-micelle transition (68.2 °C), and the third a micelle-micelle transition (84.5 °C). These transformations between different aggregate structures have been studied before with several methods, e.g., TEM, SANS, and FT-IR.<sup>[26-27, 30]</sup> The first transition is connected with an increase in *gauche* conformers of the alkyl chains as was determined by FT-IR measurements.<sup>[26]</sup> However, the fiber structure is still intact which is due to hydrogen bonding between the headgroups.

First rheological measurements showed that this transition is connected with a large drop in the elasticity of the gel structure<sup>[27]</sup> suggesting that the entanglement of the fibers is weakened. The second DSC peak was found to be connected with the transformation of the fibers into spherical micelles with a radius of 2.64 nm as determined by SANS measurements.<sup>[27]</sup> The third transition is a micelle-micelle transition during which the amount of *gauche* conformers in the alkyl chain further increases, but where the structural differences between the two types of micelles are still unclear.

In suspensions at pH 9 and 10, the first and second transitions are very broad and divided into several small peaks, but there are still peaks left at the same temperatures that were observed for suspensions at pH 5. The third transition is hardly influenced by changes in pH.

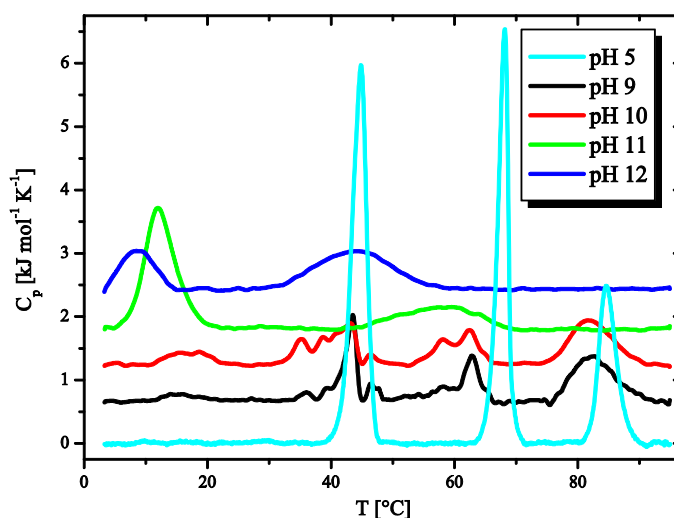


**Figure 3.1:** DSC heating curves of aqueous suspensions ( $c = 1 \text{ mg ml}^{-1}$ ) of Me<sub>2</sub>PE-C32-Me<sub>2</sub>PE in acetate buffer at pH 5 and at pH values from 9 to 12 (adjusted with NaOH solution). The heating and cooling rate was  $20 \text{ °C h}^{-1}$ . The DSC curves are shifted horizontally for clarity.

For the suspension at pH 10 a small transition below 20 °C can already be observed. A larger change becomes visible at pH 11 as the DSC curve now shows two broad peaks around 12 and 60 °C, respectively. This tendency increases at pH 12; then two broad transitions at 9 and 44 °C can be observed.

### TEM

TEM images were taken to determine the aggregate structures at the different pH values (Figure 3.2).

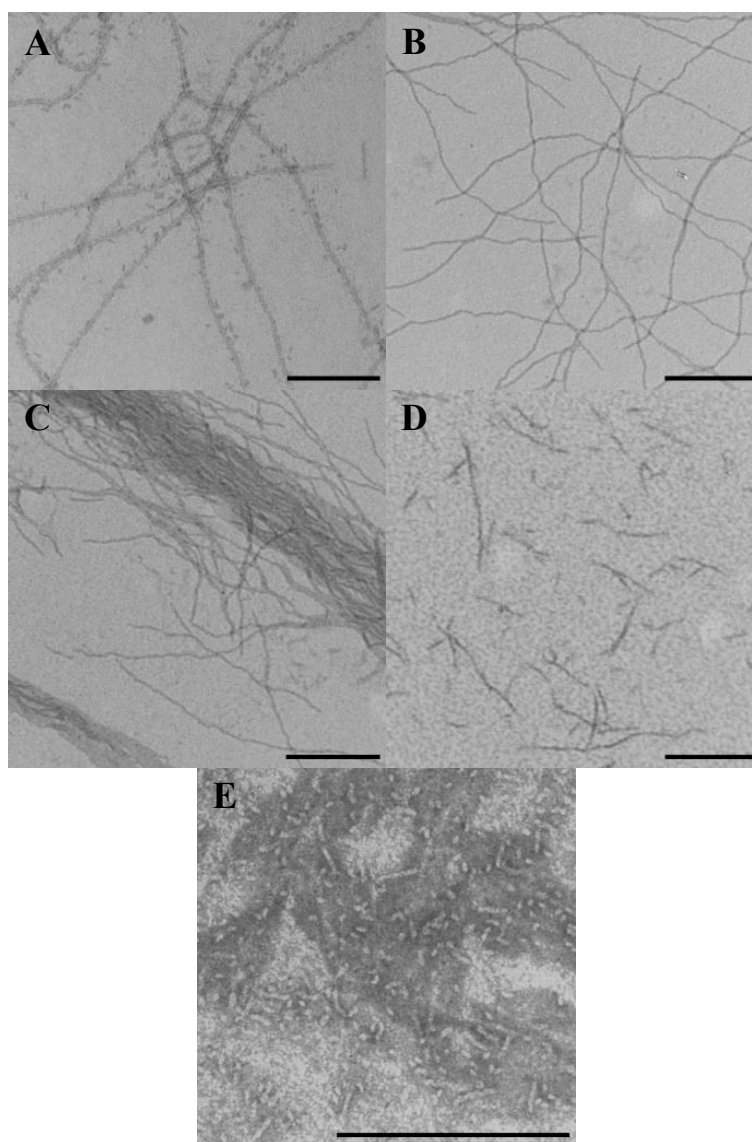


**Figure 3.2:** TEM images of aqueous suspensions of Me<sub>2</sub>PE-C32-Me<sub>2</sub>PE at (A): pH 9, 25 °C, (B): pH 10, 25 °C, (C): pH 11, 5 °C, (D): pH 12, 5 °C, and (E): pH 11, 25 °C. The bar corresponds to 200 nm. The samples were stained with uranyl acetate.

At 25 °C the suspensions at pH 9 and 10 show the presence of fibers (Figure 3.2A,B). The suspensions at pH 11 and 12 were prepared at 5 °C and these samples also show the

aggregation into fibers below the first transition (Figure 3.2C,D). The presence of short fiber segments in the sample at pH 12 is due to the very low temperature of the transition starting at 2 °C. If the suspensions are kept at 4 °C in the refrigerator for a few weeks, gelation can be observed for all pH values. The strongest gel seems to be formed at pH 9.

### DLS

Using DLS, the aggregate structure in the suspensions at pH 11 and 12 at 30 °C above the first transition was examined. The experiments reveal the presence of spherical micelles with a hydrodynamic radius of 2.6 nm for both pH values (Figure 3.3). This is also in accordance with the TEM image of a sample at pH 11 at 25 °C showing micelles (Figure 3.2E).

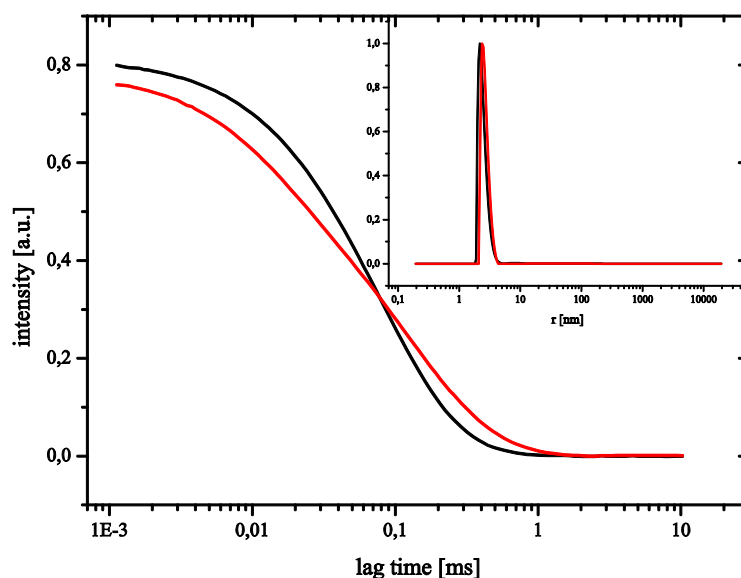


**Figure 3.3:** DLS autocorrelation functions and fits for aqueous suspensions ( $c = 1 \text{ mg ml}^{-1}$ ) of Me<sub>2</sub>PE-C32-Me<sub>2</sub>PE at pH 11 (black) and pH 12 (red) at 30 °C. The inset shows the number-weighted size distribution.

DSC and TEM prove that the fiber structure is destabilized at pH 9 and 10; the self-aggregation into fibers, however, is not completely inhibited at these pH values. The DSC curves reveal the presence of a mixture of aggregate types such as fibers, short fiber segments, and micelles as can be seen by the appearance of several small transition peaks. This was also observed in SANS measurements with the suspension in carbonate buffer at pH 10.<sup>[27]</sup> The deprotonation of the dimethylammonium headgroup does not seem to be complete at pH 10, and the changes in aggregation behavior at increasing temperature basically follow the same pattern as at pH 5. Probably, the fibers can tolerate a certain percentage of the negatively charged headgroups merely leading to reduced interactions between the fibers and to shorter fiber segments. However, the much larger shift of the transitions to lower temperature for

samples at pH 11 and 12 indicates that the effect of deprotonation with increasing negative charge of the headgroup is getting stronger and that the fibers are now only stable up to 12 or 9 °C, respectively. These results suggest that the apparent  $pK_a$  value of the dimethylammonium group is between pH 10 and 11 in solutions with low ionic strength. The previously reported  $pK_a^{\text{app}}$  value of 6.5 was obtained by using an automatic titrator with Me<sub>2</sub>PE-C32-Me<sub>2</sub>PE dissolved in 150 mM KCl.<sup>[26]</sup> As the apparent  $pK_a^{\text{app}}$  values depend on the ionic strength of a solution and are shifted to lower values with increasing salt concentration, it can be expected that the apparent  $pK_a^{\text{app}}$  value of the Me<sub>2</sub>PE headgroup deduced from the DSC measurements of pure aqueous suspensions without additional salt is higher than the previously determined one.

The fiber structure of Me<sub>2</sub>PE-C32-Me<sub>2</sub>PE is stabilized on the one hand by hydrophobic interactions between the alkyl chains. On the other hand, Me<sub>2</sub>PE-C32-Me<sub>2</sub>PE is able to form hydrogen bonds between its headgroups that further increase the stability of the aggregates and the gel structure. As the deprotonation of the Me<sub>2</sub>PE headgroup increases with higher pH values, this additional attractive interaction is overcompensated by an increasing repulsive interaction due to the negative charge of the phosphate group and the loss of the hydrogen-bond donor. The stability range of the self-assembled nanofibers is therefore shifted to lower temperature with increasing deprotonation of the dimethylammonium group.

### 3.1.2 Salt-Dependent Aggregation Behavior at pH 11

The possibility of influencing the aggregation behavior of suspensions of Me<sub>2</sub>PE-C32-Me<sub>2</sub>PE by other means besides changing the temperature or the pH value was of further interest. The negative net charge of the headgroup at high pH clearly caused a destabilization of the fiber structure. The addition of salt seems to be a suitable way of shielding this charge and enabling a better self-assembly depending on the pH value and the salinity. All further measurements were carried out at pH 11 as the previous results indicate that there are only micelles present at ambient temperature and no mixture of different aggregates such as micelles, short fiber segments, and nanofibers (Figure 3.2E).

#### DSC

In order to investigate the effect of different salts on the systems properties, DSC measurements with suspensions of Me<sub>2</sub>PE-C32-Me<sub>2</sub>PE at various concentrations of NaCl, KCl, MgCl<sub>2</sub>, and CaCl<sub>2</sub> were carried out to compare the different monovalent and divalent cations while keeping the anion the same (Figure 3.4).

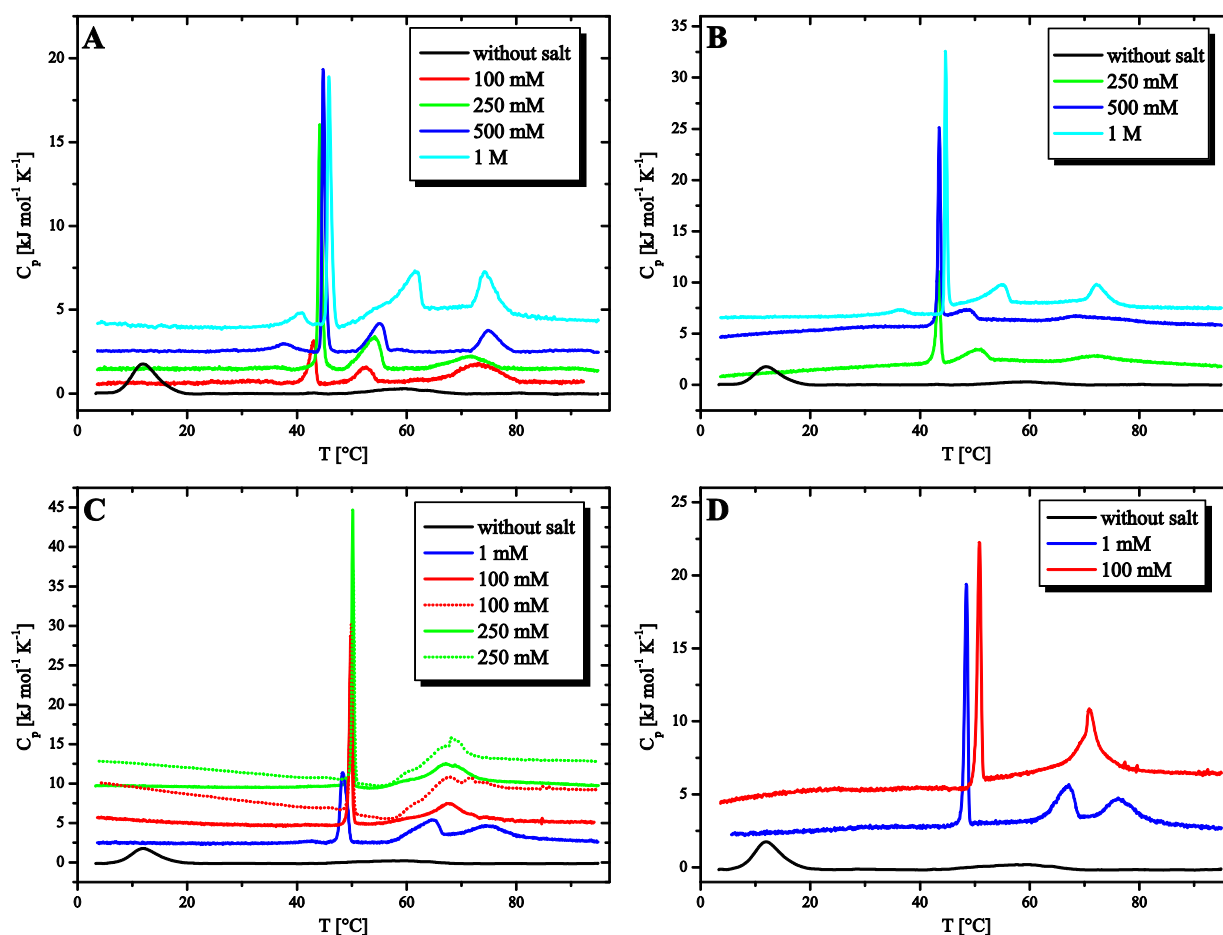


**Figure 3.4:** DSC heating curves of aqueous suspensions ( $c = 1 \text{ mg ml}^{-1}$ ) of  $\text{Me}_2\text{PE-C32-Me}_2\text{PE}$  at pH 11 with different concentrations of (A) NaCl, (B) KCl, (C)  $\text{MgCl}_2$ , and (D)  $\text{CaCl}_2$ . The heating rate was  $20 \text{ }^{\circ}\text{C h}^{-1}$  for the solid curves and  $60 \text{ }^{\circ}\text{C h}^{-1}$  for the dotted curves (C). The DSC curves are shifted horizontally for clarity.

The DSC heating curves for NaCl concentrations from 100 mM to 1 M are shown in Figure 3.4A. It is obvious that the addition of NaCl causes a general increase in the transition temperatures. Even at low concentration, the DSC curves reveal a profile comparable to that in acetate buffer at pH 5. With increasing concentration the first transition is slightly shifted to higher temperature, whereas the third transition becomes more cooperative with higher salt content. The largest effect of increasing salt concentration is observed for the second transition, where the temperature gradually increases from  $52.5 \text{ }^{\circ}\text{C}$  at 100 mM NaCl to  $61.8 \text{ }^{\circ}\text{C}$  at 1 M NaCl. At concentrations of 500 mM and 1 M NaCl a fourth transition appears at a temperature below the first one. This small transition was also observed previously for the zwitterionic bolaamphiphile PC-C32-PC.<sup>[25]</sup> The occurrence of this transition is dependent on the concentration of the bolalipid and the equilibration time before the measurement.<sup>[25]</sup> The longer a sample is equilibrated or the higher the concentration, the more pronounced the transition becomes. The DSC measurements suggest that this small transition also correlates

with the salt concentration. An overview of the transition temperatures and enthalpies determined by DSC is shown in Table 3.1.

**Table 3.1:** DSC transition temperatures and enthalpies of aqueous suspensions of Me<sub>2</sub>PE-C32-Me<sub>2</sub>PE at pH 11 with different concentrations of NaCl and KCl.<sup>a</sup>

	T [°C] ( $\Delta H$ [kJ mol <sup>-1</sup> ])						
	NaCl				KCl		
	100 mM	250 mM	500 mM	1 M	250 mM	500 mM	1 M
first transition	42.9 (4.8)	44.2 (12.8)	44.8 (12.2)	45.9 (12.8)	43.4 (8.2)	43.4 (10.8)	44.7 (12.7)
second transition	52.5 (2.7)	54.0 (7.3)	55.1 (4.9)	61.8 (8.1)	50.7 (4.4)	48.7 (2.3)	55.1 (6.5)
third transition	73.2 (8.2)	71.9 (4.9)	74.9 (5.0)	74.3 (7.1)	72.0 (4.7)	68.7 (5.7)	72.3 (5.2)

<sup>a</sup> The transition temperatures and enthalpies were determined from the DSC heating curves ( $c = 1 \text{ mg ml}^{-1}$ ) with a heating rate of  $20 \text{ }^\circ\text{C h}^{-1}$ .

The effect of KCl concentrations from 250 mM to 1 M on the transition behavior of Me<sub>2</sub>PE-C32-Me<sub>2</sub>PE suspensions at pH 11 can be seen in Figure 3.4B. Similarly as for solutions containing the sodium chloride, the DSC heating curves exhibit three distinct peaks. With increasing KCl concentration, the first transition is slightly shifted to higher temperature and the third transition becomes more cooperative. Again, the second transition shows the strongest dependence on the salt concentration, with the second and third transition for 500 mM KCl seeming to be an exception to this tendency (Table 3.1). This might be caused by experimental inaccuracy.

The binding of monovalent cations to negatively charged phosphate groups of phosphodiester is usually weak. This is different for the binding of divalent cations such as magnesium or calcium ions, as it has been studied in detail for the binding of ions to lipid vesicles containing the negatively charged lipid dimyristoyl-phosphatidylglycerol.<sup>[73]</sup> For the binding to the negatively charged headgroups of Me<sub>2</sub>PE-C32-Me<sub>2</sub>PE, effects similar to those observed for the binding to the headgroup region of flat bilayers are to be expected.

The DSC curves for Me<sub>2</sub>PE-C32-Me<sub>2</sub>PE solutions containing magnesium and calcium chlorides show significant differences as compared to curves obtained for solutions containing monovalent ions. Even for a low concentration of 1 mM the aggregation behavior changes drastically. As can be seen in Figure 3.4C, the DSC curve at 1 mM MgCl<sub>2</sub> has three peaks at 48.3, 64.8, and 74.6 °C suggesting an aggregation behavior of the bolaamphiphile similar to that in acetate buffer (pH 5). When the concentration is further increased, only two transitions at 49.8 and 67.6 °C appear. The second transition seems to be situated between the second

and the third transition of the sample with 1 mM MgCl<sub>2</sub>. Above the concentration of 250 mM MgCl<sub>2</sub> only a small further increase of the transition temperatures can be observed. Similar effects can be seen for measurements with CaCl<sub>2</sub> solutions (Figure 3.4D). However, solutions with a concentration higher than 100 mM CaCl<sub>2</sub> could not be examined because of precipitation of aggregates. Detailed information on transition temperatures and enthalpies is provided in Table 3.2.

**Table 3.2:** DSC transition temperatures and enthalpies of aqueous suspensions of Me<sub>2</sub>PE-C32-Me<sub>2</sub>PE at pH 11 with different concentrations of MgCl<sub>2</sub> and CaCl<sub>2</sub>.<sup>a</sup>

	T [°C] ( $\Delta H$ [kJ mol <sup>-1</sup> ])				
	MgCl <sub>2</sub>			CaCl <sub>2</sub>	
	1 mM	100 mM	250 mM	1 mM	100 mM
first transition	48.3 (12.7)	49.8 (15.0)	50.1 (14.3)	48.4 (12.6)	50.9 (14.1)
second transition	64.8 (10.7)	67.6 (19.0)	68.0 (17.5)	67.0 (7.7)	70.8 (16.0)
third transition	74.6 (8.5)			75.9 (8.1)	

<sup>a</sup> The transition temperatures and enthalpies were determined from the DSC heating curves ( $c = 1 \text{ mg ml}^{-1}$ ) with a heating rate of  $20 \text{ }^\circ\text{C h}^{-1}$ .

### TEM

To identify the structure of the aggregates below the first transition, TEM images of the suspensions containing 100 mM NaCl and 250 mM MgCl<sub>2</sub>, respectively, were recorded. Samples prepared at 25 °C show images with long fibers that are formed after the addition of the salt (Figure 3.5).

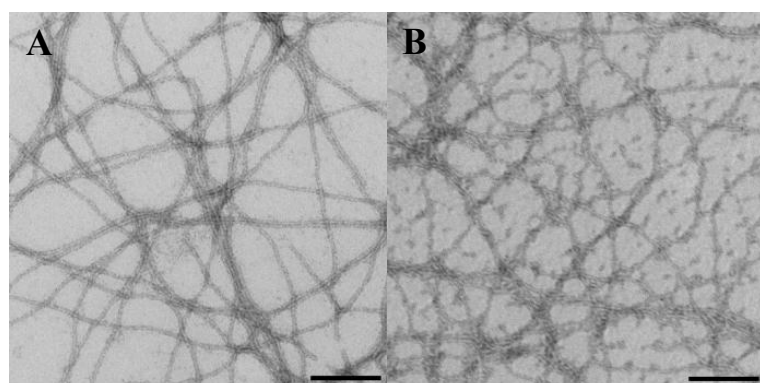


**Figure 3.5:** TEM images of aqueous suspensions of Me<sub>2</sub>PE-C32-Me<sub>2</sub>PE at pH 11 with (A) 100 mM NaCl and (B) 250 mM MgCl<sub>2</sub> at 25 °C. The bar corresponds to 50 nm. The samples were stained with uranyl acetate.

All cations are able to shield the electrostatic repulsion between the negatively charged headgroups and therefore enable a close arrangement of the headgroups in the fiber structure. Considering the similarities between the DSC curves of Me<sub>2</sub>PE-C32-Me<sub>2</sub>PE at pH 5

and pH 11 with added salts, respectively, and the corresponding TEM images (Figure 3.5), it is reasonable to assume the same aggregate structure found at pH 5. The presence of fibers

above the first transition is also in accordance with the rheological data of these samples (see rheological data in Chapter 3.1.3).

In addition, all suspensions with additional salt form a gel, with the gelling process being faster for higher salt concentration and for the divalent cations compared to the monovalent cations. As mentioned above, in the pH value range between 9 and 12 in pure water without additional salt, gelation can only be observed after a few weeks incubation at a temperature of 4 °C.

In comparing the transition temperatures for the suspensions with NaCl and KCl, it becomes obvious that the stabilizing effect of NaCl on the system is stronger. Several experiments on ion binding to lipids have revealed that monovalent cations have small association constants for binding to negatively charged lipid headgroups. The constant is higher for sodium compared to potassium.<sup>[74-75]</sup> The stronger binding of sodium to the negatively charged Me<sub>2</sub>PE headgroup compared to potassium is in line with these observations on bilayer systems; it leads to an increased stabilization of the fibers by sodium compared to potassium.

A much lower concentration of the divalent magnesium and calcium cations is necessary to achieve the same stabilizing effect as for the monovalent ions. Compared with the monovalent cations, the association constants are much higher for the divalent cations.<sup>[76-77]</sup> In addition, these cations can bind to two negatively charged headgroups. A significant difference can also be observed in the gelling process when the solution contains divalent cations. Gelation starts very fast after the addition of the divalent salts at room temperature, whereas for NaCl and KCl this process may take several days at 4 °C. The divalent cations can not only bind to two adjacent headgroups in the same fiber but can also enhance the cross-linking of the fibers by connecting two fiber strands leading to the formation of stronger gels (see rheological data in Chapter 3.1.3).

Calcium has a greater stabilizing effect on the fiber and gel structure than magnesium. The main reason is to be seen in the stronger binding of the calcium cations to the headgroups containing negatively charged phosphate groups through the formation of inner sphere complexes as shown by calorimetric measurements with DMPG<sup>[73]</sup> and in other works concerning the interaction between lipids and divalent cations.<sup>[76, 78]</sup> This apparently leads to increased stability of the fiber and the gel structure compared to the measurements with magnesium.

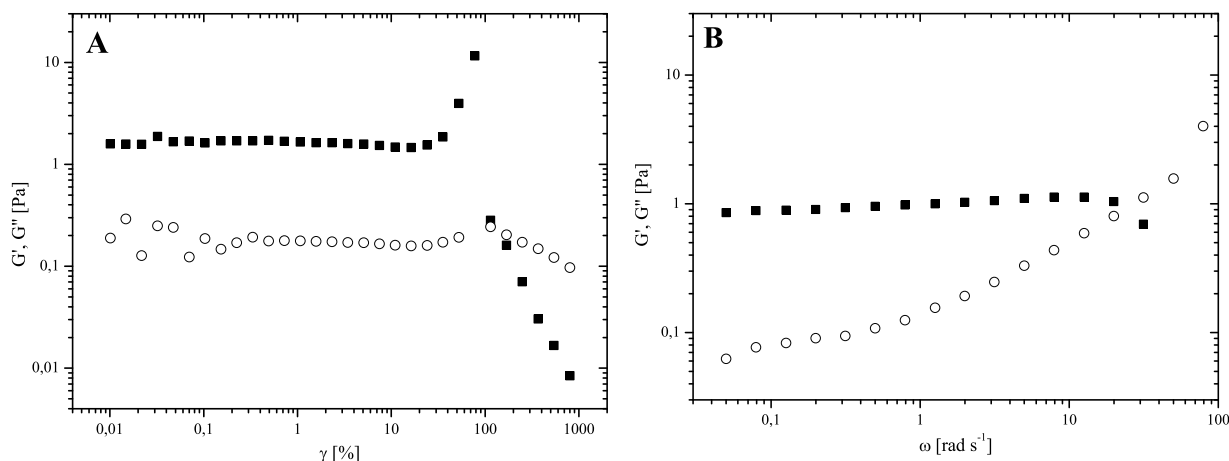
The appearance of only two transitions at higher concentration of  $\text{MgCl}_2$  can be explained when the heating curves of the suspensions containing 100 and 250 mM  $\text{MgCl}_2$  obtained with a heating rate of  $60\text{ }^\circ\text{C h}^{-1}$  are compared (Figure 3.4C, dotted curves). These curves exhibit a split second transition compared to a single transition observed with a heating rate of  $20\text{ }^\circ\text{C h}^{-1}$ . At 1 mM  $\text{MgCl}_2$ , three transitions are observed, regardless of the heating rate. The fiber-micelle transition (second transition) is shifted by  $3\text{ }^\circ\text{C}$  to higher temperature, and the micelle-micelle transition is shifted to lower temperature by  $10\text{ }^\circ\text{C}$  in contrast to the suspension in acetate buffer. At a concentration of 100 mM  $\text{MgCl}_2$  the temperature difference between both transitions is so small that they superimpose into one and can only be resolved when the heating rate is increased. This transition then combines the transformation of the fiber structure into micelles and the micelle-micelle transition, where an increase in fluidity of the alkyl chains inside the micelles takes place. This is also supported by the transition enthalpy of the merged transition, which has about the same value as the sum of the fiber-micelle and the micelle-micelle transition (Table 3.2).

For 100 mM  $\text{CaCl}_2$  the DSC cooling curves also show the splitting of the transition that was already observed for  $\text{MgCl}_2$  (data not shown).

### 3.1.3 Rheology of $\text{Me}_2\text{PE-C32-Me}_2\text{PE}$ Suspensions

In aqueous suspensions of  $\text{Me}_2\text{PE-C32-Me}_2\text{PE}$  the bolalipids form a transparent gel consisting of a dense three-dimensional network of nanofibers. This gel can be influenced depending on the pH value and the salt concentration. To investigate the gels properties such as strength and viscoelasticity oscillatory rheology was used. The rheological behavior of  $\text{Me}_2\text{PE-C32-Me}_2\text{PE}$  at pH 5 was studied before<sup>[27]</sup> and was repeated here for purposes of comparison when the influence of the salt concentration at pH 11 on the rheological behavior was studied. In addition, a higher density of data points and a wider temperature range were used to investigate the changes in  $G'$  and  $G''$  more closely.

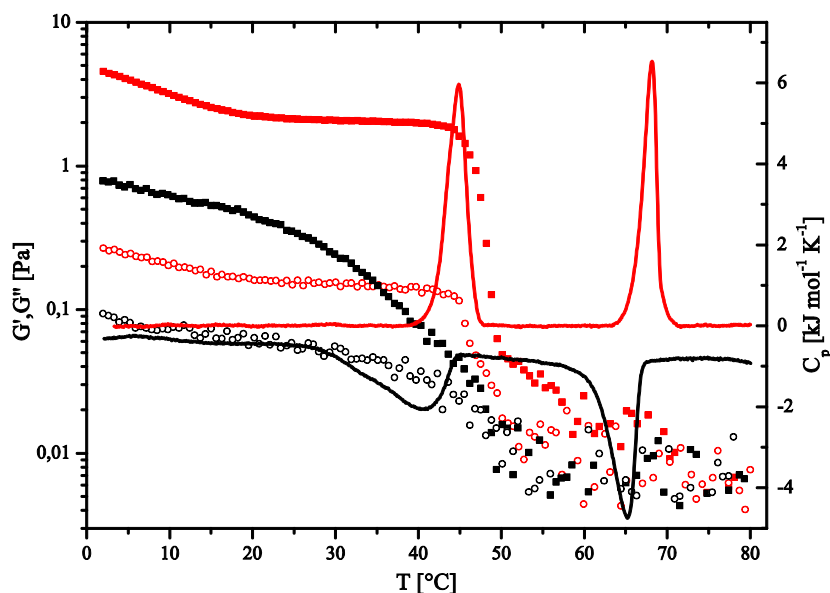
The amplitude sweep in Figure 3.6A shows that  $G'$  and  $G''$  are independent of the deformation up to approximately 30 %. At higher deformations strain stiffening is observed followed by the crossover of  $G'$  and  $G''$  indicating the transition from gel to sol. The frequency sweep at  $2\text{ }^\circ\text{C}$  shows a plateau of  $G'$  up to  $10\text{ rad s}^{-1}$  (Figure 3.6B) at the concentration  $c = 1\text{ mg ml}^{-1}$ .  $G''$  increases with increasing angular frequency until a crossover at  $20\text{ rad s}^{-1}$  occurs. This behavior is caused by the high angular frequency and probably wall slip at the interface of cone and gap with the sample.



**Figure 3.6:** (A) Amplitude sweep ( $\omega = 1 \text{ rad s}^{-1}$ ) and (B) frequency sweep ( $\gamma = 1 \%$ ) of a suspension of Me<sub>2</sub>PE-C32-Me<sub>2</sub>PE ( $c = 1 \text{ mg ml}^{-1}$ ) in acetate buffer at pH 5 at 2 °C.  $G'$ : filled squares,  $G''$ : open circles.

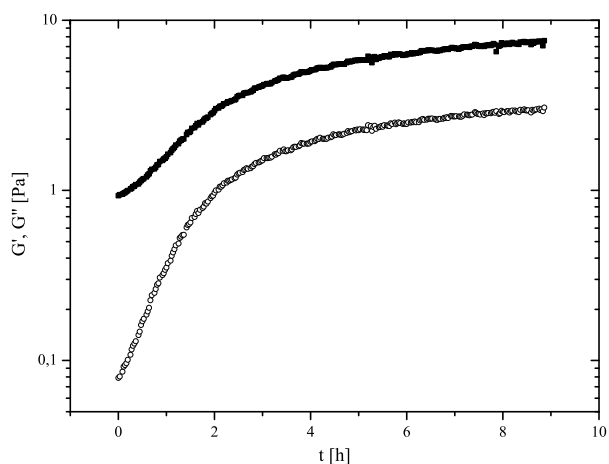
The rheological measurements were therefore performed using the same experimental conditions as the DSC measurements to ensure comparability. Deformation ( $\gamma = 1 \%$ ) and angular frequency ( $\omega = 1 \text{ rad s}^{-1}$ ) were chosen inside the linear viscoelastic (LVE) region (Figure 3.6).

Figure 3.7 displays  $G'$  and  $G''$  as a function of temperature, along with the calorimetric data of a suspension of Me<sub>2</sub>PE-C32-Me<sub>2</sub>PE in acetate buffer at pH 5. In the temperature range from 2 to 20 °C a steady decrease in  $G'$  occurs followed by constant values up to 45 °C. Up to this temperature  $G'$  is about one order of magnitude higher than  $G''$ . Both moduli are almost independent of temperature in this region. Correlating with the fiber-fiber transition, a large drop in  $G'$  and  $G''$  can be observed at 45 °C. Above this temperature the difference in  $G'$  and  $G''$  decreases, however,  $G'$  is still higher. At approximately 60 °C, which is slightly below the fiber-micelle transition of the aggregates,  $G'$  and  $G''$  have about the same magnitude and the suspension behaves as a Newtonian fluid.



**Figure 3.7:** DSC curves (solid lines) and rheological data ( $G'$ : filled squares,  $G''$ : open circles) of an aqueous suspension of  $\text{Me}_2\text{PE-C32-Me}_2\text{PE}$  in acetate buffer at pH 5 ( $c = 1 \text{ mg ml}^{-1}$ ). The heating and cooling rate was  $20 \text{ }^\circ\text{C h}^{-1}$ . Deformation ( $\gamma = 1 \%$ ) and angular frequency ( $\omega = 1 \text{ rad s}^{-1}$ ) were chosen inside the linear viscoelastic region. Heating: red, cooling: black.

Below  $45 \text{ }^\circ\text{C}$   $G'$  and  $G''$  show the characteristic behavior of a gel with viscoelastic properties. These data support the macroscopic observation of the gelation. At  $45 \text{ }^\circ\text{C}$  the macroscopic breakdown of the gel can be observed but the fiber structure and a weak viscoelasticity remain intact as was previously shown by rheology, cryo-TEM, and by SANS measurements.<sup>[26-27]</sup> At this temperature the cross-linking between the hydrophobic parts of different fiber strands via hydrophobic interactions, the hydrogen bonding between the headgroups, and the entanglement of fibers weaken.<sup>[26-27]</sup> During the fiber-micelle transition at  $68 \text{ }^\circ\text{C}$  the fiber structure breaks down and spherical micelles remain. This micellar solution exhibits no viscoelastic properties and shows Newtonian behavior. These results are in accordance with the previous measurement,<sup>[27]</sup> however, showing a nearly 10-fold lower  $G'$  value due to the almost 10-fold lower concentration. Upon cooling,  $G'$  and  $G''$  show a hysteresis and the reformation of the gel structure does not occur until the sample is cooled below  $50 \text{ }^\circ\text{C}$ . Subsequently, a slow increase can be monitored, but the initial values of  $G'$  and  $G''$  are reached only after tempering several hours at  $2 \text{ }^\circ\text{C}$  (Figure 3.8).



**Figure 3.8:** Time dependent rheological data of an aqueous suspension ( $c = 1 \text{ mg ml}^{-1}$ ) of Me<sub>2</sub>PE-C32-Me<sub>2</sub>PE in buffer at pH 5 at 2 °C after heating to 80 °C and subsequent cooling to 2 °C. The heating and cooling rate was 20 K h<sup>-1</sup>. Deformation ( $\gamma = 1 \%$ ) and angular frequency ( $\omega = 1 \text{ rad s}^{-1}$ ) were chosen inside the linear viscoelastic region.  $G'$ : filled squares,  $G''$ : open circles.

Figure 3.10.

For the monovalent cations sodium and potassium (Figure 3.10A,B) the data show the characteristics of weak viscoelastic gels with  $G'$  being larger than  $G''$  and independent of temperature up to the transition at 45 °C. This correlates well with the DSC transition temperatures of the fiber-fiber transition (Table 3.1).

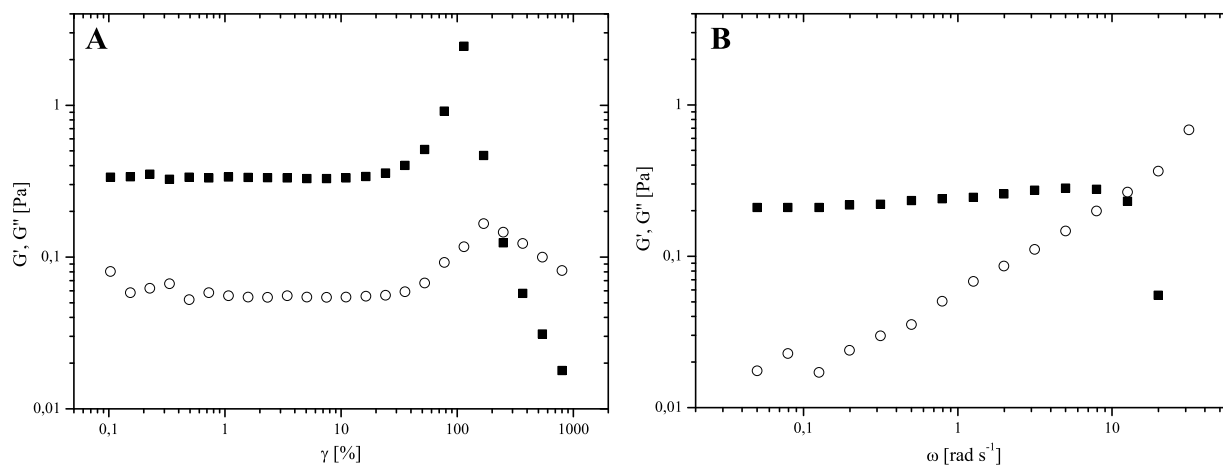


**Figure 3.9:** (A) amplitude sweep ( $\omega = 1 \text{ rad s}^{-1}$ ) and (B) frequency sweep ( $\gamma = 1 \%$ ) of a suspension of Me<sub>2</sub>PE-C32-Me<sub>2</sub>PE ( $c = 1 \text{ mg ml}^{-1}$ ) at pH 11 with 100 mM MgCl<sub>2</sub> at 2 °C.  $G'$ : filled squares,  $G''$ : open circles.

Above this temperature a fast decrease in  $G'$  and  $G''$  can be observed. At lower concentrations of NaCl the gel-sol transition ( $G''$  equal to  $G'$ ) occurs right after this decrease, indicating the loss of the gel character. With increasing concentration this transition is shifted

An amplitude sweep and a frequency sweep of a suspension at pH 11 with 100 mM MgCl<sub>2</sub> are shown in Figure 3.9. The values for deformation ( $\gamma = 1 \%$ ) and angular frequency ( $\omega = 1 \text{ rad s}^{-1}$ ) inside the LVE region are identically to the measurements at pH 5 due to the very similar amplitude and frequency sweeps of the samples.

The results of the temperature dependent rheological measurements with Me<sub>2</sub>PE-C32-Me<sub>2</sub>PE suspensions at pH 11 for some concentrations of NaCl, KCl, MgCl<sub>2</sub>, and CaCl<sub>2</sub> are shown in

to higher temperature, resulting in gels that are stable up to 55 °C. The same effects can be observed when KCl is added, but less pronounced.

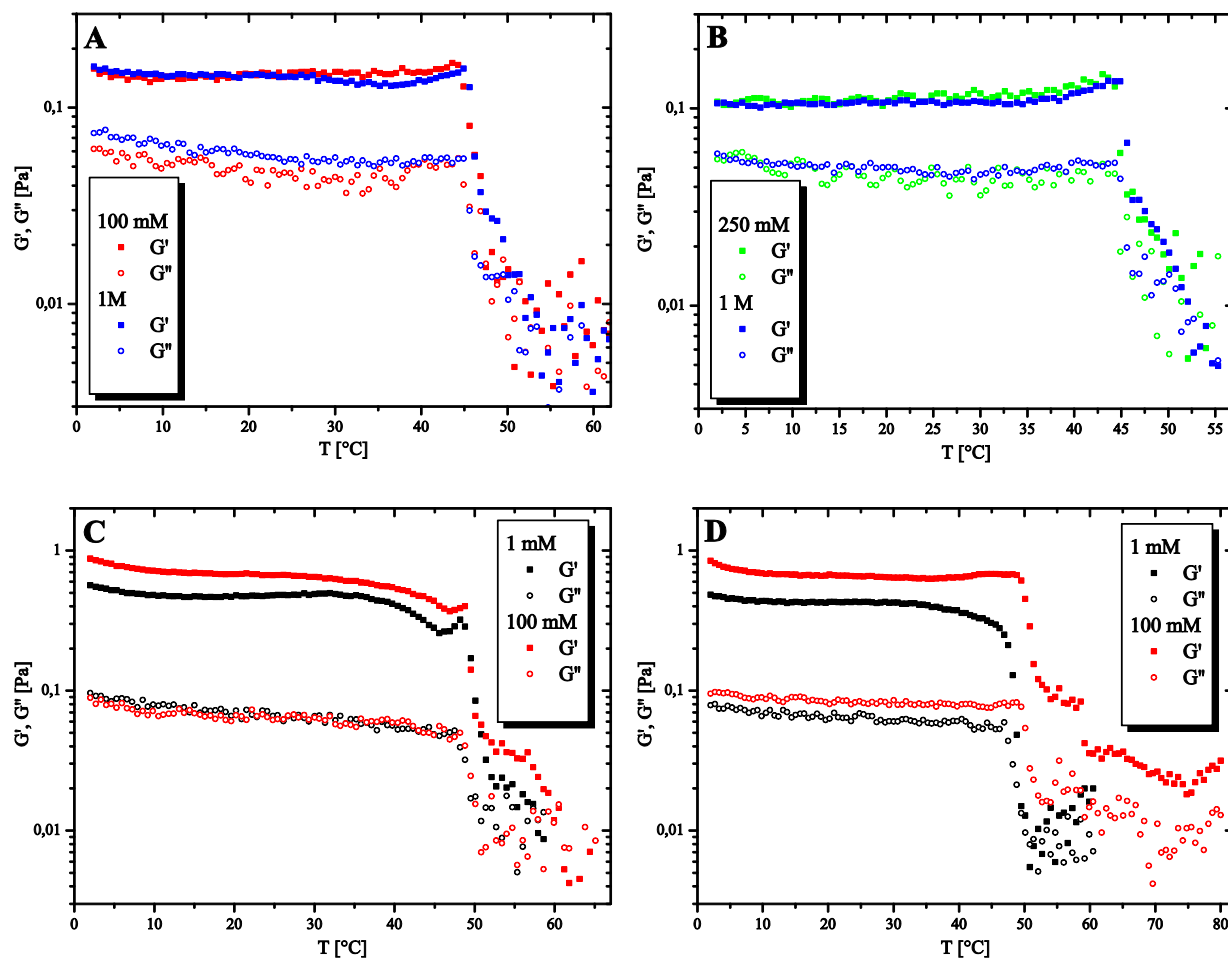


**Figure 3.10:** Temperature dependent rheological data of  $\text{Me}_2\text{PE-C32-Me}_2\text{PE}$  suspensions ( $c = 1 \text{ mg ml}^{-1}$ ) at pH 11 with (A) NaCl, (B) KCl, (C)  $\text{MgCl}_2$ , and (D)  $\text{CaCl}_2$  at selected concentrations. The heating rate was  $20 \text{ }^\circ\text{C h}^{-1}$ . Deformation ( $\gamma = 1 \%$ ) and angular frequency ( $\omega = 1 \text{ rad s}^{-1}$ ) were chosen inside the linear viscoelastic region.  $G'$ : filled squares,  $G''$ : open circles.

The reformation of the gel structure after cooling is also affected by the salt concentration and is becoming faster with increasing amount of salt (Figure 3.11). For the monovalent cations the values of  $G'$  and  $G''$  do not depend on the salt concentration.

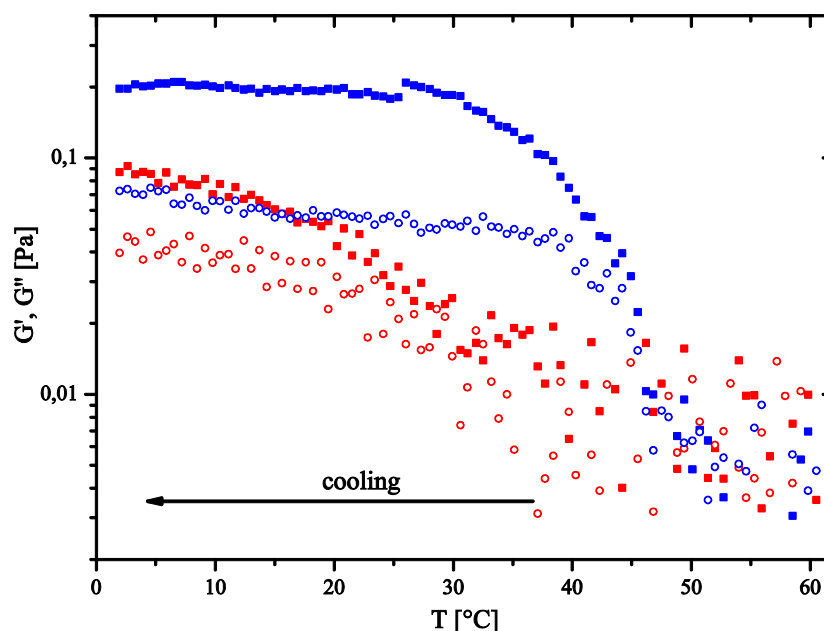


**Figure 3.11:** Temperature dependent rheological data of the  $\text{Me}_2\text{PE-C32-Me}_2\text{PE}$  suspensions ( $c = 1 \text{ mg ml}^{-1}$ ) at pH 11 with 250 mM (red) and 1 M (blue) KCl during the cooling process. The cooling rate was  $20 \text{ }^\circ\text{C h}^{-1}$ . Deformation ( $\gamma = 1 \%$ ) and angular frequency ( $\omega = 1 \text{ rad s}^{-1}$ ) were chosen inside the linear viscoelastic region.  $G'$ : filled squares,  $G''$ : open circles.

When divalent cations are present, the moduli are higher even at lower concentration, emphasizing the stronger effect on the stabilization of the fiber structure induced by calcium and magnesium (Figure 3.10C,D). The changes in  $G'$  and  $G''$  follow the same pattern as for the sodium and potassium cations, and the transition temperatures correspond well with those determined from the DSC data (Table 3.2). Even at 1 mM  $\text{MgCl}_2$  the gel stays stable up to  $52 \text{ }^\circ\text{C}$  and the stability range extends up to  $60 \text{ }^\circ\text{C}$  at 100 mM  $\text{MgCl}_2$ , which is just a little below the second transition, supporting the interpretation of this transition as the conversion of fibers into micelles. In the case of 100 mM  $\text{CaCl}_2$  this effect is even more evident as  $G'$  remains larger than  $G''$  over the whole temperature range. The second distinct step in the decrease of  $G'$  correlates with the onset of the rather broad DSC transition temperature. The stability of the gel structure even above this second DSC transition might be due to a slow breaking up of the fibers into micelles during this transition that would take more time to be fully completed at this salt concentration.

The rheological data with 100 mM  $\text{MgCl}_2$  and  $\text{CaCl}_2$  show a second plateau of  $G'$  above the fiber-fiber transition at which  $G'$  has about the same value as for all concentrations of NaCl and KCl (Figure 3.10C,D). This suggests a kind of intermediate state in the gel stability that is formed if the formation of the gel structure is disturbed, e.g., by insufficient shielding of the negative charge in the case of monovalent ions or higher temperature in the case of divalent cations.

The values for  $G'$  are much higher for Me<sub>2</sub>PE-C32-Me<sub>2</sub>PE in acetate buffer at pH 5 than at pH 11 with monovalent or divalent cations (4.5 Pa compared to 0.15 Pa and around 0.7 Pa, respectively); nevertheless it is obvious that the salts are able to transform the viscous behavior of Me<sub>2</sub>PE-C32-Me<sub>2</sub>PE suspensions at pH 11 into the behavior of a viscoelastic gel. For the divalent cations the moduli, in contrast to the monovalent ions, increase with increasing salt concentration.

As was shown by DSC and TEM investigations, the fibers can, at basic pH values, be reformed in the presence of the salts, but the shielding of the negatively charged headgroups and the cross-links between the fibers are still too weak to retain the viscoelastic gel properties above the fiber-fiber transition, at least at small salt concentration. With increasing salt concentration they are stable up to higher temperature, and at the highest concentrations up to the onset of the fiber-micelle transition. Above this temperature  $G'$  and  $G''$  become very small and the behavior can be described as that of a Newtonian fluid, as described for Me<sub>2</sub>PE-C32-Me<sub>2</sub>PE suspensions above pH 10.<sup>[27]</sup>

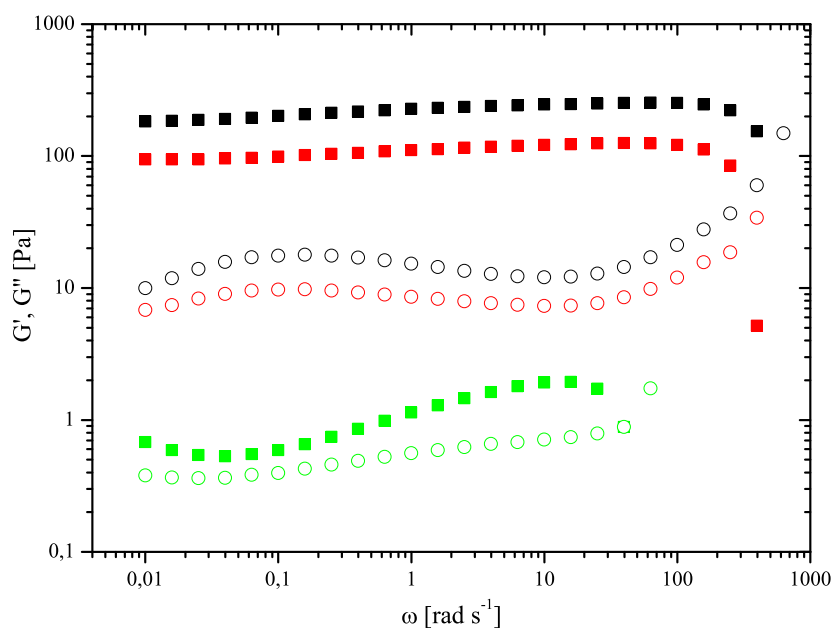


**Figure 3.12:** Frequency sweeps (with  $\gamma = 1\%$ ) of a suspension of Me<sub>2</sub>PE-C32-Me<sub>2</sub>PE ( $c = 8\text{ mg ml}^{-1}$ ) in buffer at pH 5 at 2 (black), 20 (red), and 55 °C (green).  $G'$ : filled squares,  $G''$ : open circles.

The rheological analysis of the Me<sub>2</sub>PE-C32-Me<sub>2</sub>PE gels reveals a behavior that differs distinctly from the behavior of gels formed by wormlike micelles. A very common property of these gels is their Maxwell behavior with a single relaxation time.<sup>[67-68, 79]</sup> The relaxation time is linked to the breaking time and the reptation time of the wormlike micelles. In the fast breaking limit the micelles undergo several breaking and recombination reactions in the time scale of the reptation.<sup>[68, 80]</sup> In the frequency spectra this Maxwellian behavior can be

monitored by the crossover of  $G'$  and  $G''$  at low frequency. However, this crossover cannot be observed in the frequency spectra of gels of Me<sub>2</sub>PE-C32-Me<sub>2</sub>PE at pH 5 or at pH 11 in the presence of higher amounts of salts recorded at 2 °C (Figure 3.6 and Figure 3.9). Because the gel strength increases with the concentration of the bolaamphiphile in suspension, the measurement of frequency spectra of a Me<sub>2</sub>PE-C32-Me<sub>2</sub>PE suspension ( $c = 8 \text{ mg ml}^{-1}$ ) at elevated temperature becomes possible. These measurements show that even at 55 °C no crossover can be observed at low frequencies (Figure 3.12).

The absence of a crossover of  $G'$  and  $G''$  at low frequency indicates a very long relaxation time, characteristic for the behavior of an elastic gel. Similar behavior was also described for the zwitterionic, C22-tailed surfactant EDAB (erucyl dimethyl amidopropyl betaine) suspended in water at a temperature below 40 °C.<sup>[58, 81]</sup> This surfactant self-assembles into wormlike micelles forming a hydrogel above the concentration of 2.5 mM. The storage modulus  $G'$  is approximately 0.005 Pa at 25 °C. However, the  $G'$  value for gels of Me<sub>2</sub>PE-C32-Me<sub>2</sub>PE at 25 °C is more than 1000-fold higher at this concentration ( $G' = 10 \text{ Pa}$ ), showing the high efficiency of gelation of the fibers formed from bolalipids in contrast to the system of wormlike micelles formed from EDAB.

The independence of  $G'$  and  $G''$  from frequency over a certain range is common for all gels, but gels of wormlike micelles also show high straining limits (up to 100 %) in contrast to gels of crystalline nanofibers that have straining limits as low as 2%.<sup>[18, 68]</sup> The bolaamphiphile gels are only disrupted if the deformation gets higher than about 100 %, they also exhibit strain stiffening right before an abrupt decrease in  $G'$  and  $G''$  (Figure 3.6 and Figure 3.9). This phenomenon has been reported for organogels<sup>[66]</sup> and is also common in biological materials, such as collagen, fibrin, or actin networks, which are covalently linked, fiber-like macromolecules.<sup>[82]</sup> This shows again the intermediate behavior of gels formed by the stiff bolalipid nanofibers.

The recovery of the gel structure of Me<sub>2</sub>PE-C32-Me<sub>2</sub>PE may take several hours and depends on bolalipid and salt concentration. This is due to the fact that the fibers have to be formed from single dispersed micelles. The nature of the nucleation process is not known at the moment. In addition, a relatively well ordered alignment of the all-*trans* alkyl chains inside the aggregates has to occur. Therefore, the nanofibers formed by Me<sub>2</sub>PE-C32-Me<sub>2</sub>PE have a larger similarity to the high order in crystalline nanofibers (e.g., 5 $\alpha$ -cholestan-3 $\beta$ -yl N-(2-naphthyl) carbamate (CNC)).<sup>[83]</sup> This is also the reason for the disagreement with the

Maxwell model used for wormlike micelles, as the scission and recombination of these fibers with higher chain order takes more time than for the wormlike micelles.

### 3.1.4 Rheology of PC-C32-PC Suspensions

The rheological behavior of aqueous PC-C32-PC suspensions was found to be similar to the one observed for suspensions of Me<sub>2</sub>PE-C32-Me<sub>2</sub>PE in acetate buffer at pH 5.<sup>[49]</sup> However, one significant difference between both bolalipids is the ability of the Me<sub>2</sub>PE headgroup to form hydrogen bonds between adjacent headgroups if it is in its zwitterionic state. The influence of the protonation state and charge of the Me<sub>2</sub>PE headgroup on the aggregation behavior and rheology was described above (see Chapter 3.1.3). Since there is no possibility to form hydrogen bonds between PC headgroups,<sup>[25]</sup> rheological measurements are a suitable way to investigate how hydrogen bonds affect the properties of the gels built by bolaamphiphile nanofibers.

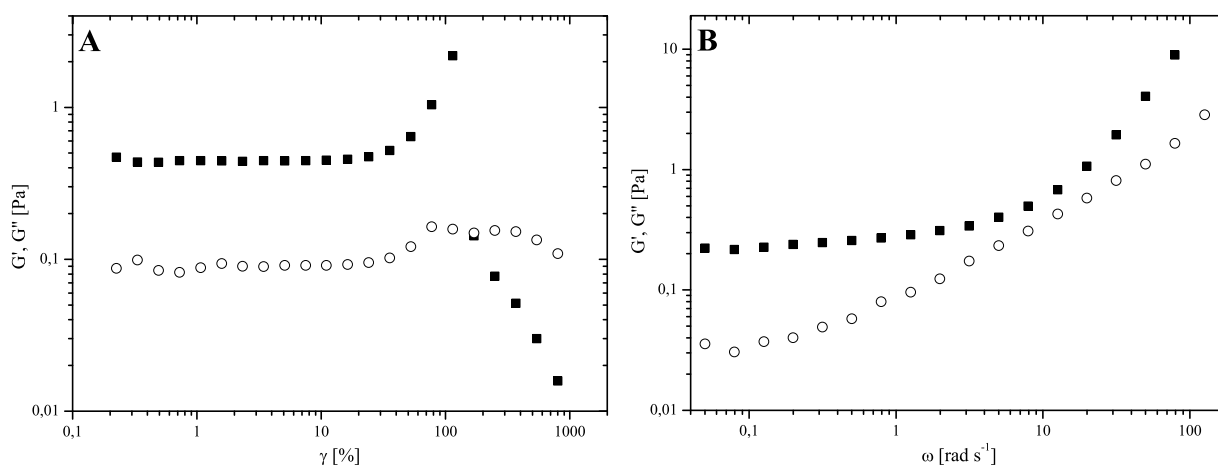


**Figure 3.13:** (A) Amplitude sweep ( $\omega = 1 \text{ rad s}^{-1}$ ) and (B) frequency sweep ( $\gamma = 1 \%$ ) of a suspension of PC-C32-PC ( $c = 1 \text{ mg ml}^{-1}$ ) in water at  $2 \text{ }^\circ\text{C}$ .  $G'$ : filled squares,  $G''$ : open circles.

An amplitude sweep and a frequency sweep of the oscillatory rheological measurements are shown in Figure 3.13. Both measurements reveal the viscoelastic behavior of the PC-C32-PC suspension ( $G' > G''$ ). The amplitude sweep shows a high straining limit that is similar to the limit determined for Me<sub>2</sub>PE-C32-Me<sub>2</sub>PE suspensions at pH 5. The strain stiffening effect can also be observed. The moduli observed in the frequency sweep are lower than those observed for the amplitude sweep. This is due to the experimental procedure with the frequency sweep succeeding the amplitude sweep after a tempering period. In this experiment, the reformation of the gel was not fully completed prior to starting the frequency sweep. However, the general behavior of the suspension is not affected by this (compare

Figure 3.6B). As in the case of Me<sub>2</sub>PE-C32-Me<sub>2</sub>PE suspensions, no Maxwell behavior can be observed.

The magnitude of the moduli already indicates a lower gel strength for the PC-C32-PC suspension compared to the Me<sub>2</sub>PE-C32-Me<sub>2</sub>PE suspension. This effect can be studied in more detail by a comparison of the temperature dependent measurements inside the LVE region. The results for the PC-C32-PC suspension are shown in Figure 3.14.

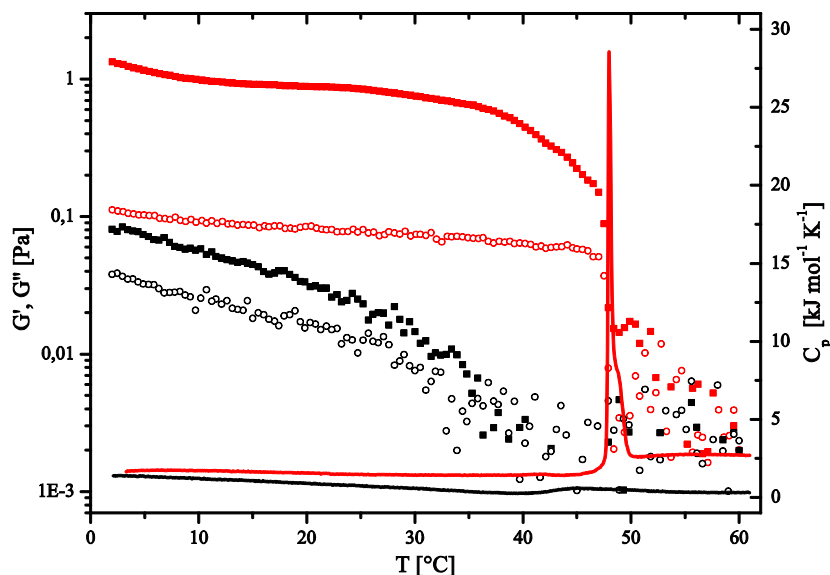


**Figure 3.14:** Calorimetric (solid lines) and rheological data ( $G'$ : filled squares,  $G''$ : open circles) of a suspension of PC-C32-PC in water ( $c = 1 \text{ mg ml}^{-1}$ ). The heating and cooling rate was  $20 \text{ }^\circ\text{C h}^{-1}$ . Deformation ( $\gamma = 1 \%$ ) and angular frequency ( $\omega = 1 \text{ rad s}^{-1}$ ) were chosen inside the linear viscoelastic region. Heating: red, cooling: black.

$G'$  is one order of magnitude higher than  $G''$  up to the temperature of the first DSC transition peak, the fiber-micelle transition, just below  $50 \text{ }^\circ\text{C}$ . Above this temperature viscous flow behavior of the suspension is observed. The loss factor  $\tan \delta$  at the beginning of the measurement at  $2 \text{ }^\circ\text{C}$  is 0.08 and increases to 0.50 after heating and cooling again to  $2 \text{ }^\circ\text{C}$ . Even after 12 hours of tempering at  $2 \text{ }^\circ\text{C}$  subsequent to the heating and cooling process the initial values of  $G'$  and  $G''$  are not reached again.

In rheological measurements with a Me<sub>2</sub>PE-C32-Me<sub>2</sub>PE suspension in acetate buffer at pH 5 the loss factor  $\tan \delta$  was determined to be 0.06 at  $2 \text{ }^\circ\text{C}$  and 0.12 after the heating and cooling process (Figure 3.7). This shows that the viscoelasticity, described by the loss factor  $\tan \delta$ , of the bolaamphiphile gels formed by PC-C32-PC and Me<sub>2</sub>PE-C32-Me<sub>2</sub>PE is very similar at low temperature. However, a difference can be observed in the magnitude of the storage and loss moduli that are higher in the case of the Me<sub>2</sub>PE-C32-Me<sub>2</sub>PE gel in acetate buffer at pH 5. Repeated measurements at  $2 \text{ }^\circ\text{C}$  showed a storage modulus of  $G' = 0.76 \pm 0.35 \text{ Pa}$  for PC-C32-PC suspensions in water and  $G' = 5.35 \pm 1.80 \text{ Pa}$  for Me<sub>2</sub>PE-C32-Me<sub>2</sub>PE suspensions in acetate buffer at pH 5. Viscoelasticity and high straining limits are

probably mainly due to entanglements of the fibers and hydrophobic interactions in the contact regions of the fibers. The reformation of the viscoelastic gel structure is faster in the suspension of Me<sub>2</sub>PE-C32-Me<sub>2</sub>PE as it can be seen by comparison of the loss factors. This is caused by a quicker reformation of the fiber structure promoted by the increased interaction between the bolaamphiphile molecules. This higher G' can be ascribed to the ability of the Me<sub>2</sub>PE headgroups to stabilize the fiber and gel structure via additional hydrogen bonding.

Although the rheological behavior of the examined viscoelastic bolaamphiphile gels did not show Maxwell behavior, which is typical of systems of wormlike micelles, the concentration dependence of the storage modulus G' at 25 °C exhibits a tendency, which is also described for these systems. The concentration dependent values of the storage modulus were measured previously<sup>[49]</sup> and were found to be higher for Me<sub>2</sub>PE-C32-Me<sub>2</sub>PE suspended in acetate buffer at pH 5 than for PC-C32-PC suspended in water at low concentration. At higher concentration the difference in G' between both suspensions decreases.<sup>[49]</sup> When the logarithm of G' at 25 °C is plotted against the logarithm of the suspensions concentration the data can be fitted with the function  $\lg y = \lg A + B \cdot \lg x$  (Figure 3.15).

The resulting values of B are 2.04 and 1.90 for PC-C32-PC suspended in water and Me<sub>2</sub>PE-C32-ME<sub>2</sub>PE suspended in acetate buffer at pH 5, respectively. The difference in B between both bolaamphiphiles is very small. Systems of wormlike micelles were found to exhibit B values of 1.8 up to 2.4.<sup>[80]</sup> This shows that the properties of the bolaamphiphile fibers and gels (e.g., all-*trans* alkyl chain, no Maxwell behavior) are, on the one hand, similar to crystalline nanofibers and on the other hand similar to wormlike micelles (e.g., high straining limit, concentration dependence of G').

### 3.1.5 Conclusions

The single-chain symmetrical bolaamphiphile Me<sub>2</sub>PE-C32-Me<sub>2</sub>PE self-assembles into fibers in aqueous suspensions depending on the pH value and the salinity. At pH values higher than

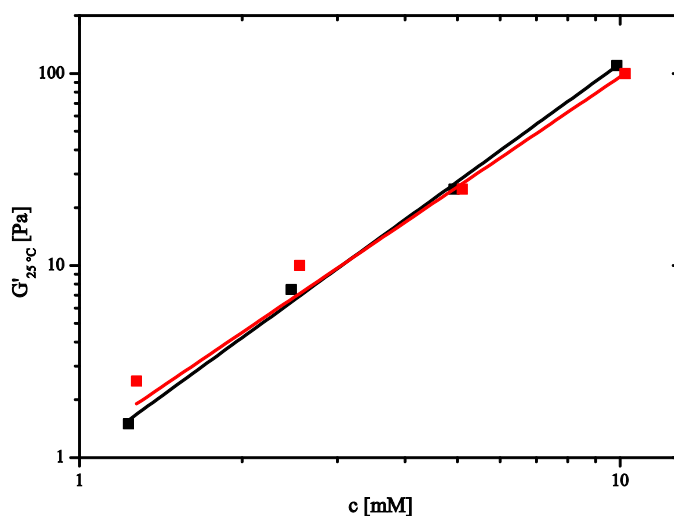


**Figure 3.15:** Dependence of the storage modulus G' on the concentration of the bolaamphiphile suspension of PC-C32-PC in water (black) and Me<sub>2</sub>PE-C32-Me<sub>2</sub>PE in acetate buffer at pH 5 (red) at 25 °C.

10, the negatively charged headgroups impede the aggregation into fibers and the fibers stability range is shifted to lower temperature. The ability of the Me<sub>2</sub>PE-C32-Me<sub>2</sub>PE fibers to form hydrogels depends on the pH value, decreasing with an increasing amount of charged headgroups. In the case of charged bolalipids, the formation of fibrous aggregates can be enhanced by the addition of cations that shield the electrostatic forces between the headgroups in the aggregates. Divalent cations such as calcium and magnesium have been shown to have a stronger stabilizing effect than the monovalent ions sodium and potassium due to the higher binding constants.

The rheological properties of Me<sub>2</sub>PE-C32-Me<sub>2</sub>PE suspensions vary from the behavior of a viscoelastic gel at pH 5 to that of a Newtonian fluid at pH 10 and higher pH values. The addition of salts at pH 11 results in the reformation of the viscoelastic gel properties. The influence of the cations on the rheological behavior exhibits the same tendencies as on the thermal stability as observed by DSC measurements. If the salinity is high enough, the viscoelastic gel structure is stable up to the fiber-micelle transition.

Although the fibers and gel structure described for Me<sub>2</sub>PE-C32-Me<sub>2</sub>PE reveal several properties that are similar to the ones described for wormlike micelles (e.g., transparent gel, high straining limit and a slope of -1 in the scattering data), the frequency spectra of the suspensions show a behavior that is uncommon in gels of wormlike micelles. Due to the high degree of order (*all-trans* alkyl chains) inside the fibers, slower breaking and reforming reactions than in the case of wormlike micelles are observed. The bolalipid gels show a higher similarity to the rheological behavior of biological materials such as collagen or actin and fibrin fiber networks, which are macromolecules consisting of covalently linked subunits.

The bolalipid suspensions can be switched between gel behavior and Newtonian fluid by changing the temperature, the pH value, or the salt concentration at high pH. However, due to slow nucleation and growth from micellar structures, the reformation of the gel is dependent on the bolalipid and salt concentration and may take several hours at low bolalipid concentration.

The rheological behavior of aqueous PC-C32-PC suspensions equals the one observed for Me<sub>2</sub>PE-C32-Me<sub>2</sub>PE suspensions. However, as no stabilizing hydrogen bonds can form between the PC headgroups, the gel is less stable.

### 3.2 Aggregation Behavior of Asymmetrical Single-Chain Bolaamphiphiles with Two Different Headgroups

The symmetrical bolaamphiphiles PC-C32-PC and Me<sub>2</sub>PE-C32-Me<sub>2</sub>PE were shown to self-assemble into helical nanofibers formed of molecules with all-*trans* alkyl chains. These nanofibers gel water in aqueous suspensions by creating a three-dimensional network.<sup>[25-26, 30-31]</sup>

A way of influencing the aggregation behavior of the single-chain bolaamphiphiles are changes in the charge of the headgroups. The pH dependence of the Me<sub>2</sub>PE headgroup and its influence on the aggregation behavior were discussed in Chapter 3.1.1.

A different way of modifying the headgroup structure is the coupling of two different headgroups to the same alkyl chain. Possible changes in aggregation compared to the self-assembly of the symmetrical bolalipids into fibers might be the formation of lamellar aggregates,<sup>[1, 15, 61]</sup> e.g., with antiparallel orientation of the different headgroups, or rods and nanotubes<sup>[15, 84]</sup> as described for other asymmetrical bolaamphiphiles. In both cases, the size difference between the two headgroups plays an important role as the molecules have to fit into either a monolayer-like structure for the lamellar aggregates or into the different curvature of the inner and outer side of the nanotubes.

A headgroup to spacer diameter ratio of 1.4 was assumed in Monte Carlo simulations concerning the aggregation behavior of the symmetrical bolalipid PC-C32-PC using a very simple molecular model.<sup>[30-31]</sup> These calculations showed that the formation of fibrous aggregates is possible for a headgroup to spacer diameter ratio from 1.25 to 2.1.<sup>[30]</sup> This indicates that a quite large difference in the size of headgroups and spacer cannot inhibit the formation of the fiber structure. Although the model for symmetrical single-chain bolaamphiphiles cannot be applied accordingly to asymmetrical bolaamphiphiles, the size of two different headgroups alone should be no obstacle for an aggregation behavior similar to the one observed for symmetrical bolaamphiphiles. However, the size difference of the two headgroups could influence the aggregation behavior.

Therefore, the question arose, whether the size difference of the two headgroups of the asymmetrical bolaamphiphile 32- $\{[\text{hydroxy}(2\text{-hydroxyethoxy})\text{phosphinyl}]\text{oxy}\}$ -dotriacontane-1-yl- $\{2\text{-}[N\text{-}(3\text{-dimethylaminopropyl})\text{-}N,N\text{-dimethylammonio}]\text{ethylphosphate}\}$  (DMAPPC-C32-POH) is large enough to result in such significant changes of the aggregation behavior in suspension. For comparison, another molecule with an even larger size difference was examined. The molecule 32-hydroxydotriacontane-1-yl- $\{2\text{-}[N\text{-}(3\text{-dimethylaminopropyl})\text{-}$

*N,N*-dimethylammonio]ethylphosphate} (DMAPPC-C32-OH) has nearly the same structure as DMAPPC-C32-POH, only the hydroxyethyl phosphate group is missing at one of the ends. Instead, the hydroxyl group is attached directly to the end of the alkyl chain. The aggregation behavior of this bolaamphiphile is discussed in Chapter 3.2.2.

### 3.2.1 Aggregation Behavior of DMAPPC-C32-POH in Aqueous Suspension

The asymmetrical bolaamphiphile DMAPPC-C32-POH consists of two different headgroups at each end of an alkyl chain with 32 methylene units. The chemical structure of the molecule is depicted in Figure 3.16. It contains four functional groups that can be protonated or deprotonated depending on the pH value, if suspended in aqueous media, as well as a positively charged dimethylammonium group. The exact  $pK_a$  values of all groups could not be determined, but it is possible to deduce a probable protonation behavior from values of similar molecules.

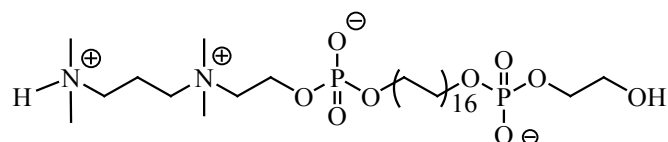


**Figure 3.16:** Chemical structure of DMAPPC-C32-POH with protonated amino group.

The bolaamphiphile was suspended in acetate buffer at pH 5 (in H<sub>2</sub>O or D<sub>2</sub>O), in water (pH 5-6), and in heavy water (pH 9-10). D<sub>2</sub>O was utilized for the neutron scattering experiments and the connection between the pD value and the pH value is  $pD = pH + 0.4$ .<sup>[85]</sup>

The two phosphate groups can be expected to be deprotonated and therefore negatively charged at pH values between 4 and 12. This is due to the  $pK_a$  value of this group, which has been determined to be 3.3 for the suspended bolaamphiphile Me<sub>2</sub>PE-C32-Me<sub>2</sub>PE containing phosphodiester groups in similar chemical surroundings.<sup>[26]</sup> The dimethylamino group at the end of the bolaamphiphile, however, assumedly changes its protonation state in the pH range from 5 to 10. The dimethylamino group of Me<sub>2</sub>PE-C32-Me<sub>2</sub>PE was shown to have a  $pK_a$  value of 6.5 in a titration experiment in 150 mM KCl solution.<sup>[26]</sup> Without additional salts in the suspension, the  $pK_a^{app}$  value seems to be between 10 and 11 as determined by DSC measurements (see Chapter 3.1.1). This is due to the different experimental conditions as there are monomers present in the titration experiment. In the DSC measurement, however, the molecules are self-assembled into nanofibers and the accumulation of charged headgroups at the fiber surface influences the  $pK_a^{app}$  value. The presence of buffer salts and their influence on the  $pK_a^{app}$  have to be taken into account, too, as the  $pK_a^{app}$  is shifted to lower values with increasing salt concentration.

The close proximity of a negatively charged phosphodiester group to the dimethylamino group in the Me<sub>2</sub>PE headgroup also influences the pK<sub>a</sub> value. Therefore, the Me<sub>2</sub>PE headgroup is not analogous to the DMAPPCC headgroup making a direct comparison difficult.

As no direct pK<sub>a</sub> measurements were possible, the previous results can be taken to estimate the pH region in which the dimethylamino group of the DMAPPCC headgroup is deprotonated. This is important to know to predict the self-assembly process, as the dimethylamino group can form hydrogen bonds to stabilize the aggregates in its protonated state but not in its deprotonated state.

At pH 5 the dimethylamino group should be protonated and positively charged. With increasing pH value the protonation will decrease, with a mixture of positively charged and neutral dimethylamino groups at intermediate pH values, to mostly deprotonated dimethylamino groups at pH 10. A schematic illustration of the proposed protonation of the functional groups at pH 5 and 10 is shown in Figure 3.17.

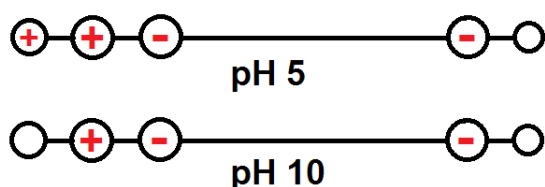


**Figure 3.17:** Schematic image of DMAPPCC-C32-POH and the charge of the functional groups.

The image shows the smaller POH headgroup with the schematic hydroxyethylphosphate group on the right side. This headgroup carries a negative net charge at all examined pH values due to the phosphodiester part. On the left, the larger DMAPPCC headgroup shows a zwitterionic part with the second phosphodiester group and the positively charged dimethylammonium group. The additional dimethylamino moiety at the end of this headgroups causes a positive net charge for this headgroup at pH 5 resulting in an overall uncharged molecule. At pH 10 however, this group remains deprotonated and the whole bolaamphiphile carries a negative net charge at the right headgroup.

Apart from the different protonation behavior, the two headgroups also differ in size as can be seen in the CPK model in Figure 3.18.

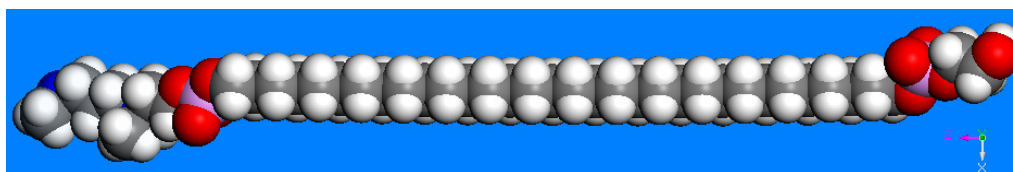


**Figure 3.18:** CPK model of DMAPPCC-C32-POH visualized with Materials Studio (Accelrys, Inc.)

The aggregation behavior of this asymmetrical bolaamphiphile in aqueous suspension is expected to be influenced by the charges of the headgroups as well as their different sizes.

DSC and FT-IR

To investigate the aggregation behavior of DMAPP-*C*32-*POH* in aqueous suspension DSC and FT-IR measurements were carried out with suspensions in water and acetate buffer at pH 5. The results are shown in Figure 3.19. Both suspensions were found to form gels at ambient temperature.

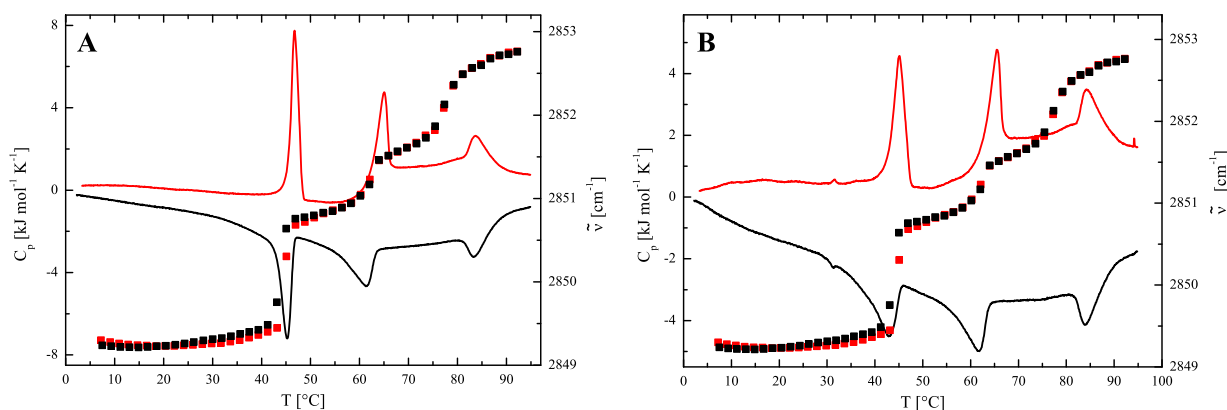


**Figure 3.19:** DSC data (solid lines,  $c = 1 \text{ mg ml}^{-1}$ ) and FT-IR spectroscopic data (symmetric methylene stretching vibration, scattered data,  $c = 50 \text{ mg ml}^{-1}$ ) of DMAPP-*C*32-*POH* in (A) water and (B) acetate buffer at pH 5. The heating rate was  $20 \text{ °C h}^{-1}$  in the DSC measurement. Heating: red, cooling: black.

The DSC heating curve of the suspension in water shows three endothermic peaks at 46.7, 65.1, and 83.8 °C (Figure 3.19A). The corresponding cooling curve shows the same peaks with a small hysteresis of the second one. The wavenumber of the symmetric methylene stretching vibrational band is below  $2849.5 \text{ cm}^{-1}$  up to the temperature of the first DSC transition peak. At approx. 45 °C an abrupt increase in the wavenumber to  $2850.7 \text{ cm}^{-1}$  can be observed. Two more stepwise increases correlate with the DSC peaks until the wavenumber reaches a value of  $2852.7 \text{ cm}^{-1}$ . The lower temperature of the third transition in the FT-IR measurement compared to the transition in the DSC curve is caused by the higher bolaamphiphile concentration used for this measurement.<sup>[26]</sup> The FT-IR data show no hysteresis in the cooling curve.

The suspension in acetate buffer at pH 5 shows very similar properties (Figure 3.19B). The DSC heating curve has three endothermic peaks at 45.1, 65.5, and 84.2 °C. A hysteresis of the second transition in the cooling curve is evident as well. The wavenumber of the symmetric stretching vibrational band of the methylene groups shows an almost identical value as for the suspension in water with a step-wise increase from below  $2849.5$  to  $2852.8 \text{ cm}^{-1}$  correlating with the three DSC transition peaks.

Both suspensions exhibit nearly equal behavior in the DSC and FT-IR measurements. It is similar to the one observed for the symmetrical bolaamphiphile  $\text{Me}_2\text{PE-C32-Me}_2\text{PE}$  suspended in buffer at pH 5 (see Chapter 3.1.1).<sup>[26]</sup>

The FT-IR measurements reveal wavenumbers below  $2850\text{ cm}^{-1}$  for the symmetric methylene stretching vibrational bands up to  $45\text{ }^{\circ}\text{C}$  for the suspensions in water and in acetate buffer at pH 5. This is an indication for an all-*trans* conformation in the alkyl chain<sup>[41]</sup> needed for the formation of the described fiber structure.<sup>[26, 30-31]</sup> The three step behavior of the wavenumber shows an increase in the amount of *gauche* conformers, which is in accordance with the interpretation of the three transitions as a fiber-fiber transition followed by a fiber-micelle transition. The third transition occurs inside the micellar range.

As no significant differences in the properties of the two DMAPPC-C32-POH suspensions could be observed, it can be assumed that the protonation state of the dimethylamino group at the end of the DMAPPC headgroup is similar in both suspensions. The utilized water initially had a pH value of 5 - 6 whereas a pH value of 8 was measured for the DMAPPC-C32-POH suspension in water. The pH value increases, as no buffer is present in the suspension. This shows that the dimethylamino group of DMAPPC-C32-POH becomes protonated after the molecule is suspended in water.

The similarities in the suspensions of DMAPPC-C32-POH in water at pH 8 and acetate buffer at pH 5 with  $\text{Me}_2\text{PE-C32-ME}_2\text{PE}$  suspensions in acetate buffer at pH 5 lead to the conclusion that the formed aggregates are the same in all cases. This is also supported by the gelation of the sample observed in all suspensions.

### TEM

To visualize the aggregate structures, TEM images of samples prepared at ambient temperature below the fiber-fiber transition were taken (Figure 3.20).

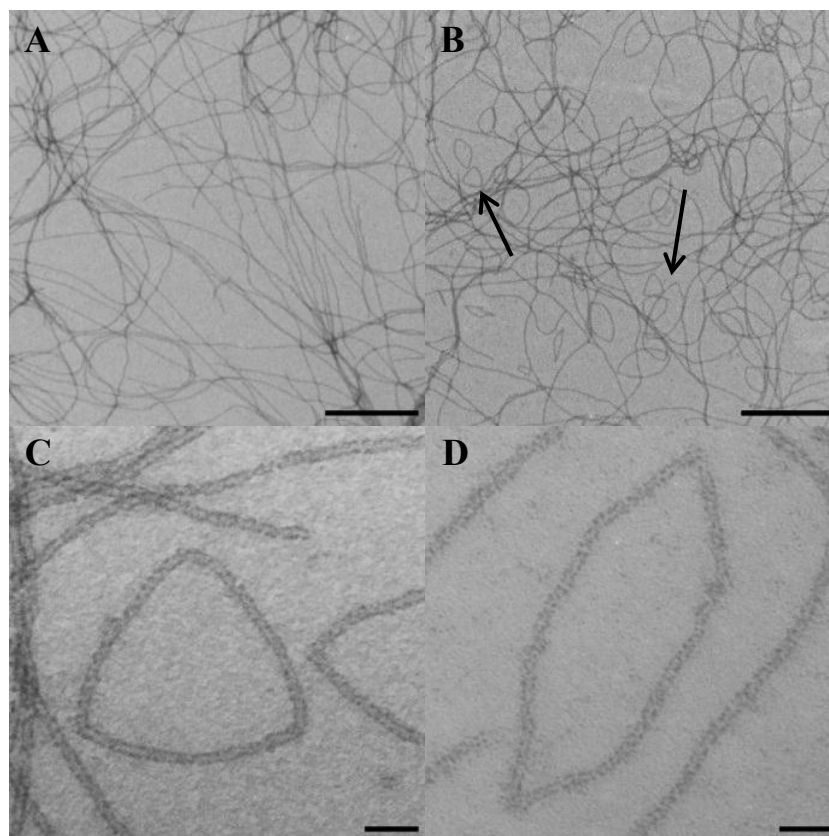


**Figure 3.20:** TEM images of DMAPPC-C32-POH suspensions in (A) water and (B-D) acetate buffer at pH 5 at 25 °C. The samples were stained with uranyl acetate. The bar corresponds to 500 nm (A,B) and to 25 nm (C,D).

The TEM image of the suspension in water displays the presence of long, regular fibers with a diameter of approximately 6 nm (Figure 3.20A). An important difference can be seen in the TEM images of the suspension in acetate buffer at pH 5. Apart from long fibers with a diameter of approximately 6 nm many fibers are visible that have formed irregular, circular structures (arrows in Figure 3.20B). When these structures are examined in detail (Figure 3.20C,D), it seems as if they are composed of short fiber segments that overlap and probably connect at the ends. This was observed in several independently prepared samples, thus preparation artifacts can be ruled out as a reason for the occurrence of this effect.

This behavior has not been observed in any other bolaamphiphile suspensions so far and seems to be a specific property of the asymmetrical molecule DMAPPC-C32-POH in acetate buffer at pH 5. As the protonation state of the dimethylamino group in the suspensions in water and in buffer is similar, the main influence on the aggregation behavior is probably the presence of buffer salts. It was shown that salts can be utilized to shield electrostatic repulsion between charged bolaamphiphile headgroups (see Chapter 3.1.2). Electrostatic attractions between the positively charged dimethylamino group and the acetate anion are possible in the buffered suspension though probably weak. This might influence the stability of the

aggregates, as the acetate anion further increases the size of the DMAPPC headgroup and then might lead to the presence of shorter fiber segments.

### SANS

To get further insight into the structure of the fibers, SANS measurements were performed at three temperatures to investigate the changes of the aggregate structures. In both suspensions heavy water was used as solvent. In acetate buffer the pH value was adjusted to pH 5, but the heavy water had a pH value of 9 to 10, which was not changed prior to the SANS measurements. Therefore, the measurement cannot be compared directly to the experiments in water described above. Only a very small fraction of the dimethylamino group will be protonated at this high pH value. However, the two examined pH values can be assumed as the two different protonation states of the dimethylamino group of DMAPPC-C32-POH and might therefore lead to new results concerning the structure of the aggregates. The scattering data of the SANS experiments and their fits are displayed in Figure 3.21.

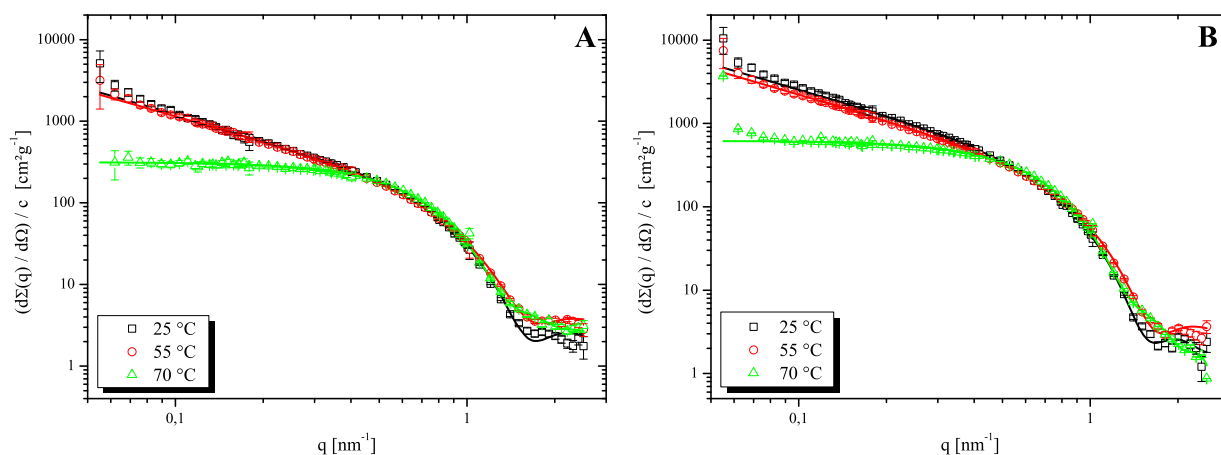


**Figure 3.21:** SANS data of suspensions of DMAPPC-C32-POH ( $c = 1 \text{ mg ml}^{-1}$ ) in (A) D<sub>2</sub>O and (B) in acetate buffer at pH 5 with IFT fits (solid lines).

The fits were done using the IFT method (see Chapter 2.2.7) and are in good agreement with the experimental data. For fitting the data at 25 and 55 °C, the model of infinitely long cylinders was used and for the data at 70 °C spherical aggregates were assumed. The results of the fits are provided in Table 3.3.

**Table 3.3:** Data obtained from IFT fits of suspensions of DMAPPC-C32-POH ( $c = 1 \text{ mg ml}^{-1}$ ) in  $\text{D}_2\text{O}$  and in acetate buffer at pH 5.<sup>a</sup>

	T [°C]	aggregate shape	$D_{\text{max}}$ [nm]	M [g] or $M_L$ [gcm <sup>-1</sup> ]	$N_{\text{agg}}$ [nm <sup>-1</sup> ] or $N_{\text{agg}}$ per micelle	$R_g$ or $R_{\text{SC},g}$ [nm]	R [nm]
<b>DMAPPC-C32- POH in D<sub>2</sub>O</b>	25	fibers	5.0	$1.31 \cdot 10^{-13}$	9	$1.65 \pm 0.05$	$2.33 \pm 0.05$
	55	fibers	5.0	$1.23 \cdot 10^{-13}$	9	$1.59 \pm 0.05$	$2.25 \pm 0.05$
<b>(pH 10)</b>	70	micelles	7.0	$9.84 \cdot 10^{-20}$	70	$2.54 \pm 0.05$	$3.28 \pm 0.05$
<b>DMAPPC-C32- POH in acetate buffer (pH 5)</b>	25	fibers	5.5	$2.74 \cdot 10^{-13}$	20	$1.78 \pm 0.05$	$2.52 \pm 0.05$
	55	fibers	5.0	$2.37 \cdot 10^{-13}$	17	$1.63 \pm 0.05$	$2.31 \pm 0.05$
	70	micelles	7.5	$1.97 \cdot 10^{-19}$	140	$2.62 \pm 0.05$	$3.38 \pm 0.05$
<b>Me<sub>2</sub>PE-C32- Me<sub>2</sub>PE in acetate buffer (pH 5)<sup>1271</sup></b>	20	fibers	6.0	$1.39 \cdot 10^{-13}$	11	$1.84 \pm 0.02$	$2.60 \pm 0.02$
	50	fibers	5.0	$1.32 \cdot 10^{-13}$	11	$1.63 \pm 0.02$	$2.31 \pm 0.02$
	75	micelles	7.5	$1.03 \cdot 10^{-19}$	79	$2.64 \pm 0.04$	$3.41 \pm 0.04$

<sup>a</sup>  $D_{\text{max}}$ : maximal size or cross-section of aggregate, M: mass,  $M_L$ : mass per unit length,  $N_{\text{agg}}$ : aggregation number,  $R_g$ : radius of gyration,  $R_{\text{SC},g}$ : radius of gyration of cross-section, R: radius.

The results of the fits support the interpretation of the aggregates structure as fibers below the first and the second DSC transition peak. The radius of the fibers is in accordance with the one determined from the TEM images (Figure 3.20). At 55 °C the radius becomes smaller due to the higher amount of gauche conformers in the alkyl spacer chain reducing the effective length of the spacer chain. No pronounced difference between the size of the aggregates at pH 5 and 10 can be observed.

The values determined for a suspension of Me<sub>2</sub>PE-C32-Me<sub>2</sub>PE in acetate buffer at pH 5 are provided in Table 3.3 for comparison. The size of the aggregates is very similar to the one determined for the DMAPPC-C32-POH suspensions. However, the aggregation number of the DMAPPC-C32-POH aggregates at pH 5 is twice as high as for the suspension in heavy water or the suspension of Me<sub>2</sub>PE-C32-ME<sub>2</sub>PE in acetate buffer (Table 3.3).

The fibers are formed starting with a micellar solution. The orientation of the molecules upon forming of the fibers is controlled by electrostatic and steric effects. Therefore, a statistical orientation of the asymmetrical molecules in the fibers is expected, i.e., parallel and antiparallel orientations of the two headgroups occur. The positive charge of the dimethylamino group at the end of the DMAPPC headgroup in the suspensions in water and in acetate buffer enables electrostatic attraction to the negatively charge POH headgroup in an antiparallel orientation of the molecules. A model for the antiparallel packing of two DMAPPC-C32-POH molecules was made using Materials Studio (Accelrys Inc.). The

conformation of the adjacent headgroups was optimized taking into account the different charges of the functional groups. A CPK model and a ball and stick model for two antiparallel arranged DMAPPC-C32-POH molecules are displayed in Figure 3.22.

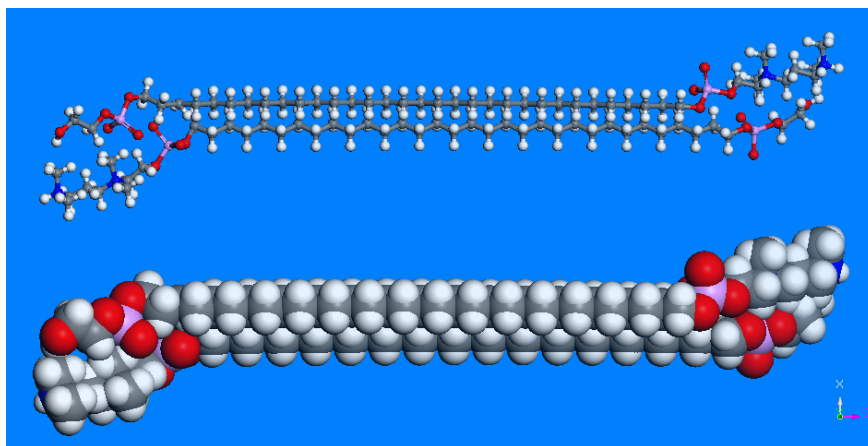


**Figure 3.22:** CPK and ball and stick model for the antiparallel arrangement of two asymmetrical DMAPPC-C32-POH bolaamphiphiles at pH 5.

The electrostatic interaction between headgroups in the antiparallel orientation is weaker in the suspension at pH 10 due to the reduced amount of protonated dimethylamino groups in the DMAPPC headgroup. However, this difference cannot explain the higher aggregation numbers found in the SANS experiment for the buffered suspension. The packing assumed for the molecules inside the fibers is quite dense (Figure 1.3) and an orientation with a two-fold denser packing seems unlikely. In addition, no significant changes were found for the wavenumber of the symmetric methylene stretching vibrational band, indicating no differences in the order and packing of the alkyl chains. An influence of the bolaamphiphile monomer concentration on the analysis of the scattering data can be neglected, as the monomer concentration is very low due to the long hydrophilic alkyl chain of the molecules. So far, the results of the SANS measurement of the suspension at pH 5 remain inconsistent.

At pH 10, most DMAPPC headgroups carry a zwitterionic charge whereas the POH headgroups are negatively charged. Without any additional salt present in the suspension, this charge cannot be shielded. The aggregation numbers are similar to the ones for Me<sub>2</sub>PE-C32-Me<sub>2</sub>PE at pH 5 and indicate no differences in the general structure of the fibers. In addition, small amounts of negatively charged headgroups were shown to be tolerated by the fiber structure also for Me<sub>2</sub>PE-C32-Me<sub>2</sub>PE suspensions at basic pH values (see Chapter 3.1.1). Additional SANS measurements are necessary to further investigate the fiber structure in these suspensions.

DSC, FT-IR, and SANS examinations with suspensions of DMAPPC-C32-POH did not show pronounced differences between the aggregate structures at pH 5 in acetate buffer, in water, and in heavy water at pH 10. However, TEM images showed a tendency of the fibers to form shorter segments and irregular circles in the suspension at pH 5. This behavior might influence the rheological properties of the suspensions via fewer entanglements caused by the shorter fibers or via electrostatic interactions between the headgroups with different charge.

### *Rheology*

Oscillatory rheological measurements were used to examine the properties of DMAPPC-C32-POH suspensions that were observed to form gels at ambient temperature. The results of the amplitude and frequency sweeps, for determining of the linear viscoelastic (LVE) region, are provided in Figure 3.23. The amplitude sweep with  $\omega = 10 \text{ rad s}^{-1}$  shows that the storage modulus  $G'$  is larger than the loss modulus  $G''$  at low deformations. This is the typical behavior ascribed to viscoelastic gels.<sup>[56-57]</sup> In acetate buffer at pH 5, the value of  $G'$  is more than twice as high as for the suspension in water whereas  $G''$  has the same value for both samples. A comparison of the loss factor for the suspension in acetate buffer ( $\tan \delta = 0.14$ ) and the suspension in water ( $\tan \delta = 0.37$ ) demonstrates that it is significantly smaller for the suspension in pure water. The hydrogel with buffer has therefore higher elasticity.

The second obvious difference in the properties of both suspensions is the straining limit indicated by the crossover from gel ( $G' > G''$ ) to sol ( $G' < G''$ ). For the suspension at pH 5, this limit is found at 20 % deformation, but in water the limit is as high as 110 %. Strain stiffening can be observed in both suspensions as can be seen in the increase in  $G'$  and  $G''$  just before the crossover point. This phenomenon has also been observed in samples of symmetrical bolaamphiphiles (see Chapters 3.1.3 and 3.1.4) as well as in biological systems of collagen or actin fibers.<sup>[82]</sup>

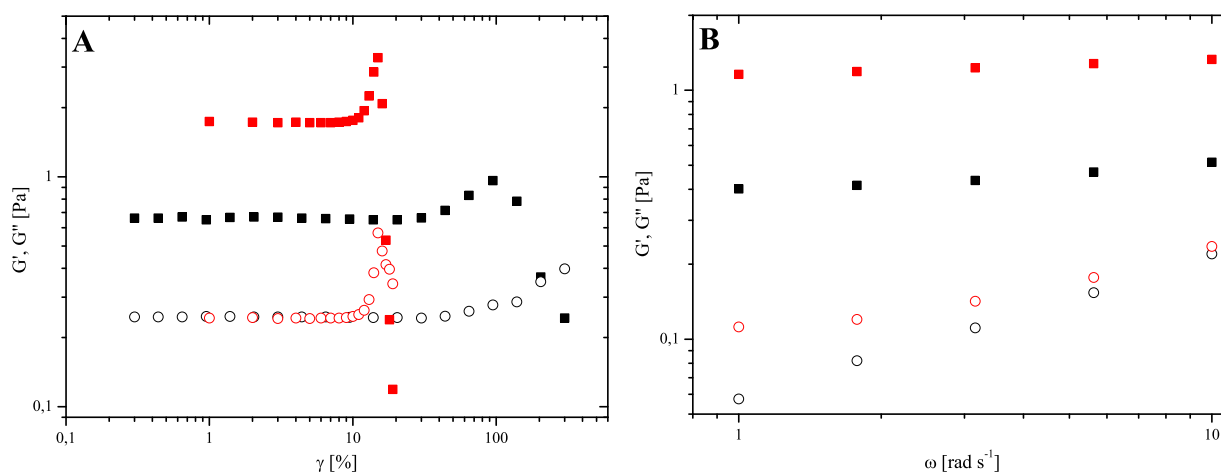


**Figure 3.23:** (A) Amplitude sweeps of DMAPP-C32-POH suspensions ( $c = 1 \text{ mg ml}^{-1}$ ) in water (black) and acetate buffer at pH 5 (red) at  $20 \text{ }^\circ\text{C}$  ( $\omega = 10 \text{ rad s}^{-1}$ ). (B) Frequency sweeps of DMAPP-C32-POH suspensions in water (black) and acetate buffer at pH 5 (red) at  $20 \text{ }^\circ\text{C}$  ( $\gamma = 1\%$ ).  $G'$ : solid squared,  $G''$ : open circles.

Frequency sweeps were carried out with a deformation of 1 %. In the frequency range from 1 to  $10 \text{ rad s}^{-1}$  the values of  $G'$  remain constant and the values of  $G''$  show a slight increase.  $G'$  is larger than  $G''$  over the whole range indicating the presence of viscoelastic gels in both samples. No crossover of  $G'$  and  $G''$  at low angular frequencies can be observed indicating again very long relaxation times and no Maxwell behavior (see Chapter 3.1.3).<sup>[68]</sup> The values of the buffered suspension exceed again the ones determined for the suspension in water.

The LVE region reaches up to 10 % and 30 % deformation, respectively, for the suspensions in acetate buffer and water and up to an angular frequency of  $10 \text{ rad s}^{-1}$ .

The comparison of both suspensions shows a higher gel strength and elasticity for the sample at pH 5 inside the LVE region. However, the low straining limit indicates a certain inflexibility of the fibers to deformation or easy breaking of the cross-links and entanglements under high straining conditions. This is a common behavior of crystalline nanofibers such as 12-hydroxystearic acid (HSA), which can have straining limits as low as 2 % and break easily.<sup>[86]</sup> The TEM images of the suspension of DMAPP-C32-POH at pH 5 support this observation as short fiber segments are present and entanglements with these segments can be supposed to break more easily under strain than in suspensions with longer fibers (Figure 3.20B-D).

No short fibers are present in the TEM images of the suspension in water (Figure 3.20A), which is in accordance with the high straining limit having similar values as for the symmetrical bolalipids (see Chapter 3.1.3 and 3.3.1). The fiber network is stabilized by

entanglements of the fibers but also by interactions between the hydrophobic parts of the fibers exposed to the surface.<sup>[25]</sup> Additional stabilization can occur via hydrogen bonds, as in the case of Me<sub>2</sub>PE-C32-Me<sub>2</sub>PE,<sup>[26]</sup> or even electrostatic interaction. This depends on the kind and protonation of the headgroups and buffer salts present in the examined bolaamphiphile suspension. The dimethylamino group of the DMAPPCC headgroup is protonated in both examined suspension, but in the suspension at pH 5 there are also buffer salts present that can interact with the two headgroups. This apparently influences buffered sample and leads to lower strength and elasticity of suspension in water. This can be explained by weaker interactions between the fiber strands.

Further measurements inside the LVE region were performed with a suspension of DMAPPCC-C32-POH in acetate buffer at pH 5 ( $\omega = 1 \text{ rad s}^{-1}$  and  $\gamma = 1 \%$ ) to examine the temperature dependence of the rheological properties. The change in  $G'$  and  $G''$  was monitored in the temperature range between 20 and 75 °C and is shown in Figure 3.24.

The values of  $G'$  and  $G''$  decrease from approximately 2 and 0.2 Pa, respectively, in two steps around 40 and 60 °C, which is in accordance with the transition peaks observed in the DSC measurements (Figure 3.19B).  $G'$  is about one order of magnitude higher than  $G''$  up to 60 °C. Above this temperature both moduli have about the same value.

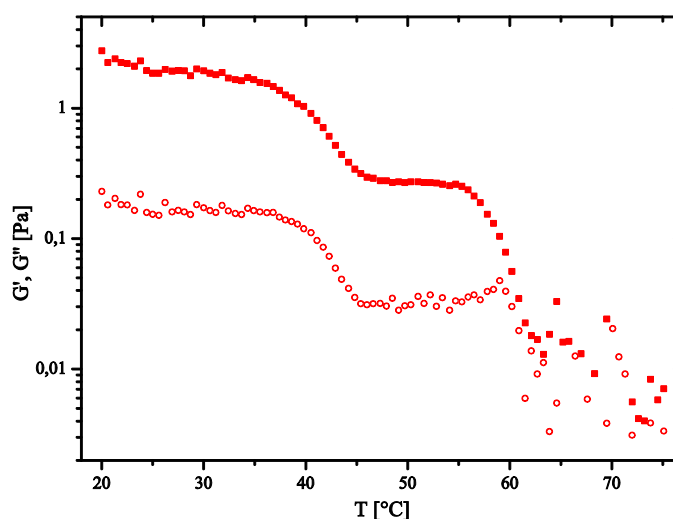


**Figure 3.24:** Rheological data of a DMAPPCC-C32-POH suspension in acetate buffer at pH 5 ( $c = 1 \text{ mg ml}^{-1}$ ) with  $\omega = 1 \text{ rad s}^{-1}$  and  $\gamma = 1 \%$  inside the linear viscoelastic region. The heating rate was  $60 \text{ °C h}^{-1}$ .  $G'$ : filled squares,  $G''$ : open circles.

This proves the presence of a viscoelastic gel state up to 60 °C and supports the interpretation of the DSC peaks as a fiber-fiber transition followed by a fiber-micelle transition. At higher temperature the suspension has the properties of a Newtonian fluid.<sup>[87]</sup>

Compared to the gel of Me<sub>2</sub>PE-C32-Me<sub>2</sub>PE in acetate buffer at pH 5 the gel of DMAPPCC-C32-POH is weaker but it is a little stronger than the gel formed by Me<sub>2</sub>PE-C32-Me<sub>2</sub>PE at

pH 11 with divalent ions shielding the negatively charged headgroups (see Chapter 3.1.3). The second plateau value of  $G'$  has about the same value as observed in the case of  $\text{Me}_2\text{PE-C32-Me}_2\text{PE}$  at pH 11 with divalent ions and seems to be a state of intermediate gel stability formed at higher temperature or insufficient shielding of opposing charges (see Chapter 3.1.3).

### 3.2.1.1 Mixing Behavior with Symmetrical Bolaamphiphiles

The ability of the bolaamphiphile DMAPPC-C32-POH to self-assemble into nanofibers when it is suspended in water or in buffer at pH 5 suggests an investigation of the miscibility of this bolaamphiphile with the symmetrical bolaamphiphiles PC-C32-PC in water or  $\text{Me}_2\text{PE-C32-Me}_2\text{PE}$  in acetate buffer at pH 5.

#### 3.2.1.1.1 Miscibility with PC-C32-PC in Water

The miscibility of DMAPPC-C32-POH with PC-C32-PC suspended in water was tested in a mixture with a molar ratio of  $x = 0.63$  of PC-C32-PC.

#### DSC

The DSC heating curve of this mixture is shown in Figure 3.25 along with the heating curves of the two pure suspended bolaamphiphiles. Just as the suspensions of the separate bolaamphiphiles were observed to gel the solvent, the mixture of both molecules also forms a homogenous gel after 24 hours at 4 °C.

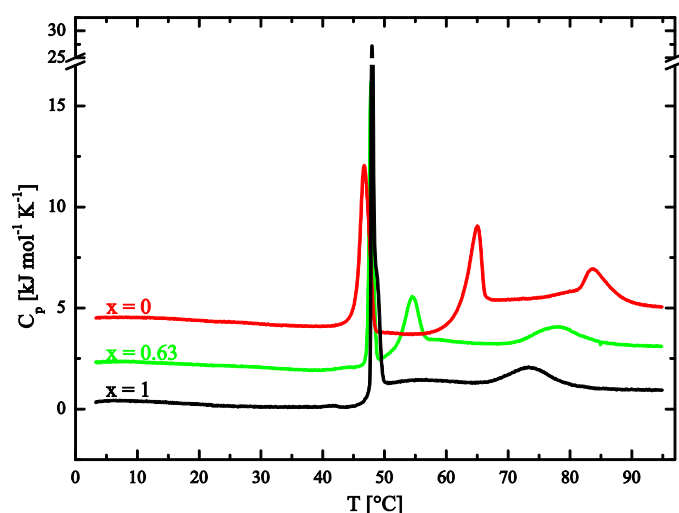


**Figure 3.25:** DSC heating scans of suspensions of PC-C32-PC ( $x = 1$ ), DMAPPC-C32-POH ( $x = 0$ ) and a mixture of both ( $x = 0.63$ ) in water. The curves are shifted horizontally and the heating rate was 20 °C h<sup>-1</sup>.

The DSC heating scan of the mixture has three endothermic peaks at 47.9, 54.5, and 77.8 °C. This behavior shows more resemblance to the curve of the asymmetrical DMAPPC-C32-POH, which also exhibits three transitions, than to the curve of the symmetrical PC-C32-PC with two transitions. The first peak appears at nearly the same position in all measurements. In the curve of the mixture, the second peak is shifted by 10 °C to lower temperature, whereas

the third peak becomes more uncooperative and is decreased by 6 °C compared to the DMAPPC-C32-POH suspension.

For the mixture, this makes a similar aggregate structure probable as found for the asymmetrical bolaamphiphile with a fiber-fiber transition followed by a fiber-micelle and a micelle-micelle transition (see Chapter 3.2.1).

### TEM

A TEM image of the mixture, prepared at 25 °C, reveals long, regular fibers with a diameter of 5 to 6 nm, just as for the DMAPPC-C32-POH suspension in water (Figure 3.26).

This suggests that the two different bolaamphiphiles are miscible and form fibers consisting of both molecules. The stability range of the fibers above the fiber-fiber transition is, however, decreased in this mixture, which is probably caused by the high amount of PC-C32-PC molecules which shows no fiber-fiber transition at all.

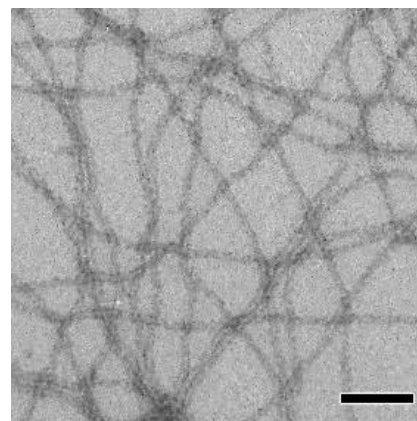


**Figure 3.26:** TEM image of a suspension of PC-C32-PC and DMAPPC-C32-POH ( $x(\text{PC}) = 0.63$ ) at 25 °C. The bar corresponds to 50 nm. The sample was stained with uranyl acetate.

#### 3.2.1.1.2 Miscibility with Me<sub>2</sub>PE-C32-Me<sub>2</sub>PE in Acetate Buffer at pH 5

The miscibility of DMAPPC-C32-POH and Me<sub>2</sub>PE-C32-Me<sub>2</sub>PE suspended in acetate buffer at pH 5 was tested using DSC measurements and TEM.

### DSC

A mixture with the molar ratio  $x = 0.63$  for Me<sub>2</sub>PE-C32-Me<sub>2</sub>PE was examined using DSC and compared with the DSC scans of the pure substances. The result of this measurement is shown in Figure 3.27. During the preparation of the sample gelation of the solvent could be observed after 24 hours at 4 °C.

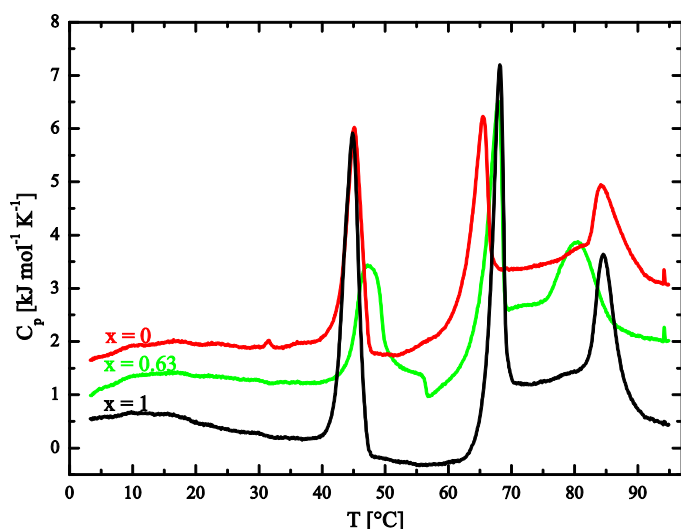


**Figure 3.27:** DSC heating scans of suspensions ( $c = 1 \text{ mg ml}^{-1}$ ) of  $\text{Me}_2\text{PE-C32-Me}_2\text{PE}$  ( $x = 1$ ),  $\text{DMAPPC-C32-POH}$  ( $x = 0$ ) and a mixture of both ( $x = 0.63$ ) in acetate buffer at pH 5. The curves are shifted horizontally. The heating rate was  $20 \text{ }^\circ\text{C h}^{-1}$ .

The DSC heating scan of the mixture shows three endothermic peaks at 47.5, 68.0, and 80.3  $^\circ\text{C}$ , just like the two separate bolaamphiphiles. The first peak is more uncooperative and has a distinct shoulder at higher temperature that does not change its shape in the consecutive scans. The second peak appears at the same temperature as the one of the  $\text{Me}_2\text{PE-C32-Me}_2\text{PE}$  suspension and the third one is shifted to lower temperature (see

Chapter 3.1.1).

Apparently, a similar sequence of aggregate structures can be observed for the mixture of the two bolaamphiphiles. The most prominent difference is the change of the first peak, the fiber-fiber transition.

### TEM

TEM images of the mixture show the presence of fibers with a diameter of 5 to 6 nm at 25  $^\circ\text{C}$ . As also observed in the TEM images of the pure asymmetrical  $\text{DMAPPC-C32-POH}$  at pH 5 (Figure 3.20), many short fiber segments are arranged into irregular circles (Figure 3.28).

The mixture contains less of the asymmetrical bolalipid, but its influence on the aggregates can be seen. Although the molecules are miscible and able to form fibers, an increased tendency towards the breaking of fiber strands seems to be caused by

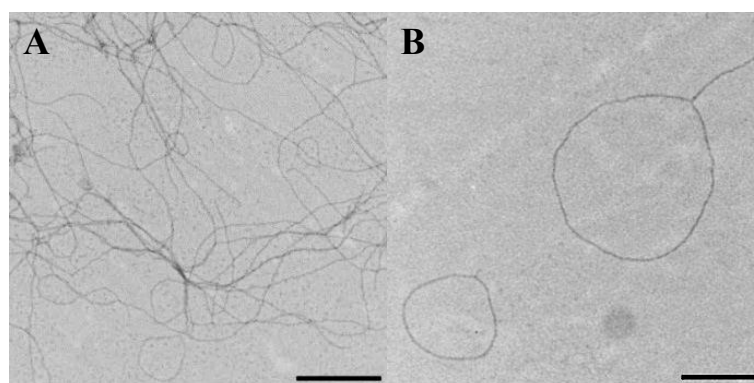


**Figure 3.28:** TEM images of a suspension of  $\text{Me}_2\text{PE-C32-Me}_2\text{PE}$  and  $\text{DMAPPC-C32-POH}$  ( $x(\text{Me}_2\text{PE}) = 0.63$ ) at 25  $^\circ\text{C}$  in acetate buffer (pH 5) in different magnifications. The samples were stained with uranyl acetate. The bar corresponds to (A): 500 nm and (B): 25 nm.

DMAPPC-C32-POH. This is probably due to the different size and charge of the involved headgroups.

### 3.2.2 Aggregation Behavior of DMAPPC-C32-OH in Aqueous Suspension

The size difference of the two asymmetrical headgroups of DMAPPC-C32-POH is not big enough to prevent the formation of nanofibers and to induce the formation of new structures such as nanotubes or lamellar aggregates. The bolaamphiphile DMAPPC-C32-OH has a much higher asymmetry, as only one hydroxyl group is present at one end.<sup>[88]</sup> The chemical structure and a CPK model are shown in Figure 3.29.

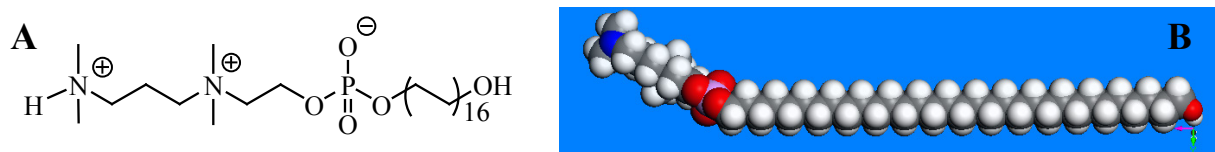


**Figure 3.29:** (A) Chemical structure and (B) CPK model of DMAPPC-C32-OH visualized with Materials Studio (Accelrys, Inc.)

The protonation of the large DMAPPC headgroup is identical to the similar molecule DMAPPC-C32-POH discussed above (see Chapter 3.2.1).

#### DSC

The bolalipid was suspended in water and acetate buffer at pH 5 for DSC measurements. It took several minutes of sonication at high temperature to achieve a homogenous suspension instead of merely heating to 80 °C and subsequent vortexing of the sample. In addition, no gelation of the suspensions was observed.

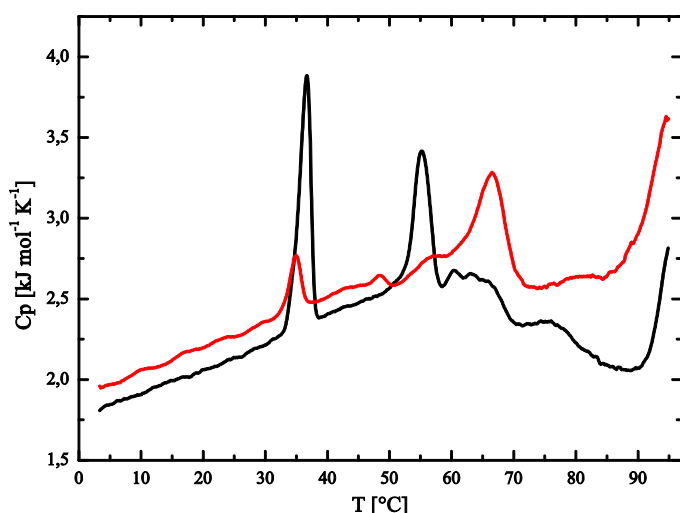


**Figure 3.30:** DSC heating scans of DMAPPC-C32-OH suspensions ( $c = 1 \text{ mg ml}^{-1}$ ) in water (black) and acetate buffer at pH 5 (red). The heating rate was  $20 \text{ °C h}^{-1}$ .

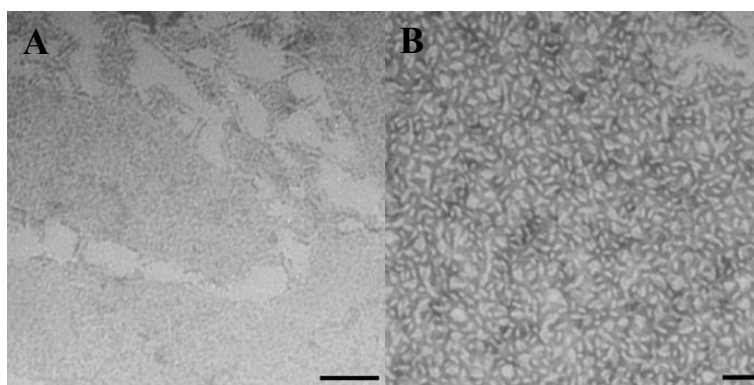
The DSC heating scans of DMAPPC-C32-OH suspended in water and acetate buffer at pH 5 are displayed in Figure 3.30. The DSC curve of the suspension in water shows four endothermic transitions, two cooperative transitions at 36.6 and 55.2 °C, and two broad ones around 65 and 75 °C. The onset of another peak can be observed above 90 °C.

For the suspension in acetate buffer at pH 5 two peaks appear at 35.0 and 66.5 °C in the DSC curve. Between these peaks two smaller ones can be discerned and furthermore the onset of an additional peak above 90 °C. The first peak of both DSC curves shows at almost the same temperature but has a higher enthalpy for the suspension in water. The peak between 60 and 70 °C, however, has a higher enthalpy for the buffered suspension.

### TEM

TEM images were taken to identify the structure of the aggregates formed at 25 °C (Figure 3.31).

In Figure 3.31A large, laminar aggregates are visible but also short segments of fibers (approx. 25 nm) for the suspension of DMAPPC-C32-OH in water. The image of the suspension in acetate buffer at



pH 5 reveals the presence of a mixture of laminar aggregates and short segments of fibers or

elongated micelles (approx. 25 nm). The structure of the molecules inside the laminar aggregates is not yet known. Future X-ray scattering experiments can support the determination of the structure of the laminar aggregates.

**Figure 3.31:** TEM images of DMAPPC-C32-OH suspensions in (A) water and (B) acetate buffer (pH 5) prepared at 25 °C. The bar corresponds to 50 nm. The samples were stained with uranyl acetate.

The TEM images of the suspension in water and acetate buffer reveal different structures, which is also supported by the different DSC scans. Both suspensions consist of a mixture of aggregates. However, the DSC scans show two peaks at similar temperature with different transition enthalpies for the two suspensions indicating the presence of a similar kind of aggregate only in different concentrations

This shows that the structure of the bolaamphiphile DMAPPC-C32-OH leads to an intermediate type of aggregation property. Both, the formation of fibrous as well as laminar aggregates is possible without one dominating aggregate structure.

The formation of more defined lamellar aggregates, as also described for suspensions of PC-C32-OH,<sup>[88]</sup> MePE-C32-MePE,<sup>[54]</sup> Me<sub>2</sub>PE-C34-Me<sub>2</sub>PE,<sup>[29]</sup> and Me<sub>2</sub>PE-C36-ME<sub>2</sub>PE<sup>[29]</sup>

seems to require either symmetrical or asymmetrical molecules with smaller headgroups, longer chains or an even larger difference in the size of the asymmetrical headgroups within the bolaalipid molecule to enforce an antiparallel orientation of the molecules inside a monolayer.<sup>[89]</sup>

### 3.2.3 Conclusions

The formation of a fiber structure is possible in suspensions of the asymmetrical bolaamphiphile DMAPPC-C32-POH in acetate buffer at pH 5, in water, and in heavy water (pH 10). The fibers contain bolaamphiphiles with alkyl chains in the all-*trans* conformation and they exhibit a fiber-fiber transition as also described for the symmetrical molecule Me<sub>2</sub>PE-C32-Me<sub>2</sub>PE.<sup>[26]</sup> SANS measurements in heavy water showed that the fibers are comparable in their aggregation number to fibers of Me<sub>2</sub>PE-C32-Me<sub>2</sub>PE at pH 5 showing no significant difference in the aggregate structure.

In the suspension at pH 5, the fibers of DMAPPC-C32-POH show an increased tendency to break into smaller segments that form irregular, circular aggregates.

Rheological measurements revealed similar viscoelastic gel behavior for the DMAPPC-C32-POH fibers in water compared to the Me<sub>2</sub>PE-C32-Me<sub>2</sub>PE fibers at pH 5. However, DMAPPC-C32-POH fibers in the suspension at pH 5 show a much lower strain resistance due to the presence of the short fiber segments that decrease the stability of the entanglements supporting the formation of viscoelastic gels.

Miscibility experiments showed that DMAPPC-C32-POH is miscible with PC-C32-PC suspended in water and with Me<sub>2</sub>PE-C32-Me<sub>2</sub>PE suspended in acetate buffer at pH 5. The resulting aggregate structure equals the one found for pure DMAPPC-C32-POH suspensions with a fiber-fiber, a fiber-micelle, and a micelle-micelle transition.

In the asymmetrical bolaamphiphile DMAPPC-C32-OH the headgroups have an even larger size difference than in the molecule DMAPPC-C32-POH. The presence of a mixture of aggregates is observed in the suspensions of this bolaamphiphile.

### 3.3 Aggregation Behavior of Bolaamphiphiles Containing Thioether Groups in the Spacer Chain

The synthetic route to bolaamphiphiles containing two thioether units within the spacer chain has been described recently.<sup>[34]</sup> Compared to the pure alkyl chains of PC-C32-PC and Me<sub>2</sub>PE-C32-Me<sub>2</sub>PE two methylene units at the positions C12 and C21 were each replaced by one sulfur atom. Phosphocholine (PC) or dimethylphosphoethanolamine (Me<sub>2</sub>PE) headgroups were attached to the modified chain to yield the two symmetrical bolaamphiphiles 12,21-dithiadotriacontane-1,32-diyl-bis[2-(trimethylammonio)ethylphosphate] (PC-C32SS-PC) and 12,21-dithiadotriacontane-1,32-diyl-bis[2-(dimethylammonio)ethylphosphate] (Me<sub>2</sub>PE-C32SS-Me<sub>2</sub>PE). The chemical structure of the bolalipids is shown in Figure 3.32A.

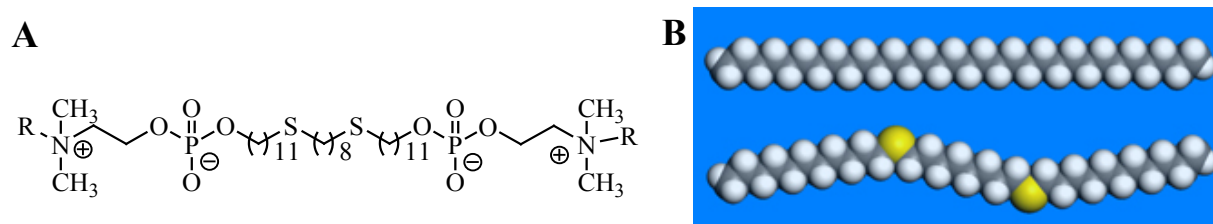


**Figure 3.32:** (A) Chemical structure of PC-C32SS-PC with R = CH<sub>3</sub> and of Me<sub>2</sub>PE-C32SS-Me<sub>2</sub>PE with R = H and (B) CPK model of a C32 (top) and a C32SS (bottom) spacer chain visualized with Materials Studio (Accelrys, Inc.)

The sulfur atoms reduce the angle of the bonds in comparison to the regular bond angle between the carbon atoms in the alkyl chain from 113.3° to 96.1° leading to a chain with two pronounced kinks.<sup>[34]</sup> Preliminary experiments on the aggregation behavior of PC-C32SS-PC in aqueous suspension were made resulting in the conclusion that the formation of the specific fiber structure is still possible. However, the stability range of the fibers is shifted to lower temperature.<sup>[34]</sup>

The aim of this work was to expand the knowledge of the aggregation behavior of PC-C32SS-PC and to examine how the heteroatoms change the characteristics of the fiber structure compared to PC-C32-PC. In addition, Me<sub>2</sub>PE-C32SS-Me<sub>2</sub>PE was investigated by means of DSC, FT-IR spectroscopy, DLS, cryo-TEM and SANS. Also the miscibility of the bolalipids with and without sulfur atoms in the alkyl spacer chain was studied.

#### 3.3.1 Aggregation Behavior of PC-C32SS-PC and Me<sub>2</sub>PE-C32SS-Me<sub>2</sub>PE in Aqueous Suspension

##### DSC

DSC measurements with suspensions of PC-C32SS-PC in water and Me<sub>2</sub>PE-C32SS-Me<sub>2</sub>PE in acetate buffer at pH 5 show only one transition at 14 and 24.5 °C, respectively (Figure 3.33).

The transition enthalpies for the transitions are 56.2 and 66.2 kJ mol<sup>-1</sup>. The DSC cooling scans shows a broader peak than observed in the heating scan and a hysteresis for the reformation of the fiber structure.

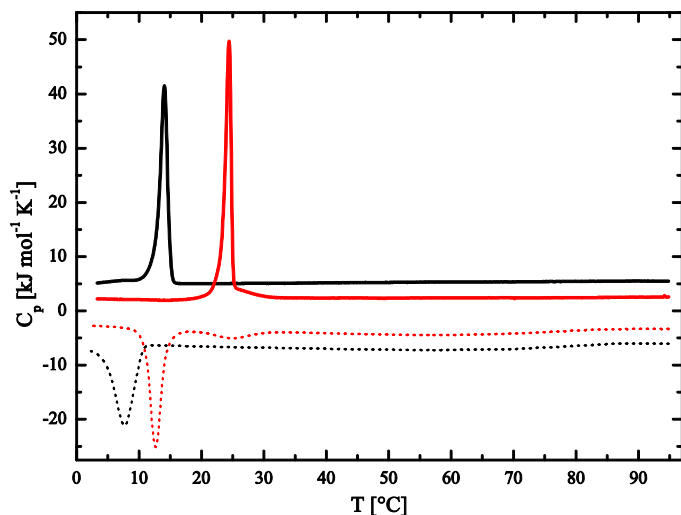


**Figure 3.33:** DSC curves of aqueous suspensions of PC-C32SS-PC (black) in water and of Me<sub>2</sub>PE-C32SS-Me<sub>2</sub>PE (red) in acetate buffer at pH 5 ( $c = 1 \text{ mg ml}^{-1}$ ). The curves are shifted horizontally for clarity. The heating rate was 20 °C h<sup>-1</sup>. Heating: solid lines, cooling: dotted lines.

### TEM

For PC-C32SS-PC and Me<sub>2</sub>PE-C32SS-Me<sub>2</sub>PE suspensions, previous TEM images of samples prepared at 5 °C have proven the presence of a fiber structure. However, the fibers of PC-C32SS-PC seemed to have an irregular structure with diameters ranging from 5 to 10 nm.<sup>[34]</sup> Cryo-TEM images of a PC-C32SS-PC suspension reveal long regular fibers with a uniform diameter of 5 to 6 nm for PC-C32SS-PC and also for Me<sub>2</sub>PE-C32SS-Me<sub>2</sub>PE indicating that

the observed irregularity originates from the preparation and drying process of the TEM samples stained with uranyl acetate (Figure 3.34).

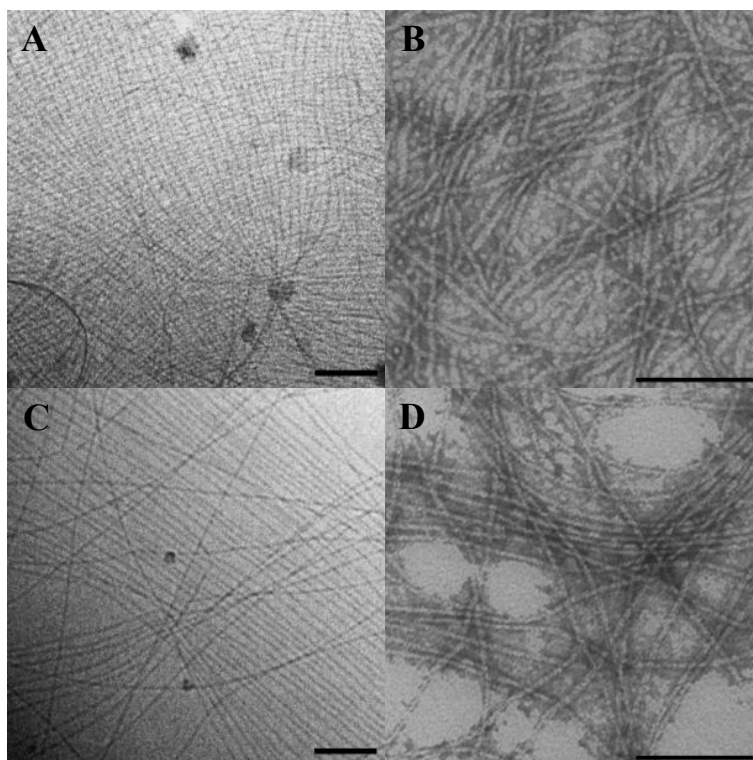


**Figure 3.34:** Cryo-TEM images of suspensions of (A) PC-C32SS-PC and (C) Me<sub>2</sub>PE-C32SS-Me<sub>2</sub>PE (acetate buffer, pH 5) at 7 and 15 °C, respectively. TEM images of suspensions of (B) PC-C32SS-PC and (D) Me<sub>2</sub>PE-C32SS-Me<sub>2</sub>PE (acetate buffer, pH 5) prepared at 5 °C. The bar corresponds to 100 nm.

Although the macroscopical appearance of the fibers does not differ from the structure of PC-C32-PC and Me<sub>2</sub>PE-C32-Me<sub>2</sub>PE fibers described before,<sup>[25-26]</sup> a difference in properties might arise from the changes in the chain geometry.

### FT-IR

FT-IR spectroscopy shows that the wavenumbers of the symmetric stretching vibrational bands of the methylene groups are at 2850.2 cm<sup>-1</sup> for Me<sub>2</sub>PE-C32SS-Me<sub>2</sub>PE and 2850.4 cm<sup>-1</sup> for PC-C32SS-PC at a temperature of 5 °C (Figure 3.35). These values are almost 1 cm<sup>-1</sup> higher than for the analogues without sulfur.<sup>[25-26]</sup> As the wavenumber of the methylene stretching vibration is a measure of order within the alkyl chain,<sup>[41]</sup> it is obvious that the amount of all-*trans* conformers in the alkyl chain is diminished by the replacement of methylene groups by sulfur atoms. Another reason for the higher values is that the maximal length of the methylene group segment is reduced to 8 or 11, respectively.

The interaction between the chains seems to be weakened by the sulfur atoms, which have a higher polarity compared to the methylene groups and disturb the regular arrangement of the methylene groups due to the presence of kinks in the chains.

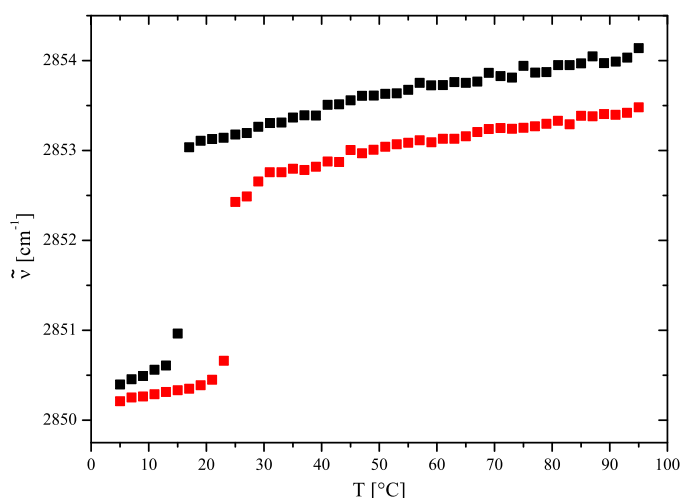


**Figure 3.35:** Temperature dependent wavenumber of the symmetric methylene stretching vibrational band of suspensions of PC-C32SS-PC in water (black) and Me<sub>2</sub>PE-C32SS-Me<sub>2</sub>PE in acetate buffer at pH 5 (red) with  $c = 50 \text{ mg ml}^{-1}$ .

PC and Me<sub>2</sub>PE-C32-Me<sub>2</sub>PE suspensions the wavenumber of the symmetric methylene stretching vibrational band does not reach these high values until the micelle-micelle transition above 70 °C.<sup>[25-26]</sup>

With further increasing temperature a continually growing amount of *gauche* conformers in the chain inside the micelles of PC-C32SS-PC and Me<sub>2</sub>PE-C32SS-Me<sub>2</sub>PE can be observed. A micelle I to micelle II transition as for PC-C32-PC and Me<sub>2</sub>PE-C32-Me<sub>2</sub>PE cannot be observed.<sup>[25-26]</sup>

### DLS

At 25 °C, the PC-C32SS-PC micelles have a hydrodynamic radius of  $2.7 \pm 0.1 \text{ nm}$  as was shown by DLS measurements. The micelles of Me<sub>2</sub>PE-C32SS-Me<sub>2</sub>PE have a slightly larger hydrodynamic radius of  $3.1 \pm 0.1 \text{ nm}$  at 35 °C (Figure 3.36).

The DSC transition temperatures correlate with a large increase in the wavenumbers observed for both bolalipids to  $2853.0 \text{ cm}^{-1}$  for PC-C32SS-PC and to  $2852.5 \text{ cm}^{-1}$  for Me<sub>2</sub>PE-C32SS-Me<sub>2</sub>PE, respectively. This transition is linked to the collapse of the fiber structure into micelles and the transformation of the all-*trans* alkyl chain into a more flexible chain with a high amount of *gauche* conformers. Compared to the FT-IR measurements with PC-C32-

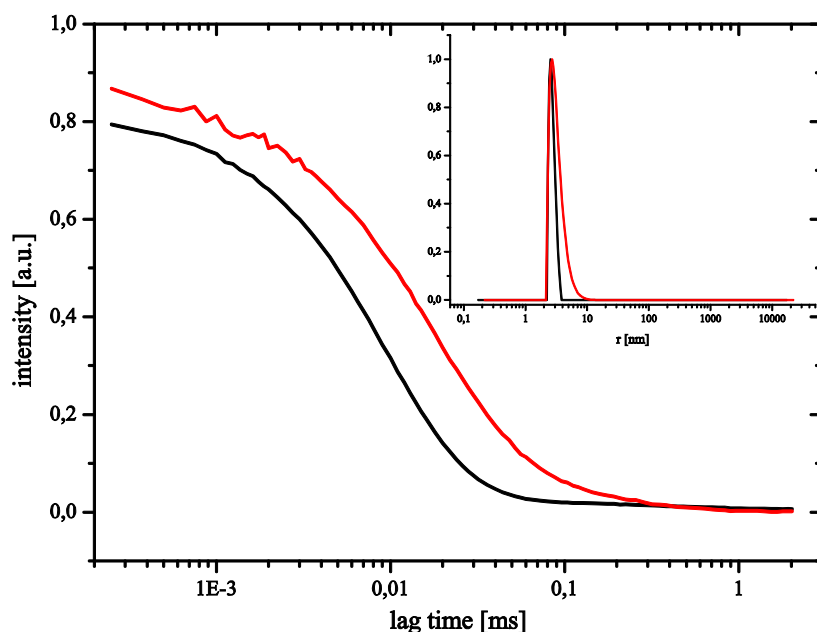


**Figure 3.36:** DLS autocorrelation functions and fits for aqueous suspensions ( $c = 1 \text{ mg ml}^{-1}$ ) of PC-C32SS-PC (black) and of Me<sub>2</sub>PE-C32SS-Me<sub>2</sub>PE in acetate buffer at pH 5 (red) at 25 and 35 °C, respectively. The inset shows the number-weighted size distribution.

The enthalpy of the single transition observed for both sulfur containing bolaamphiphiles is higher than the sum of the enthalpies of all transitions observed for the analogues without sulfur.<sup>[25-26]</sup> In combination with the FT-IR results this suggests that, at low temperature above the transition, the micelles in suspensions of PC-C32SS-PC and Me<sub>2</sub>PE-C32SS-Me<sub>2</sub>PE have a structure, which is similar to the high temperature conformation of the micelles (micelles II) in suspensions of PC-C32-PC and Me<sub>2</sub>PE-C32-Me<sub>2</sub>PE above the micelle I to micelle II transition. The large increase in the wavenumber during the fiber-micelle transition of the sulfur containing molecules explains the high enthalpy found for this transition as the disordering of the spacer chain takes place in one step and not in two separate ones as for the PC-C32-PC and Me<sub>2</sub>PE-C32-Me<sub>2</sub>PE aggregates.

### SANS

In addition, SANS measurements were carried out to identify the aggregate structure and to determine the structural parameters for both bolalipids at temperatures below and above the fiber-micelle transition. In Figure 3.37 the scattering data of PC-C32SS-PC and Me<sub>2</sub>PE-C32SS-Me<sub>2</sub>PE suspensions are shown. The data were analyzed by the Indirect Fourier Transformation (IFT) method (see Chapter 2.2.7). For the low temperature measurements the model of stiff infinite long cylinders was used and for the high temperature measurements the model of a sphere.

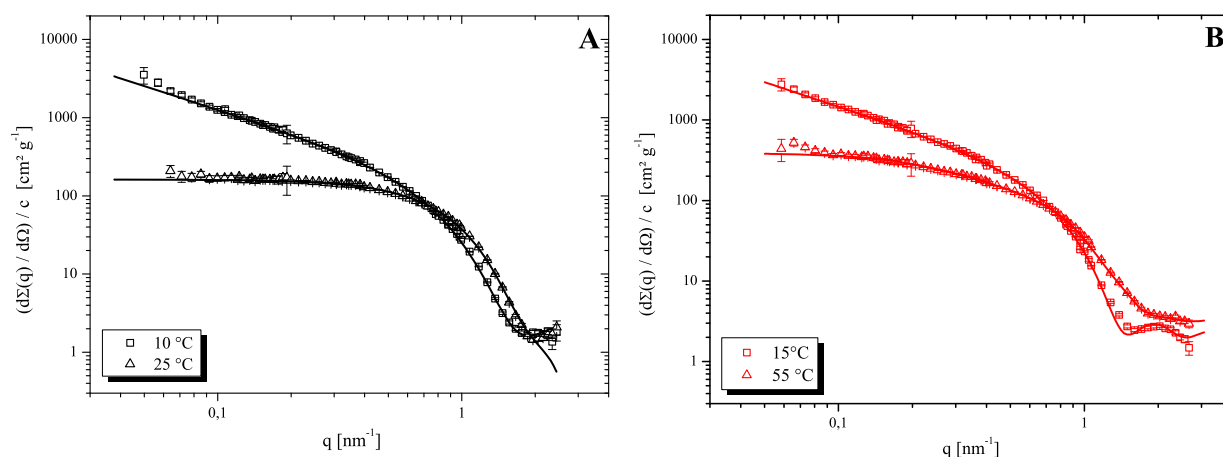


**Figure 3.37:** SANS data and IFT fits (solid lines) of suspensions of (A) PC-C32SS-PC in D<sub>2</sub>O and (B) Me<sub>2</sub>PE-C32SS-Me<sub>2</sub>PE in acetate buffer at pH 5 with  $c = 1 \text{ mg ml}^{-1}$ .

The results of the fits of the scattering data are listed in Table 3.4. The radius of the fibers matches the one determined by cryo-TEM. The higher aggregation number per nanometer ( $N_{\text{agg}}$ ) of the Me<sub>2</sub>PE analogue compared to the PC counterpart is due to the smaller size of the headgroup leading to a slightly denser arrangement of the molecules. The size of the micelles of PC-C32SS-PC matches the results of the DLS measurements at 25 °C (Figure 3.36). In the case of Me<sub>2</sub>PE-C32SS-Me<sub>2</sub>PE suspensions at 55 °C the analysis of the fit becomes difficult as the pair distance distribution function  $p(r)$  shows two maxima around 3 and 10 nm indicating

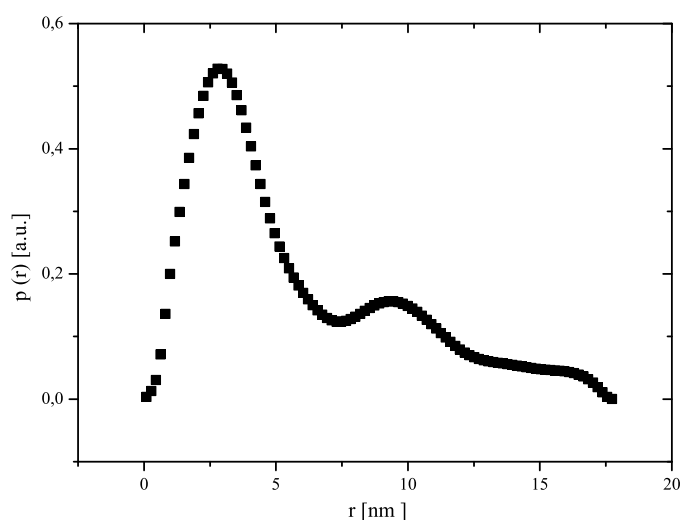


**Figure 3.38:** Pair distance distribution function  $p(r)$  for a Me<sub>2</sub>PE-C32SS-Me<sub>2</sub>PE suspension ( $c = 1 \text{ mg ml}^{-1}$ ) at 55 °C.

the presence of a multicomponent system of short fiber segments and micelles.

This is also evident from the slope of the scattering data at intermediate and small  $q$  values, which is higher compared to the data of the PC-C32SS-PC suspension. A reason for this behavior might be that the system has not reached its equilibrium during the tempering period probably caused by experimental problems with the temperature control. This is also supported by the intensity of the two maxima of the pair distance distribution function (Figure 3.38). The higher intensity of the peak at 3 nm indicates that the number of small aggregates in the suspension is higher than the

number of the aggregates with a radius of 10 nm. The size of 3 nm for the smaller aggregates has the same value as determined by DLS measurements (Figure 3.36) and observed for other single-chain bolaamphiphile micelles.<sup>[27-28]</sup> This shows that most fiber aggregates have transformed into micellar aggregates at 55 °C.

**Table 3.4:** Results of the IFT fit of the SANS data for suspensions of PC-C32SS-PC in D<sub>2</sub>O and Me<sub>2</sub>PE-C32SS-Me<sub>2</sub>PE in acetate buffer at pH 5.<sup>a</sup>

	T [°C]	aggregate shape	D <sub>max</sub> [nm]	M <sub>L</sub> [g cm <sup>-1</sup> ] M [g]	N <sub>agg</sub> [nm <sup>-1</sup> ] N <sub>agg</sub> per micelle	R <sub>CS,g</sub> or R <sub>g</sub> [nm]	R [nm]
<b>PC-C32SS-PC</b>	10	fibers	6.0	1.59·10 <sup>-13</sup>	11	1.80 ± 0.01	2.55 ± 0.01
	25	micelles	6.0	6.06·10 <sup>-20</sup>	43	2.04 ± 0.01	2.63 ± 0.01
<b>Me<sub>2</sub>PE-C32SS-</b>	15	fibers	5.5	1.84·10 <sup>-13</sup>	14	1.84 ± 0.01	2.60 ± 0.01
<b>Me<sub>2</sub>PE</b>	55	fiber segments and micelles	20.0			5.2 ± 0.2	≈ 3 and ≈ 10 nm

<sup>a</sup>D<sub>max</sub>: maximal size or cross-section of aggregate, M: mass, M<sub>L</sub>: mass per unit length, N<sub>agg</sub>: aggregation number, R<sub>g</sub>: radius of gyration, R<sub>CS,g</sub>: radius of gyration of cross-section, R: radius.

In comparison with results for suspensions of PC-C32-PC at 25 °C (R<sub>CS,g</sub> = 1.51 nm, R = 2.14 nm, N<sub>agg</sub> = 11 nm<sup>-1</sup>) and Me<sub>2</sub>PE-C32-Me<sub>2</sub>PE at 20 °C (R<sub>CS,g</sub> = 1.84 nm, R = 2.60 nm, N<sub>agg</sub> = 11 nm<sup>-1</sup>),<sup>[27]</sup> the fiber radii are slightly higher for the PC-C32SS-PC and the same for the Me<sub>2</sub>PE-C32SS-Me<sub>2</sub>PE fibers. The additional stabilizing hydrogen bonds between the headgroups of the Me<sub>2</sub>PE-C32SS-Me<sub>2</sub>PE molecules seem to be able to compensate the disorder induced by the sulfur atoms in the spacer chain. This leads to an almost identical fiber structure to the one observed for Me<sub>2</sub>PE-C32-Me<sub>2</sub>PE. In the case of PC-C32SS-PC the larger radius of the fiber structure might be caused by irregularities in the ordering of the molecules inside the fibers that cannot be compensated by stabilizing interactions between the zwitterionic headgroups.

The number of bolaamphiphile molecules per micelle (N<sub>agg</sub>) is 77 for micelles (micelles I) in PC-C32-PC suspensions at 60 °C, which is below the micelle-micelle transition.<sup>[27]</sup> The corresponding number for PC-C32SS-PC micelles is only 43 at 25 °C showing the difference in the two micellar aggregates again. There are no data available on the aggregation number of PC-C32-PC micelles II above the micelle-micelle transition but for analogue molecules with shorter alkyl chain lengths measurements in this temperature region could be performed as all transitions are shifted to lower temperature.<sup>[28]</sup> In suspensions of PC-C26-PC the aggregation number per micelle of the high temperature aggregates (micelles II) is 28 at 75 °C. This suggests that even at low temperature the micelles in the PC-C32SS-PC

suspensions have more similarities to the high temperature micellar aggregates (micelles II) with lower aggregation numbers as is also indicated by the wavenumber of the symmetric methylene stretching vibrational band determined by the FT-IR measurements.

### *Rheology*

In contrast to PC-C32-PC and Me<sub>2</sub>PE-C32-Me<sub>2</sub>PE the sulfur containing molecules do not gel water at a concentration of 1 mg ml<sup>-1</sup>. When the concentration is increased to 4 mg ml<sup>-1</sup>, however, gelation is observed in both systems at temperatures below the DSC transition temperature.

Amplitude sweeps were recorded following a 12 hour period of incubation of the sample at 2 °C (Figure 3.41) and the results are shown in Figure 3.39. In this experiment, the reformation of the gel was not fully completed prior to starting the amplitude sweep. However, the general behavior of the suspension is not affected by this.

Despite the low G' and G'' values of the PC-C32SS-PC suspension, the straining limit is above 100 %. This is also the case for the Me<sub>2</sub>PE-C32SS-ME<sub>2</sub>PE suspension. This value is similar to the ones determined for the bolalipid suspensions of PC-C32-PC and Me<sub>2</sub>PE-C32-Me<sub>2</sub>PE (see Chapter 3.1.3). A significant difference in the amplitude sweeps can be noted prior to the crossover of storage and loss modulus indicating the transition from gel to sol.

The Me<sub>2</sub>PE-C32SS-Me<sub>2</sub>PE suspension exhibits strain stiffening whereas the PC-C32SS-PC suspension shows a continual decrease of G' and G''. The absence of this increase of the moduli in the case of the PC analogue might be due to the low values of G' and G'' as well as the high loss factor at the beginning of the amplitude sweep. However, this strain stiffening effect was observed in numerous measurements with different bolaamphiphiles (e.g., Me<sub>2</sub>PE-C32-Me<sub>2</sub>PE, see Chapter 3.1.3) and the level of strain stiffening generally seems to be a good indication of strength and viscoelasticity in the specific sample.

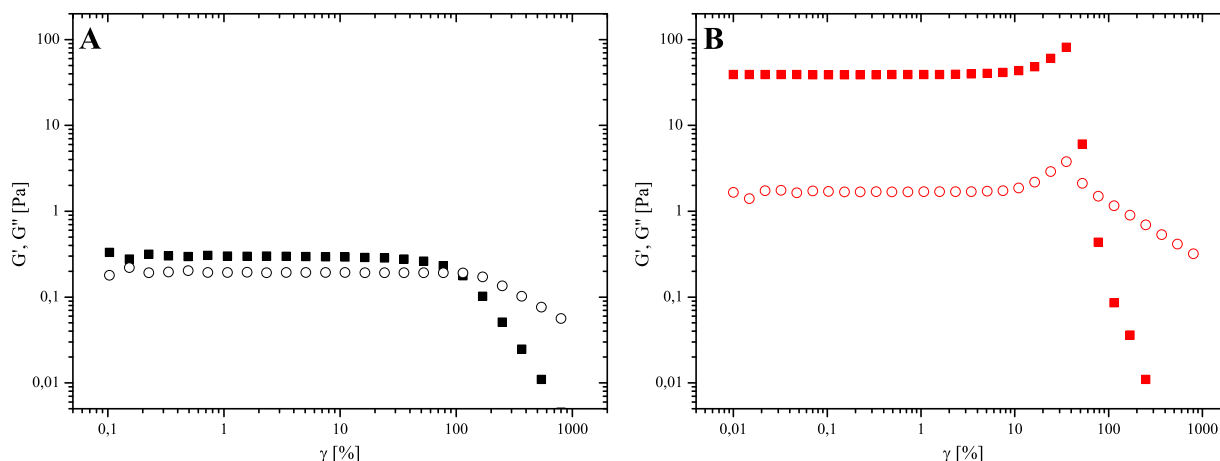


**Figure 3.39:** Amplitude sweeps of aqueous suspensions of (A) PC-C32SS-PC and (B) Me<sub>2</sub>PE-C32SS-Me<sub>2</sub>PE (acetate buffer at pH 5) with  $c = 4 \text{ mg ml}^{-1}$  at 2 °C.  $G'$ : filled squares,  $G''$ : open circles.

With values of deformation and angular frequency inside the LVE region ( $\gamma = 1 \%$  and  $\omega = 1 \text{ rad}^{-1}$ ), temperature dependent rheological measurements were carried out (Figure 3.40).

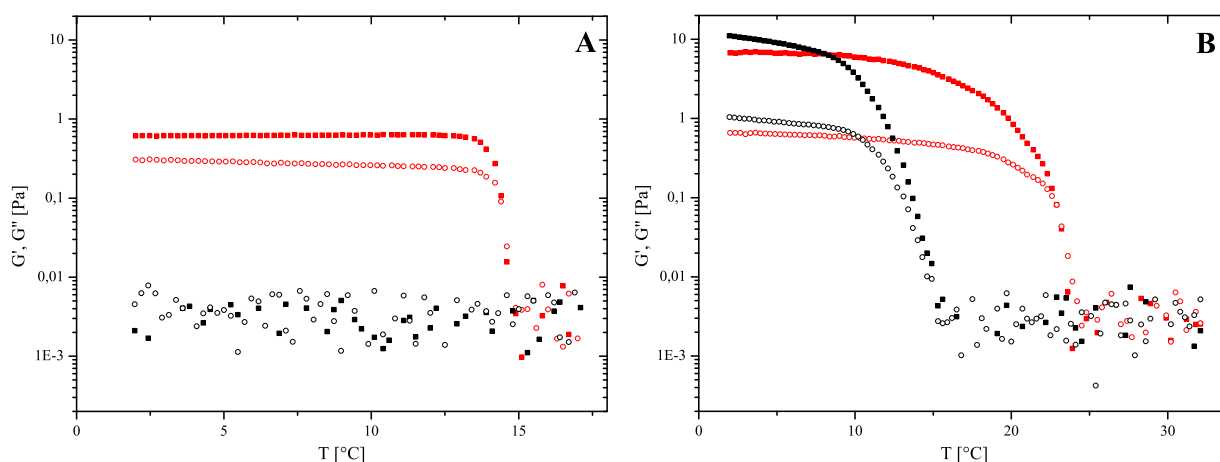


**Figure 3.40:** Temperature dependent rheological data of (A) an aqueous suspension of PC-C32SS-PC and (B) of a suspension of Me<sub>2</sub>PE-C32SS-Me<sub>2</sub>PE in acetate buffer at pH 5 ( $c = 4 \text{ mg ml}^{-1}$ ). The values of deformation ( $\gamma = 1 \%$ ) and angular frequency ( $\omega = 1 \text{ rad s}^{-1}$ ) were chosen inside the linear viscoelastic region.  $G'$ : filled squares,  $G''$ : open circles. Heating: red and cooling: black.

Even though the concentration is four times higher, the PC-C32SS-PC suspension shows smaller storage and loss moduli than the PC-C32-PC suspension at  $1 \text{ mg ml}^{-1}$  (see Chapter 3.1.4). Both moduli are independent of temperature with  $G'$  being larger than  $G''$  up to the DSC transition at 14 °C. The loss factor  $\tan \delta$  is 0.51 indicating a high degree of viscosity in the viscoelastic gel. Above the transition  $G'$  and  $G''$  have about the same value and show the break-down of the viscoelastic gel into a viscous solution. However, upon cooling of the sample no immediate reformation of the gel structure can be monitored.

The data of the Me<sub>2</sub>PE-C32SS-Me<sub>2</sub>PE suspension exhibit a similar trend with gradual decrease in  $G'$  and  $G''$  prior to the DSC transition at 25 °C. The loss factor  $\tan \delta$  is 0.10 and implies a higher elasticity in the gel structure than for the PC analogue. During the cooling

process,  $G'$  and  $G''$  are starting to increase at 13 °C. This correlates well with the peak observed in the DSC cooling scan showing a hysteresis of approximately 10 °C for the fiber reformation (Figure 3.33). At 2 °C  $G'$  is larger than  $G''$  and both moduli have values slightly above their initial ones.

By comparing the behavior of both bolaamphiphiles during a 12 hour period at constant temperature (2 °C) subsequent to the cooling, the different properties of the gels become apparent (Figure 3.41). The moduli of the Me<sub>2</sub>PE-C32SS-Me<sub>2</sub>PE sample merely show a small increase and the loss factor reaches 0.10 again. In the case of PC-C32SS-PC the transformation from sol to gel cannot be observed until after 5 hours of incubation at 2 °C. The loss factor ( $\tan \delta = 0.64$ ) reveals the very weak viscoelasticity of the gel network and the initial values of  $G'$  and  $G''$  are not reached even after 12 hours of incubation.

This shows that the disordering influence of the sulfur containing chain is more pronounced for the bolaamphiphile PC-C32SS-PC resulting in a gel structure that is weaker by a factor of 10.

The higher gel strength of the suspensions of PC-C32-PC and Me<sub>2</sub>PE-C32-Me<sub>2</sub>PE indicates that the three-dimensional network of the fibers formed by the sulfur containing bolalipids is not as strong. The cross-linking of the fibers via hydrophobic interactions between parts of the chain structure that are exposed at the

fiber surface is weakened due to the disorder induced by the thioether moieties. The Me<sub>2</sub>PE headgroups increase the stability of the fiber structure via additional hydrogen bonds and therefore minimize the effect of the disorder induced by the sulfur containing chains.

Overall, it can be concluded that the incorporation of sulfur into the spacer chain decreases the stability range of the fiber structures. The inserted kink caused by the angle between carbon and sulfur atoms affects the order and packing of the chain in the fiber

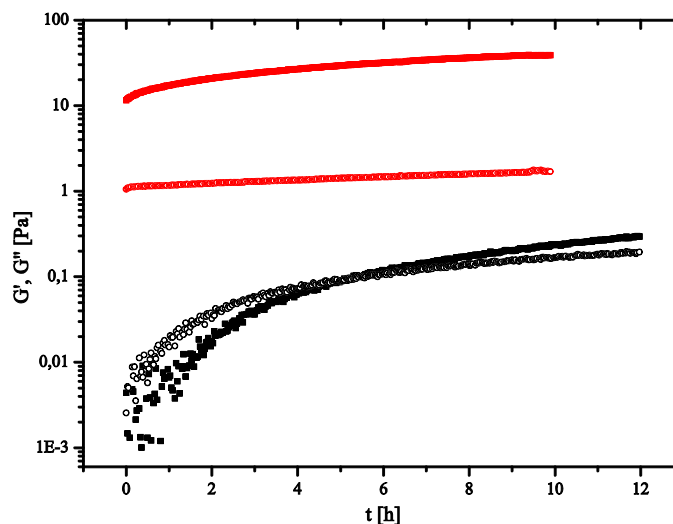


**Figure 3.41:** Time dependent rheological data at 2 °C of aqueous suspensions of PC-C32SS-PC (black) and Me<sub>2</sub>PE-C32SS-Me<sub>2</sub>PE in acetate buffer at pH 5 (red) with  $c = 4 \text{ mg ml}^{-1}$  after heating above the transition temperature and subsequent cooling to 2 °C. The values of deformation ( $\gamma = 1 \%$ ) and angular frequency ( $\omega = 1 \text{ rad s}^{-1}$ ) were chosen inside the linear viscoelastic region.  $G'$ : squares,  $G''$ : open circles.

structure as it was discussed previously.<sup>[34]</sup> In the case of Me<sub>2</sub>PE-C32SS-Me<sub>2</sub>PE, no fiber-fiber transition as for the Me<sub>2</sub>PE-C32-Me<sub>2</sub>PE analogue can be observed. However, the additional stabilization via hydrogen bonds increases the temperature stability of the fibers compared to the PC-C32SS-PC fibers. This is also supported by the FT-IR measurements that show a higher degree of order in the chain for Me<sub>2</sub>PE-C32SS-Me<sub>2</sub>PE leading also to a stronger gel structure and higher viscoelasticity.

### 3.3.1.1 Mixing Behavior of PC-C32SS-PC and Me<sub>2</sub>PE-C32SS-Me<sub>2</sub>PE with Bolaamphiphiles with Non-Modified Alkyl Chains

As the fiber structure of the sulfur containing bolaamphiphiles is not significantly different from the ones without sulfur, it is of interest to examine the miscibility of these molecules and the structure of the resulting aggregates.

#### 3.3.1.1.1 Miscibility of PC-C32SS-PC with PC-C32-PC

##### DSC

To investigate the miscibility of PC-C32-PC and PC-C32SS-PC DSC measurements of aqueous suspensions with different mixing ratios were carried out. Heating and cooling curves of the suspensions of the pure samples and the mixtures are shown in Figure 3.42. Shape and position of the peaks remained the same in all consecutive scans.

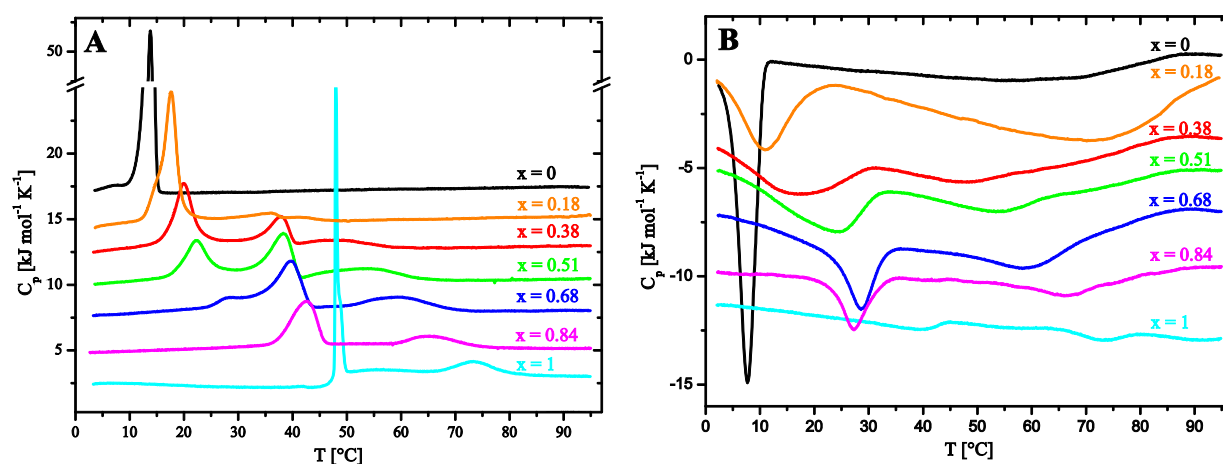


**Figure 3.42:** (A) heating and (B) cooling DSC curves of suspensions ( $c = 1 \text{ mg ml}^{-1}$ ) containing PC-C32SS-PC and PC-C32-PC in different mixing ratios.  $x$  represents the molar ratio of PC-C32-PC. The curves are shifted horizontally for clarity. The heating rate was  $20 \text{ }^{\circ}\text{C h}^{-1}$ .

Even at a low content of PC-C32-PC with  $x = 0.18$ , the first peak is shifted to higher temperature compared to the scan of the pure PC-C32SS-PC suspension and two very small and broad peaks appear between 30 and 50  $^{\circ}\text{C}$ . The curves with  $x = 0.38$  and  $x = 0.51$  show three peaks each and the distance between the first and second one decreases with increasing molar fraction. The third peak moves to higher temperature with increasing amount of PC-

C32-PC. At higher molar ratio, the first peak is shifted closer to the second one until it is just a shoulder at  $x = 0.68$ . The position of the second peak shifts much less. At  $x = 0.84$  the curve exhibits a symmetrical transition a little below the position of the fiber-micelle transition of pure PC-C32-PC.

The diagram with the cooling curves in Figure 3.42B only shows two exothermic peaks for all suspensions. The high temperature transition of the heating scans can be observed again in the cooling curves at similar temperature except in the cooling scan with  $x = 0.18$ , which is due to problems with the measurements baseline.

However, the two peaks of the heating scan lying between the temperatures of the fiber-micelle transitions of the two pure substances do not reappear as separate peaks during the cooling process but as one broad peak. For the higher values of the molar ratio this transition has a hysteresis of approximately 10 °C.

The difference in DSC transition temperatures and enthalpies for the two pure substances is very large. The significant asymmetry and near separation into two peaks, observed for the first transition in the heating scans of the mixtures, can result from this fact. Miscibility experiments and calculations of DSC scans of mixtures of lipids, e.g., of DMPC and DSPC, showed similar peak profiles.<sup>[90]</sup>

The high temperature transition can be ascribed to a micelle-micelle transition that is observed for most bolaamphiphile suspensions.<sup>[25-26]</sup> The shift to lower temperature compared to the micelle-micelle transition of the pure PC-C32-PC suspension is caused by the incorporation of PC-C32SS-PC molecules that destabilize the micellar aggregates due to their different spacer chain structure.

### TEM

TEM images taken of samples incubated and prepared at 5 °C below all observed DSC transitions show the presence of fibers (Figure 3.43). For  $x = 0.51$ , a TEM image was also taken of a sample prepared at 30 °C.

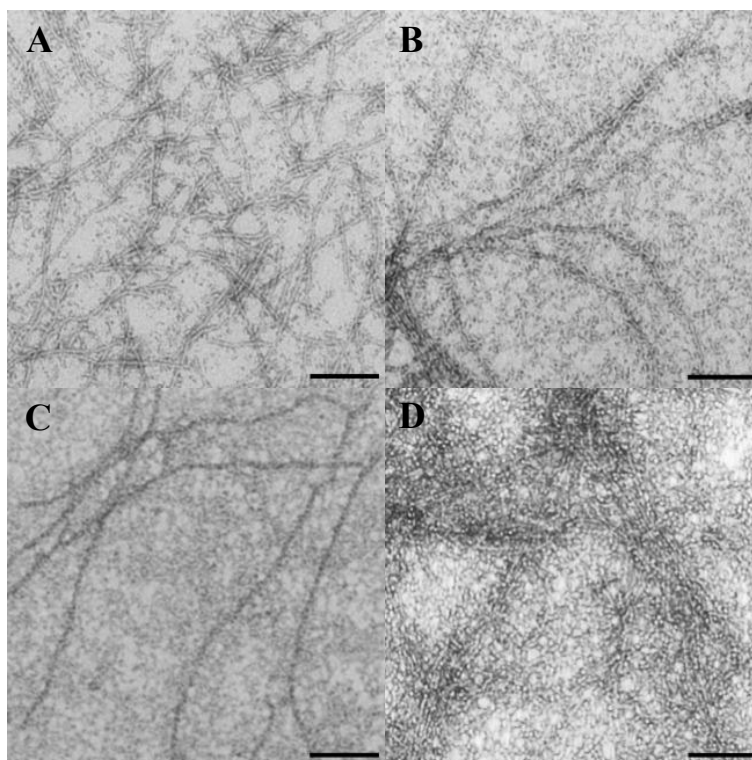


**Figure 3.43:** TEM images of suspensions containing PC-C32SS-PC and PC-C32-PC in different mixing ratios at 5 °C (**A-C**) and 30 °C (**D**). The bar corresponds to 100 nm. The samples were stained with uranyl acetate.  $x$  represents the molar ratio of PC-C32-PC. (**A**):  $x = 0.38$ , (**B,D**):  $x = 0.51$ , (**C**):  $x = 0.68$ .

For the mixture with  $x = 0.38$ , the fibers are shorter than for the pure samples (Figure 3.43A). For samples with  $x = 0.51$  and  $x = 0.68$  many short fiber segments are present (shorter than 50 nm) in addition to the longer fibers (Figure 3.43B,C). For the sample with  $x = 0.51$  prepared at 30 °C fiber aggregates are still present as the temperature is located inside the transition peak (Figure 3.42).

Apparently, the structural problems that arise from the different chain structure in the middle part of both molecules are reflected in the occurrence of shorter fiber segments.

### FT-IR

To analyze structural changes inside the bolaamphiphile aggregates as a function of the temperature of the suspension, FT-IR measurements of a mixture with  $x = 0.47$  were carried out (Figure 3.44).

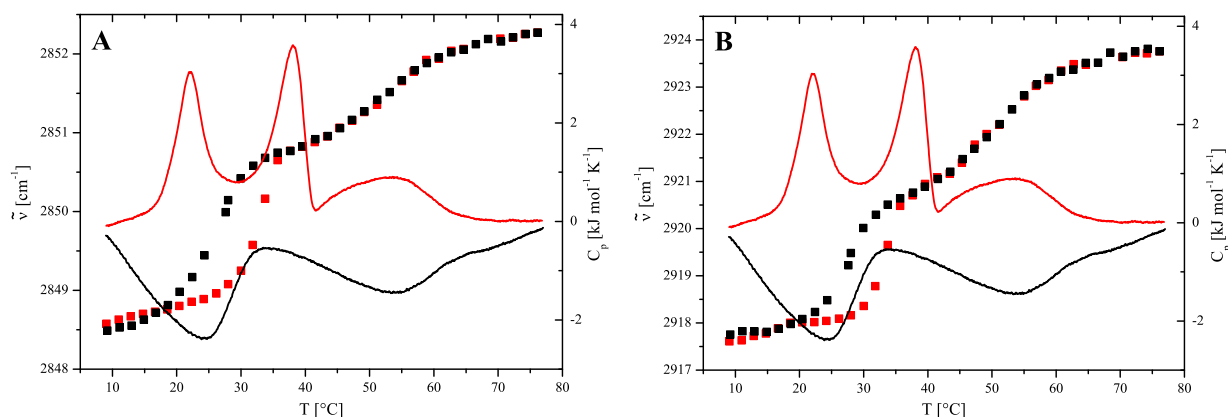


**Figure 3.44:** Calorimetric (solid lines,  $c = 1 \text{ mg ml}^{-1}$ ) and FT-IR spectroscopic (filled squares,  $c = 50 \text{ mg ml}^{-1}$ ) data of a suspension containing a mixture of PC-C32SS-PC and PC-C32-PC with the molar ratio of PC-C32-PC of  $x = 0.5$ . Temperature dependent wavenumber of the (A) symmetric and (B) asymmetric methylene stretching vibrational band. Heating: red, cooling: black.

Upon heating, the wavenumber of the symmetric methylene stretching vibrational band has a value below  $2849 \text{ cm}^{-1}$  up to  $30 \text{ }^{\circ}\text{C}$  and then increases to  $2850.6 \text{ cm}^{-1}$ . This step in the wavenumber correlates with the temperature of the second DSC peak. The high temperature peak of the DSC scan represents the micelle I to micelle II transition and is connected with a further increase in the wavenumber. The data for the asymmetric methylene stretching vibration follow a similar pattern but they additionally show a small increase of the wavenumber at the onset temperature of the first DSC peak. Upon cooling, the change of the wavenumber of both vibrational bands coincides with the transition in the DSC cooling curves.

Compared with the results of FT-IR measurements for the two pure components, the structure of the mixed aggregates obviously is similar at low temperature (see Chapter 3.3.1). In all suspensions, the wavenumber of the methylene vibrational band indicates an all-*trans* conformation of the alkyl spacer chains inside the aggregates. The increase of the wavenumber observed for the symmetric methylene stretching vibrational band at  $30 \text{ }^{\circ}\text{C}$  is similar to the change observed for the PC-C32-PC suspension but smaller than the one found for the PC-C32SS-PC suspension.

The appearance of only one increase of the wavenumber at  $30 \text{ }^{\circ}\text{C}$  in contrast to two DSC transition peaks is not yet completely understood. It might be an indication that only one conformational change occurs in this temperature region, namely during the transition of fibrous into micellar aggregates. However, in this case the increase of the wavenumber would be expected to correlate with the onset temperature of the first DSC peak. Differences in the

bolaamphiphile concentration and the experimental conditions of the FT-IR and DSC measurements could also influence temperature and shape of the observed transitions.

Another explanation for the appearance of two DSC peaks in the mixtures is the formation of a second fiber region as also described for Me<sub>2</sub>PE-C32-Me<sub>2</sub>PE.<sup>[26]</sup> Hence, the first DSC peak would be connected with a fiber-fiber transition and the second with a fiber-micelle transition. In this case the stability range of the second fiber region would decrease with increasing amount of PC-C32-PC in the mixture until the two transitions superimpose. The fibers would then have different conformations, e.g., increased flexibility or mobility, below and above the fiber-fiber transition. However, in comparison with the results for suspensions of mixtures of Me<sub>2</sub>PE-C32SS-Me<sub>2</sub>PE and Me<sub>2</sub>PE-C32-Me<sub>2</sub>PE this seems unlikely (see Chapter 3.3.1.1.2). The strong effect of the sulfur containing chain on the fiber structure of Me<sub>2</sub>PE-C32-Me<sub>2</sub>PE diminishes the possibility that the analogue mixtures with the PC headgroups exhibit a structure with a fiber-fiber transition. This applies in particular as the structures with Me<sub>2</sub>PE headgroups always show the more stable aggregates due to the additional stabilization via hydrogen bonds between the headgroups.<sup>[25-26]</sup> This is also evident from a comparison of the TEM images that do not show any short fiber segments in the case of the mixtures of the Me<sub>2</sub>PE analogues (Figure 3.48).

Based on the results of the DSC and FT-IR measurements and the TEM images, it is possible to draw a schematic “phase diagram” of the suspensions of PC-C32SS-PC and PC-C32-PC mixtures (Figure 3.45).

The onset and completion temperatures of the peaks in the DSC scans were corrected for the finite width of the peaks found for the pure components.<sup>[90]</sup> To the onset temperature the quantity  $x_A \cdot \Delta T_{1A} + x_B \cdot \Delta T_{1B}$  was added.  $x_A$  and  $x_B$  are the molar ratios of PC-C32-PC and PC-C32SS-PC, respectively, and  $\Delta T_{1A/B}$  is the difference between the main transition temperature of component A or B and the onset temperature of this transition. The completion temperature was decreased by the amount of  $x_A \cdot \Delta T_{2A} + x_B \cdot \Delta T_{2B}$ , where  $\Delta T_{2A/B}$  is the difference between the completion temperature of the transition of the component A and B and the main transition temperature of this transition.

The diagram resembles a “phase diagram” indicating a non-ideal mixing between the two components with “two-phase” regions enclosed by the lines. The behavior of the micelle I to micelle II transition at low molar ratios was not examined in detail, but it can be expected that the “two phase” region ends in a loop (Figure 3.45).

### DLS

An additional method to gain information about the size and distribution of aggregates is DLS. At

higher temperature the autocorrelation functions can be fitted to obtain the radii of the micelles that are formed. In Figure 3.46A the time autocorrelation functions of the mixture with  $x = 0.51$  at four different temperatures in the transition range are displayed. The midpoint of the autocorrelation function shifts to shorter times with increasing temperature. As this time is linked to the translational self-diffusion coefficient of the aggregates, it indicates that the aggregate size decreases with increasing temperature.<sup>[50]</sup> This is in accordance with the “phase diagram” based on the DSC measurements (Figure 3.45).

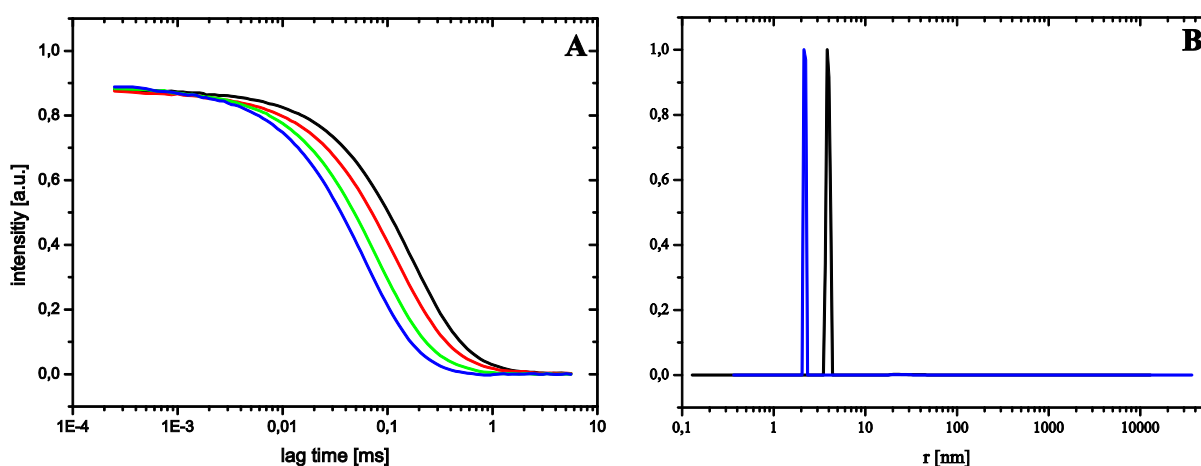


**Figure 3.46:** (A) DLS autocorrelation functions for a suspension ( $c = 1 \text{ mg ml}^{-1}$ ) containing PC-C32SS-PC and PC-C32-PC at 15 (black), 30 (red), 45 (green), and 60 °C (blue). (B) Number-weighted size distribution of the measurements at 15 (black) and 60 °C (blue). The molar ratio of PC-C32-PC is  $x = 0.51$ .

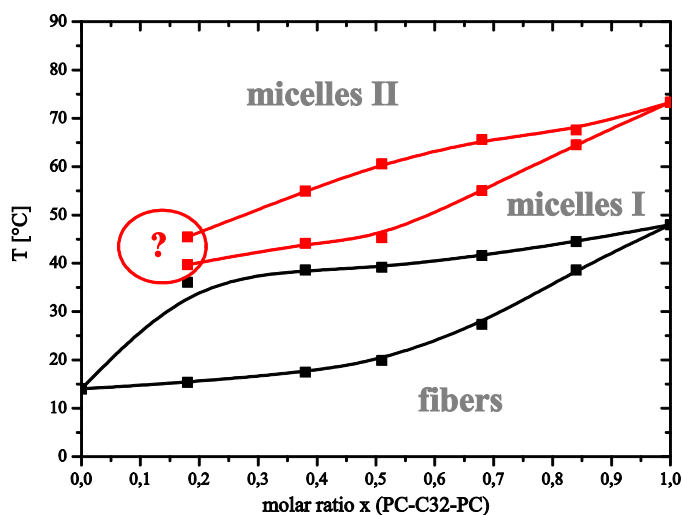


**Figure 3.45:** Schematic “phase diagram” for the suspension of the mixture of PC-C32SS-PC and PC-C32-PC. The squares represent the onset and completion temperatures of the transitions determined by DSC measurements and are corrected for the width of the transition peak of the pure substances. The lines are drawn as a guide to the eye and connect the onset and completion temperatures of the observed peaks.

The largest aggregates are found at 15 °C, which is in agreement with the TEM images showing fibers. When the temperature is increased to 45 and 60 °C, the aggregates become smaller and micelles are formed. The hydrodynamic radii are  $3.6 \pm 0.4$  and  $2.8 \pm 0.7$  nm, respectively. These values have the same order of magnitude as the radii determined for other bolaamphiphile micelles.<sup>[24, 34]</sup> Number-weighted size distributions obtained from fits of the autocorrelation functions of measurements carried out at 15 and 60 °C are shown in Figure 3.46B. They prove that the size of the aggregates decreases from large aggregates to small aggregates from 15 to 60 °C. The autocorrelation functions of the other mixtures exhibit the same tendency.

#### 3.3.1.1.2 Miscibility of Me<sub>2</sub>PE-C32SS-Me<sub>2</sub>PE with Me<sub>2</sub>PE-C32-Me<sub>2</sub>PE

##### DSC

The DSC heating curves of mixtures of Me<sub>2</sub>PE-C32SS-Me<sub>2</sub>PE with Me<sub>2</sub>PE-C32-Me<sub>2</sub>PE and of the pure substances are shown in Figure 3.47. Shape and position of the peaks remained the same in all consecutive scans.

Up to the molar ratio  $x = 0.55$  the transition temperature of the first peak is increased to higher temperature with increasing molar ratio and a shoulder appears that develops into a second peak while the first peak decreases in intensity. A small and very broad transition can be observed at high temperature at all mixing ratios. At  $x = 0.65$  the second peak is slightly shifted to higher temperature and has a broad shoulder at lower temperature.

When the molar ratio is increasing further ( $x = 0.80$ ) the DSC curve shows a broad peak that seems to develop out of the first and second transition observed for the three highest molar ratios. The temperature difference between these two peaks, identified as fiber-fiber and fiber-micelle for Me<sub>2</sub>PE-C32-Me<sub>2</sub>PE suspensions,<sup>[26-27]</sup> decreases with the addition of the sulfur analogue until they superimpose. The resulting peak is shifted to higher temperature compared to the fiber-fiber transition indicating a small stabilization of the fiber structure.

The enthalpy for the single transition at  $x = 0.80$  is somewhat lower than for the two transitions at  $x = 0.87$  and  $0.91$  taken together, which is reasonable as the order and interaction between the molecules inside the fiber is disturbed by the sulfur containing chains.

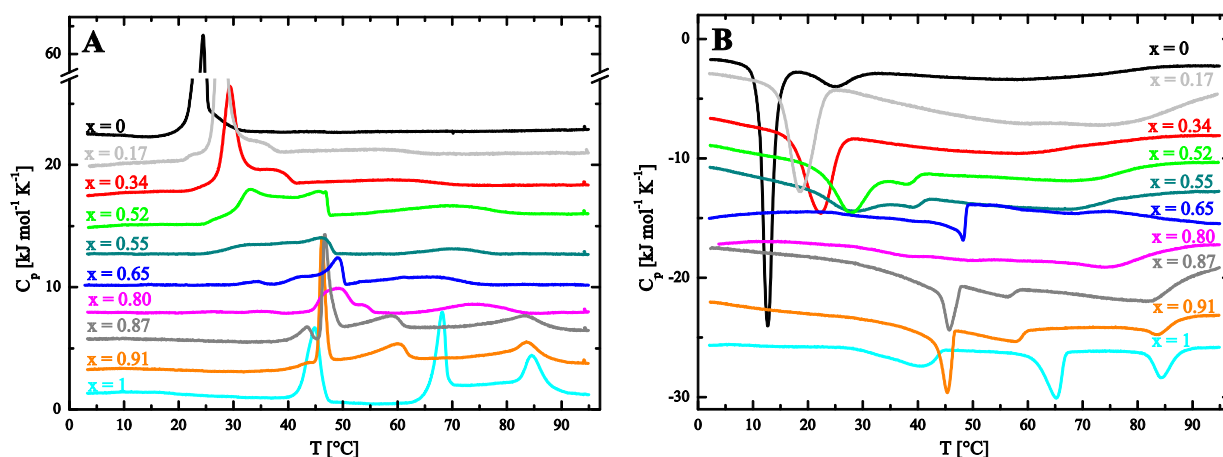


**Figure 3.47:** (A) heating and (B) cooling DSC curves of suspensions ( $c = 1 \text{ mg ml}^{-1}$ ) containing  $\text{Me}_2\text{PE-C32SS-Me}_2\text{PE}$  and  $\text{Me}_2\text{PE-C32-Me}_2\text{PE}$  in different mixing ratios in acetate buffer at pH 5.  $x$  represents the molar ratio of  $\text{Me}_2\text{PE-C32-Me}_2\text{PE}$ . The curves are shifted horizontally for clarity. The heating rate was  $20 \text{ }^\circ\text{C h}^{-1}$ .

In contrast to the DSC cooling scans of suspensions of  $\text{PC-C32SS-PC}$  and  $\text{PC-C32-PC}$  mixtures, the peaks observed in the cooling scans for the suspensions of mixtures of  $\text{Me}_2\text{PE-C32SS-Me}_2\text{PE}$  and  $\text{Me}_2\text{PE-C32-Me}_2\text{PE}$  show the same profile with a split peak as in the heating scans at intermediate molar ratios (Figure 3.47B). At  $x = 0.8$  the lower temperature peak is very broad. This might be connected with structural difficulties in the reformation of a fiber structure due to the fiber-micelle and the fiber-fiber transition that are combined in this peak.

### TEM

TEM images of samples prepared at  $5 \text{ }^\circ\text{C}$  show the presence of long, regular fibers for the molar ratios  $x = 0.34$ ,  $x = 0.52$  and  $x = 0.65$  (Figure 3.48).

The absence of short fiber segments, as observed in  $\text{PC-C32SS-PC}$  and  $\text{PC-C32-PC}$  mixtures, indicates that the structure of the mixed fiber aggregates is more stable for the bolaamphiphiles with the  $\text{Me}_2\text{PE}$  headgroups.

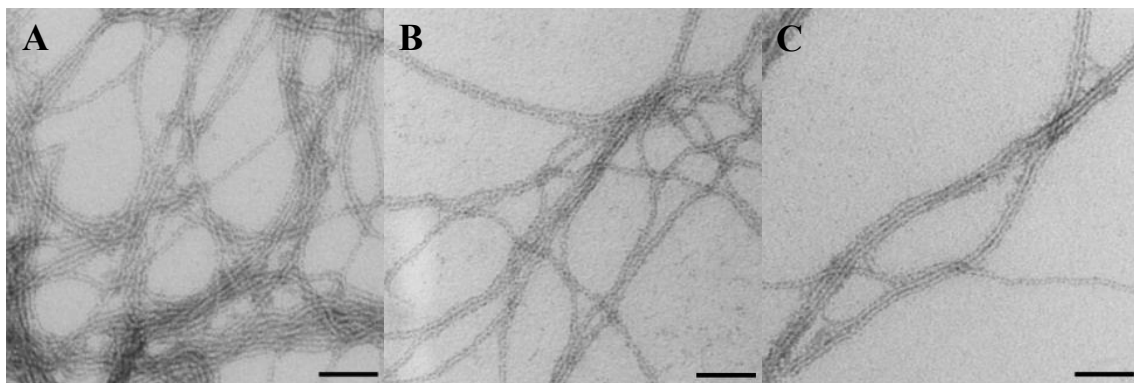


**Figure 3.48:** TEM images of suspensions containing  $\text{Me}_2\text{PE-C32SS-Me}_2\text{PE}$  and  $\text{Me}_2\text{PE-C32-Me}_2\text{PE}$  in different mixing ratios at 5 °C in acetate buffer at pH 5. The bar corresponds to 50 nm. The samples were stained with uranyl acetate.  $x$  represents the molar fraction of  $\text{Me}_2\text{PE-C32-Me}_2\text{PE}$ . (A):  $x = 0.34$ , (B):  $x = 0.52$ , (C):  $x = 0.65$ .

The profile of the observed DSC scans can be explained by the occurrence of two separate effects. First, the mixture of the two bolaamphiphile components causes the presence of broad, split peaks indicating a non-ideal miscibility of the two molecules inside the aggregates. The second effect can be observed at high molar ratios of  $\text{Me}_2\text{PE-C32-Me}_2\text{PE}$ . The fiber-fiber and the fiber-micelle transition of the  $\text{Me}_2\text{PE-C32-Me}_2\text{PE}$  suspension converge upon the addition of the sulfur containing analogue. At  $x = 0.80$  and 0.65 the

superimposition of these two transformations causes broad peaks.

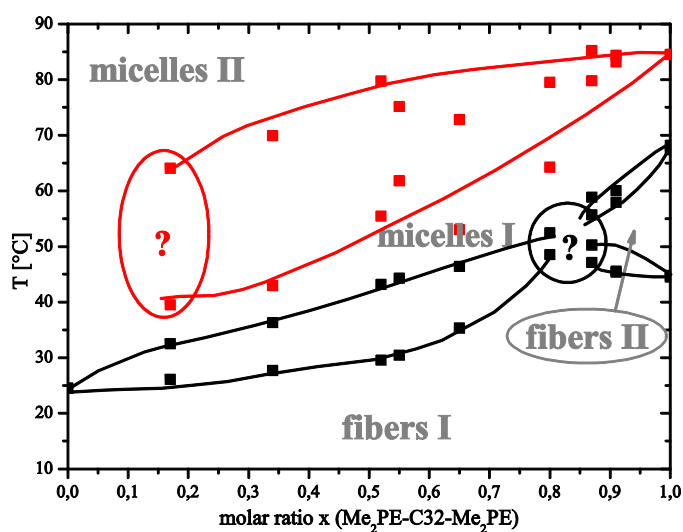


**Figure 3.49:** Schematic “phase diagram” of the mixture of  $\text{Me}_2\text{PE-C32SS-Me}_2\text{PE}$  and  $\text{Me}_2\text{PE-C32-Me}_2\text{PE}$  in acetate buffer at pH 5. The squares represent the onset and completion temperatures of the transitions determined by DSC measurements and are corrected for the width of the transition peak of the pure substances. The lines are drawn as a guide to the eye and connect the onset and completion temperatures of the observed peaks.

The onset and completion temperatures of the DSC peaks were corrected for the finite width of the peaks of the pure components as described in Chapter 3.3.1.1.1 and were used to create a schematic “phase diagram” of the  $\text{Me}_2\text{PE-C32SS-Me}_2\text{PE}$  and  $\text{Me}_2\text{PE-C32-Me}_2\text{PE}$  mixtures (Figure 3.49). The “phase diagram” indicates non-ideal mixing between the two components with “two-phase” regions enclosed by the lines.

The behavior of the micelle I to micelle II transition at low molar ratios was not examined in detail but it can be expected that

the “two phase” region ends in a loop as in the case of the PC-C32SS-PC and PC-C32-PC mixtures. Another not completely analyzed region is between the molar ratios 0.8 and 0.9. Further measurements are necessary to determine the limits of the “two phase” regions.

### DLS

In addition, DLS measurements were performed to gain information on the size of the aggregates. The time autocorrelation functions, obtained for the suspension of the mixture with  $x = 0.55$  at four temperatures, are shown in Figure 3.50.

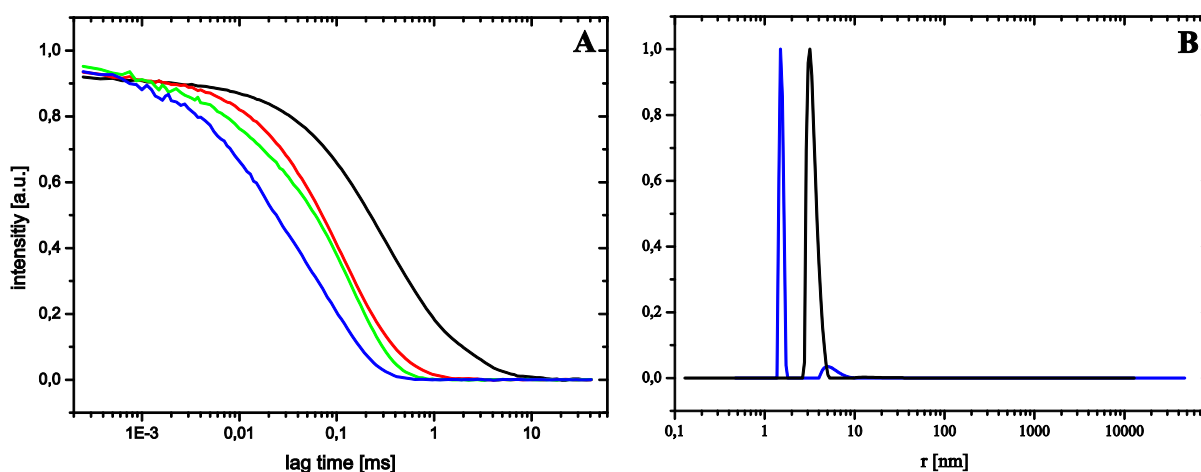


**Figure 3.50:** (A) DLS autocorrelation functions for a suspension ( $c = 1 \text{ mg ml}^{-1}$ ) in acetate buffer at pH 5 containing Me<sub>2</sub>PE-C32SS-Me<sub>2</sub>PE and Me<sub>2</sub>PE-C32-Me<sub>2</sub>PE at 15 (black), 35 (red), 55 (green), and 75 °C (blue). (B) Number-weighted size distribution of the measurement at 15 (black) and 75 °C (blue). The molar ratio of Me<sub>2</sub>PE -C32- Me<sub>2</sub>PE is  $x = 0.55$ .

The aggregates formed at 15 °C are the largest as the midpoint of the autocorrelation function is at a longer time compared to the measurements at higher temperature. This is in accordance with the TEM images showing fibers formed by the mixtures of Me<sub>2</sub>PE-C32SS-Me<sub>2</sub>PE and Me<sub>2</sub>PE-C32-Me<sub>2</sub>PE at 5 °C. At 35 °C the aggregates are considerably smaller as the temperature is chosen inside the broad DSC transition between 25 and 49 °C. At 55 °C the micellar hydrodynamic radius is  $3.3 \pm 0.2 \text{ nm}$  and at 75 °C  $1.9 \pm 0.2 \text{ nm}$ . The aggregate sizes are in accordance with the “phase diagram” and the ascribed aggregate types shown in Figure 3.49. The number-weighted size distribution obtained from the fit of the autocorrelation function of the measurements taken at 15 and 75 °C show that most aggregates are at 15 °C and that mainly small aggregates are present at 75 °C (Figure 3.50B). However, even at 75 °C some larger aggregates seem to be present.

The results for the other mixtures exhibit the same tendency concerning the dependence of aggregate size on temperature

### 3.3.2 Conclusions

The modification of the bolaamphiphile spacer chains of PC-C32-PC and Me<sub>2</sub>PE-C32-Me<sub>2</sub>PE through exchanging of two methylene groups at the positions C12 and C21 for sulfur atoms has not significantly altered the aggregation behavior in aqueous suspensions. The order of the spacer chains is indeed disturbed by the heteroatoms caused by different bond angles, but the aggregation into fibers is still possible. However, the stability range of the fibers is shifted to lower temperature and, in the case of Me<sub>2</sub>PE-C32SS-Me<sub>2</sub>PE, no fiber-fiber transition can be observed. The properties of the micelles formed by the sulfur containing bolaamphiphiles in suspensions above the fiber-micelle transition resemble the highly unordered micellar aggregates (micelles II) formed by the analogue bolaamphiphiles without sulfur at high temperature.

Gelation of aqueous suspensions can be observed at a concentration higher than necessary for the molecules without sulfur containing chains and the viscoelastic gels are also less stable.

Miscibility experiments with mixtures of the bolalipids with and without sulfur show non-ideal miscibility. The formation of fibers is observed for the mixtures of the different molecules as well.

### 3.4 Aggregation Behavior of Bolaamphiphiles Containing Polymerizable Diacetylene Groups in the Spacer Chain

Molecules containing diacetylene groups in the alkyl chain can be polymerized via irradiation with UV light. Self-assembly of such molecules into films or membranes and subsequent 1,4-photopolymerization enable the formation of specific aggregates, in which the single molecules are connected via covalent bonds.<sup>[63, 91-94]</sup> Polymerization leads to the generation of a system of conjugated double and triple bonds as backbone of the polymer. The conformation of the bonds is also referred to as the enyne conformation.<sup>[91]</sup>

Diacetylene compounds have successfully been utilized to stabilize membrane structures,<sup>[63, 95-96]</sup> including systems of bolaamphiphiles.<sup>[97-99]</sup> The extended, delocalized  $\pi$ -electron system also enables applications of polydiacetylenes (PDAs) as nanowires.<sup>[100-102]</sup>

If symmetrical single-chain bolaamphiphiles with diacetylene-modified spacer chains are able to self-assemble into fibers, polymerization is a suitable way to create fibers in which the single molecules are linked via covalent bonds instead of just hydrophobic interactions. Such polymerized fibers should be stable against break-up at high temperature, as only the conformation of the side chains attached to the polymerized middle part could change with increasing temperature. The covalent bonds in the PDA backbone would then prevent the collapse of the aggregate structure as it, e.g., occurs in systems unmodified of PC-C32-PC<sup>[25]</sup> and Me<sub>2</sub>PE-C32-Me<sub>2</sub>PE.<sup>[26]</sup>

A second interesting feature of diacetylene compounds is their ability to form colored phases upon polymerization, e.g., colored Langmuir-Blodgett films.<sup>[63, 103]</sup> This renders them suitable for applications in sensor devices.<sup>[93-94, 98, 104]</sup> Colored phases arise from the presence of  $\pi$ -electron systems that absorb light with wavelengths in the visible spectrum. An interpretation of the different observable colors with respect to the structure of the PDAs is difficult, however, the presence of a blue phase, a purple phase, and a red phase have been described.<sup>[63, 91]</sup> PDAs dissolved in good solvents tend to exhibit a yellow phase.<sup>[105-106]</sup>

Diacetylene modification of the headgroup region of symmetrical bolaamphiphiles would be another way to add the functionality of these polymerizable groups to the bolalipid systems. Thereby however, the functionalization of the bolaamphiphile headgroups with further groups such as sulfur containing moieties or structurally different headgroups would be inhibited making the diacetylene modification of the spacer chain a better choice.

### 3.4.1 Aggregation Behavior of Diacetylene-Modified Bolaamphiphiles

Symmetrical, diacetylene-modified bolaamphiphiles with phosphocholine (PC) or dimethylphosphoethanolamine (Me<sub>2</sub>PE) headgroups and spacer chain lengths from 30 to 36 carbon atoms were synthesized according to the procedure described recently.<sup>[35]</sup> The chemical structure of the diacetylene-modified bolaamphiphiles is shown in Figure 3.51A. The insertion of two triple bonds into the spacer chain leads to a perturbation of the otherwise regular C-C-C bond angle of 113.3°. The bond angle of 180° for triple bonds results in a linear segment in the middle of the spacer chain.

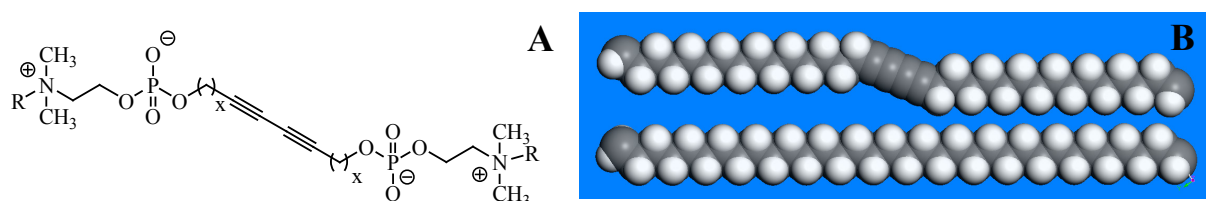


**Figure 3.51:** (A) Chemical structure of PC-C32diAc-PC (R = CH<sub>3</sub>, x = 14), PC-C34diAc-PC (R = CH<sub>3</sub>, x = 15), PC-C36diAc-PC (R = CH<sub>3</sub>, x = 16), Me<sub>2</sub>PE-C32diAc-Me<sub>2</sub>PE (R = H, x = 14), Me<sub>2</sub>PE-C34diAc-Me<sub>2</sub>PE (R = H, x = 15), and Me<sub>2</sub>PE-C36diAc-Me<sub>2</sub>PE (R = H, x = 16). (B) CPK models of the spacer chains C34diAc (top) and C34 (bottom) visualized with Materials Studio (Accelrys, Inc.).

CPK models for comparison of the chain structure of the bolaamphiphiles with C34 and C34diAc spacer chains are given in Figure 3.51B.

The length of the spacer chain is hardly affected by the changes of the bond structure. However, the two triple bonds increase the rigidity and lead to a kink in the spacer chain. This change may result in difficulties in the self-assembly of these molecules, as the packing is more restrained than in the case of pure all-*trans* alkyl chains without triple bonds. In addition, the polarity in the middle part of the chain increases slightly due to the high electron density of the triple bonds.

Apart from the structural changes caused by the diacetylene groups, the modified bolaamphiphiles establish new possibilities regarding the stabilization of the aggregates via polymerization and formation of covalent bonds between the single molecules.

The aggregation behavior of PC-C32diAc-PC and Me<sub>2</sub>PE-C32diAc-Me<sub>2</sub>PE in aqueous suspension was examined before, but a detailed analysis was difficult due to the very low transition peaks observed in the DSC scans (Figure 3.52).<sup>[49]</sup> The aggregation behavior of PC-C34diAc-PC and PC-C36diAc-PC as well as Me<sub>2</sub>PE-C34diAc-Me<sub>2</sub>PE and Me<sub>2</sub>PE-C36diAc-Me<sub>2</sub>PE was investigated in aqueous suspension using DSC, FT-IR spectroscopy, SANS and TEM.

Due to limited sample resources not all measurements could be carried out with all of the diacetylene-modified bolaamphiphiles. Recent results showed that the properties of

symmetrical single-chain bolaamphiphiles are very similar for different bolaamphiphiles. With increasing chain length the stability range of the fiber aggregates is shifted to higher temperature.<sup>[28]</sup> Therefore, the behavior observed for one of the diacetylene containing bolaamphiphiles also enables a prediction of the behavior of the longer or shorter chain analogues.

### 3.4.1.1 Diacetylene-Modified Bolaamphiphiles with PC Headgroups

#### DSC

The DSC heating scans for three suspensions of PC-C32diAc-PC, PC-C34diAc-PC, and PC-C36diAc-PC are shown in Figure 3.52. Only one DSC transition is observed.

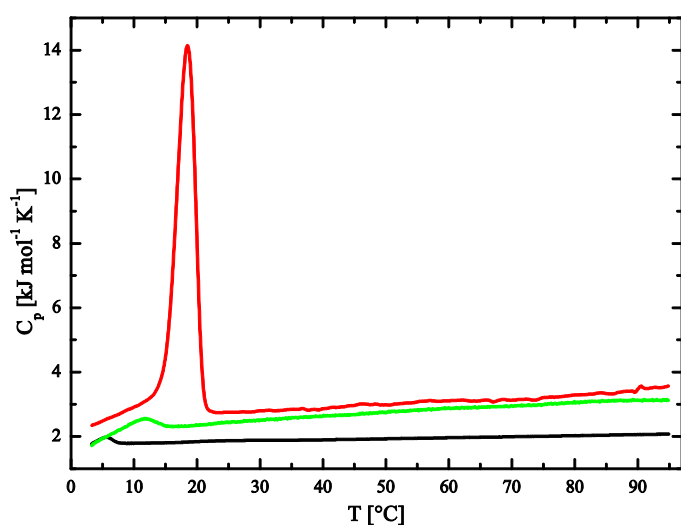


**Figure 3.52:** DSC heating scans of suspensions of PC-C32diAc-PC (black,  $c = 10 \text{ mg ml}^{-1}$ ),<sup>[49]</sup> PC-C34diAc-PC (green,  $c = 1 \text{ mg ml}^{-1}$ ), and PC-C36diAc-PC (red,  $c = 1 \text{ mg ml}^{-1}$ ) in water. The heating rate was  $20 \text{ }^\circ\text{C h}^{-1}$ .

The temperature of the peak increases from 6 to 11.8 to 18.5 °C with increasing chain length. The enthalpy of the transition also increases. Upon cooling, the transitions of the suspensions of PC-C34diAc-PC and PC-C36diAc-PC show a hysteresis of approximately 10 °C.

#### FT-IR

FT-IR spectroscopic measurements of a suspension of PC-C34diAc-PC show a wavenumber around  $2848.2 \text{ cm}^{-1}$  for the symmetric methylene stretching vibrational band up to a temperature of approximately 10 °C (Figure 3.53). The subsequent step-wise increase of the wavenumber correlates with the transition peak observed in the DSC heating scan of this bolaamphiphile although the temperature is a little higher than in the DSC scan. This is probably due to the higher concentration of the bolaamphiphile and different experimental conditions.

Up to 50 °C, the wavenumber increases further up to a value of approx.  $2851.8 \text{ cm}^{-1}$ . These values are similar to the ones determined for a suspension of PC-C32-PC at this temperature corresponding to micellar aggregates (micelles I).<sup>[25]</sup> Upon cooling a hysteresis is again seen as was already observed in the DSC scans.

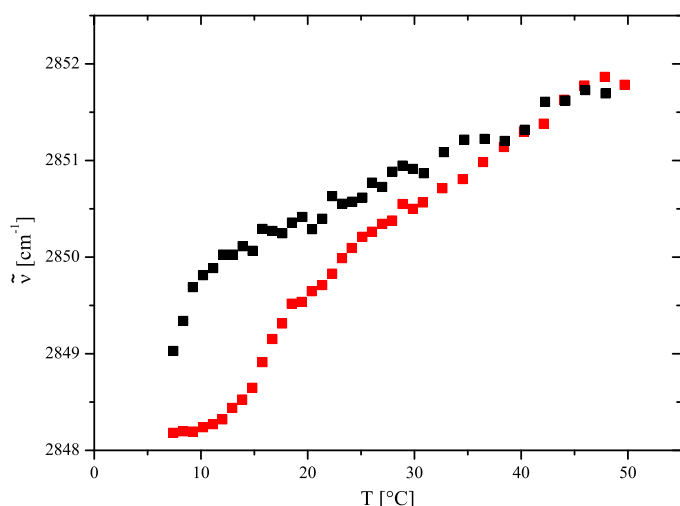


**Figure 3.53:** FT-IR spectroscopic data (wavenumber of the symmetric methylene stretching vibrational band) of an aqueous suspension of PC-C34diAc-PC ( $c = 50 \text{ mg ml}^{-1}$ ). Red: heating, black: cooling.

diameter seems to be too high for single bolaamphiphile fiber strands. This may be caused by a parallel orientation of two fiber strands or due to preparation artifacts as the preparation temperature is very close to the DSC transition temperature. The fiber segments are considerably shorter than the fibers formed in PC-C32-PC suspensions.<sup>[25]</sup>

### SANS

SANS measurements should give further information on the structure of aggregates in aqueous suspensions. The results of neutron scattering experiments at 5 and 30 °C with a suspension of PC-C36diAc-PC in heavy water are shown in Figure 3.55. For the sample at 5 °C, the scattering data exhibit characteristics typical for the fiber structure of the bolaamphiphiles.<sup>[27-28]</sup> The slope of the scattering data at low and intermediate  $q$  values decreases at higher temperature indicating the formation of smaller aggregates. The data were fitted with the IFT method (see Chapter 2.2.7) and the model of cylinders and spheres at 5 and 30 °C, respectively (Table 3.5). The fits are in good agreement with the experimental data and lead to the conclusion that the PC-C36diAc-PC molecules

### TEM

Cryo-TEM images of a suspension of PC-C32diAc-PC revealed the presence of micellar aggregates at 7 °C.<sup>[49]</sup> This is due to the very low onset temperature of the transition observed in the DSC scans. In the TEM image of a PC-C34diAc-PC suspension, prepared at 5 °C, which is below the DSC transition temperature, the presence of fibrous aggregates with a diameter of 14 nm is evident (Figure 3.54). The

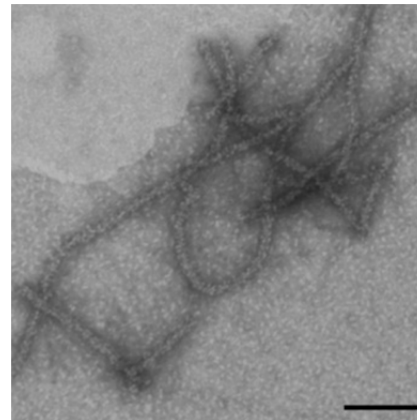


**Figure 3.54:** TEM image of a suspension of PC-C34diAc-PC prepared at 5 °C. The sample was stained with uranyl acetate. The bar corresponds to 100 nm.

self-assemble into fibers below the DSC transition peak. The transition at 18.5 °C is connected with the collapse of these fibers into spherical micelles.

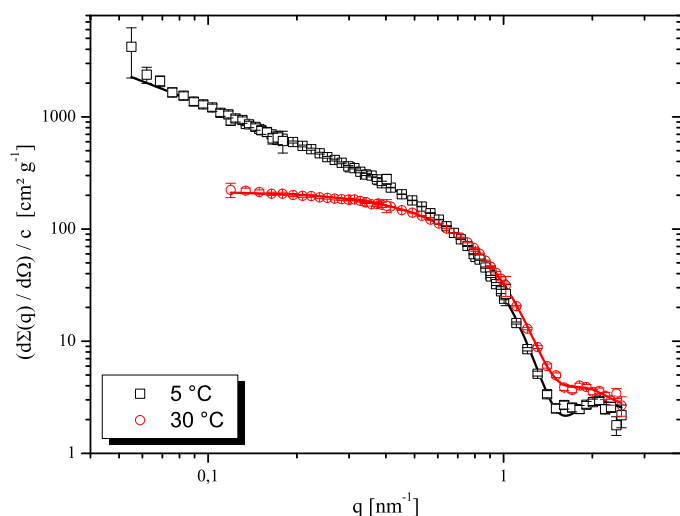


**Figure 3.55:** SANS data and IFT fits (solid lines) of measurements of a PC-C36diAc-PC suspension ( $c = 1 \text{ mg ml}^{-1}$ ) in  $\text{D}_2\text{O}$ .

fiber region (fibers II) as was also found for  $\text{Me}_2\text{PE-C32-Me}_2\text{PE}$  and its analogues with longer chains.<sup>[29]</sup> This effect is not evident in the suspension of PC-C34diAc-PC and PC-C36diAc-PC and furthermore, no micelle-micelle transition as for PC-C32-PC and PC-C36-PC was observed.<sup>[25, 29]</sup>

Compared to SANS experiments with PC-C36-PC at 25 °C the fibers formed by PC-C36diAc-PC at 5 °C seem to be very similar, showing that the fiber formation is not inhibited by the diacetylene segments.

However, the thermal stability of the fibers is significantly decreased for the diacetylene-modified bolaamphiphiles. The bolaamphiphiles PC-C34-PC and PC-C36-PC show the presence of an additional

**Table 3.5:** Results of IFT fits of the SANS measurements with PC-C36diAc-PC suspended in  $\text{D}_2\text{O}$  ( $c = 1 \text{ mg ml}^{-1}$ ) at 5 and 30 °C.<sup>a</sup>

	T [°C]	aggregate shape	$D_{\text{max}}$ [nm]	$N_{\text{agg}}$ [nm <sup>-1</sup> ] $N_{\text{agg}}$ per micelle	$M_L$ [g cm <sup>-1</sup> ] M [g]	$R_g$ or $R_{\text{CS},g}$ [nm]	R [nm]
PC-C36diAc-PC	5	fibers	5	9	$1.30 \cdot 10^{-13}$	$1.73 \pm 0.05$	$2.45 \pm 0.05$
	30	micelles	6.5	25	$3.56 \cdot 10^{-20}$	$2.30 \pm 0.05$	$2.96 \pm 0.05$
PC-C36-PC <sup>[29]</sup>	25	fibers	5.5	10	$1.46 \cdot 10^{-13}$	$1.86 \pm 0.01$	$2.63 \pm 0.01$

<sup>a</sup> $D_{\text{max}}$ : maximal size or cross-section of aggregate, M: mass,  $M_L$ : mass per unit length,  $N_{\text{agg}}$ : aggregation number,  $R_g$ : radius of gyration,  $R_{\text{SC},g}$ : radius of gyration of cross-section, R: radius.

### 3.4.1.2 Diacetylene-Modified Bolaamphiphiles with $\text{Me}_2\text{PE}$ Headgroups

#### DSC

DSC heating scans of suspensions of  $\text{Me}_2\text{PE-C32diAc-Me}_2\text{PE}$ ,<sup>[49]</sup>  $\text{Me}_2\text{PE-C34diAc-Me}_2\text{PE}$ , and  $\text{Me}_2\text{PE-C36diAc-Me}_2\text{PE}$  in acetate buffer at pH 5 are shown in Figure 3.56. As for the analogue bolaamphiphiles with PC headgroups, an increase of the transition temperature from

14.3 to 19.7 and 29.5 °C can be observed with increasing chain length. No further peaks occur at higher temperature.

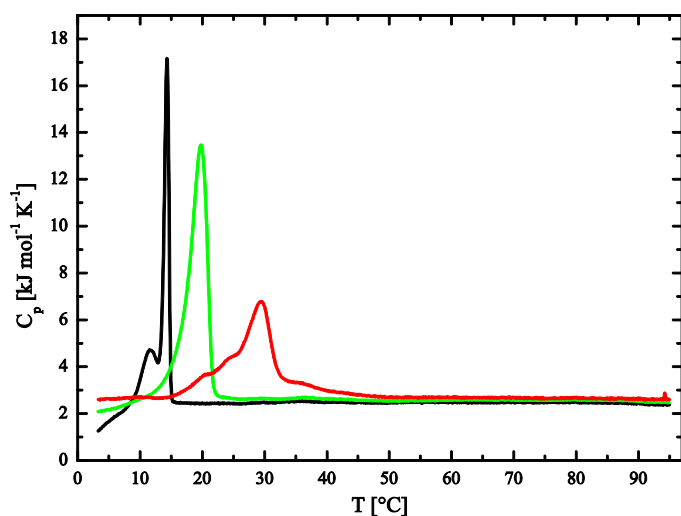


**Figure 3.56:** DSC heating scans of suspensions of Me<sub>2</sub>PE-C32diAc-Me<sub>2</sub>PE (black,  $c = 5 \text{ mg ml}^{-1}$ ),<sup>[49]</sup> Me<sub>2</sub>PE-C34diAc-Me<sub>2</sub>PE (green,  $c = 1 \text{ mg ml}^{-1}$ ), and Me<sub>2</sub>PE-C36diAc-Me<sub>2</sub>PE (red,  $c = 1 \text{ mg ml}^{-1}$ ) in acetate buffer at pH 5. The heating rate was  $20 \text{ °C h}^{-1}$ .

The higher transition temperatures compared to the diacetylene compounds with PC headgroups can be explained by the additional stabilization via hydrogen bonds between the Me<sub>2</sub>PE headgroups formed in this case.

### TEM

TEM images of a Me<sub>2</sub>PE-C32diAc-Me<sub>2</sub>PE suspension at 25 °C revealed micelles.<sup>[49]</sup> TEM images of suspensions of Me<sub>2</sub>PE-C34diAc-Me<sub>2</sub>PE

and Me<sub>2</sub>PE-C36diAc-Me<sub>2</sub>PE prepared at 5 °C are displayed in Figure 3.57.

In both cases long fibers can be observed, however, the diameters of fiber strands differ in the sample of the bolaamphiphile with the longer spacer chain. The fibers of Me<sub>2</sub>PE-C36diAc-Me<sub>2</sub>PE have diameters ranging from 3 to 8 nm, whereas the Me<sub>2</sub>PE-C34diAc-Me<sub>2</sub>PE fibers seem to exhibit more uniform diameters of 4 nm.

### SANS

SANS experiments were carried out with a suspension of Me<sub>2</sub>PE-C36diAc-Me<sub>2</sub>PE in deuterated acetate buffer at 5 and 55 °C. The scattering data and IFT fits (see Chapter 2.2.7)

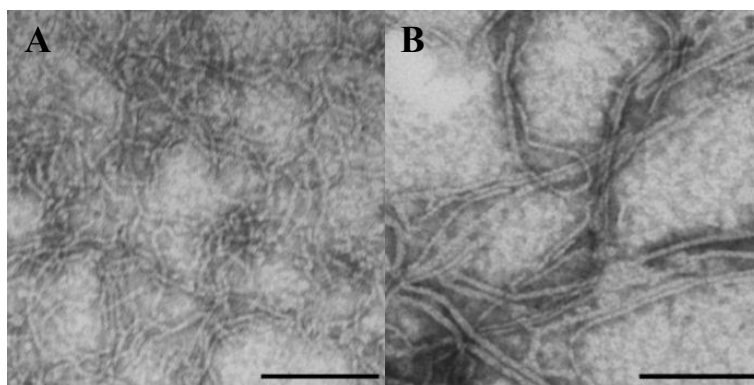


**Figure 3.57:** TEM images of suspensions of (A) Me<sub>2</sub>PE-C34diAc-Me<sub>2</sub>PE and (B) Me<sub>2</sub>PE-C36diAc-Me<sub>2</sub>PE prepared at 5 °C. The samples were stained with uranyl acetate. The bar corresponds to 100 nm.

as well as the pair distance distribution function  $p(r)$  are provided in Figure 3.58.

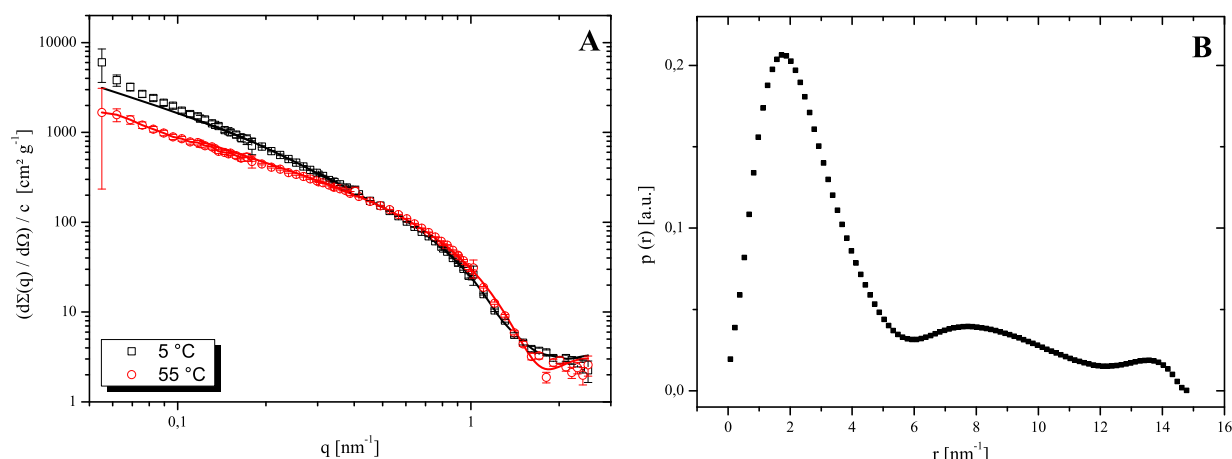


**Figure 3.58:** (A) Scattering data and IFT fits (solid lines) of SANS measurements of a suspension of Me<sub>2</sub>PE-C36diAc-Me<sub>2</sub>PE ( $c = 1 \text{ mg ml}^{-1}$ ) in acetate buffer at 5 and 55 °C. (B) Pair distance distribution function  $p(r)$  of the scattering data at 5 °C.

The IFT fits for the data at 5 and 55 °C were done with the model of infinitely long cylinders and are in good agreement with the experimental data (Table 3.6).

The pair distance distribution function of the measurement at 5 °C is asymmetric and has three maxima around 2, 8, and 14 nm (Figure 3.58B). This indicates that the aggregates present in the suspension have different radii which can be explained by the formation of bundles of individual fiber strands. Fibers with larger radii are also obtained from the IFT fit of the scattering data at 5 °C with the model of long cylinders. The radius is approximately twice as high as determined for other bolaamphiphile systems (Table 3.6)<sup>[27-28]</sup> and is an average over all aggregates in the suspension. TEM images support these results as they show fibers with a range of radii for the Me<sub>2</sub>PE-C36diAc-Me<sub>2</sub>PE suspension at 5 °C (Figure 3.57B).

**Table 3.6:** Results of IFT fits of the SANS measurements with Me<sub>2</sub>PE-C36diAc-Me<sub>2</sub>PE suspended in acetate buffer ( $c = 1 \text{ mg ml}^{-1}$ ) at 5 and 55 °C.<sup>a</sup>

	T [°C]	aggregate shape	D <sub>max</sub> [nm]	N <sub>agg</sub> [nm <sup>-1</sup> ] or N <sub>agg</sub> per micelle	M <sub>L</sub> [g cm <sup>-1</sup> ] or M [g]	R <sub>g</sub> or R <sub>CS,g</sub> [nm]	R [nm]
Me <sub>2</sub> PE- C36diAc-Me <sub>2</sub> PE	5	bundles of fibers	15	12	$1.70 \cdot 10^{-13}$	$3.99 \pm 0.05$	$5.64 \pm 0.05$
	55	fibers	4.5	7	$9.46 \cdot 10^{-14}$	$1.51 \pm 0.05$	$2.14 \pm 0.05$
Me <sub>2</sub> PE-C36- Me <sub>2</sub> PE <sup>[29]</sup>	70	fibers	5.5	11	$1.51 \cdot 10^{-13}$	$1.65 \pm 0.01$	$2.33 \pm 0.01$

<sup>a</sup>D<sub>max</sub>: maximal size or cross-section of aggregate, M: mass, M<sub>L</sub>: mass per unit length, N<sub>agg</sub>: aggregation number, R<sub>g</sub>: radius of gyration, R<sub>SC,g</sub>: radius of gyration of cross-section, R: radius.

In contrast to the measurements with the PC-C36diAc-PC suspension the scattering data of the high temperature measurement exhibit a slope at small and intermediate  $q$  values that indicates the presence of fibers even at 55 °C.<sup>[27-28]</sup> This is an unexpected observation for the diacetylene bolaamphiphiles. In fact, fiber structures have been observed at elevated temperature above a fiber-fiber transition for bolaamphiphiles with Me<sub>2</sub>PE headgroups, but this transition was always followed by a high temperature transition of the fibrous aggregates into micellar aggregates.<sup>[26, 29]</sup> A transition of this kind, however, cannot be observed in the DSC scans of Me<sub>2</sub>PE-C36diAc-Me<sub>2</sub>PE (Figure 3.56).

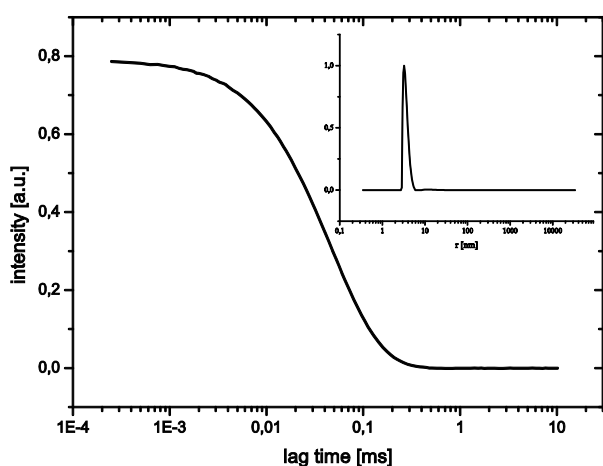


**Figure 3.59:** DLS autocorrelation function and fit for an aqueous suspension of Me<sub>2</sub>PE-C36diAc-Me<sub>2</sub>PE ( $c = 1 \text{ mg ml}^{-1}$ ) at 55 °C. The inset shows the number-weighted size distribution.

### DLS

To check the size and type of the aggregates present in the Me<sub>2</sub>PE-C36diAc-Me<sub>2</sub>PE suspension at 55 °C DLS measurements were carried out. The time autocorrelation function and a number-weighted fit are shown in Figure 3.59. They indicate the presence of micelles with a hydrodynamic radius of  $r = 3.8 \pm 0.4 \text{ nm}$ .

In combination with the results of the DSC scan of this sample it seems probable that the high temperature SANS measurement is inaccurate. This might be due to experimental errors in the temperature control or the preparation of the sample.

However, TEM images and SANS measurements show that the formation of fibers is possible for the suspensions of Me<sub>2</sub>PE-C34diAc-Me<sub>2</sub>PE and Me<sub>2</sub>PE-C36diAc-Me<sub>2</sub>PE at 5 °C. The stability range of these fibers is again shifted to lower temperature compared to the non-modified bolaamphiphiles.

### **3.4.2 Polymerization of Diacetylene-Modified Bolaamphiphiles**

It was shown that the diacetylene containing bolaamphiphiles self-assemble into fibers below the temperature of the DSC transition peak. Polymerization of these aggregates using UV irradiation is a way to examine the possibility of developing thermostable fibers via the formation of covalent bonds between the single molecules that form the fibers. The

polymerization process is very sensitive to the distance and relative orientation of the diacetylene units. Both parameters were shown to determine the reactivity of the diacetylene monomers.<sup>[103, 107]</sup> A distance between 0.47 and 0.52 nm and an inclination angle of 45° between the diacetylene axes are necessary for an efficient polymerization reaction.<sup>[108]</sup> A schematic representation of the polymerization process is given in Figure 3.60A. This reaction leads to an alternating double-triple bond structure with changed orientation of the side chains R and R'. A model of four polymerized diacetylene-modified bolaamphiphile chains is given in Figure 3.60B.

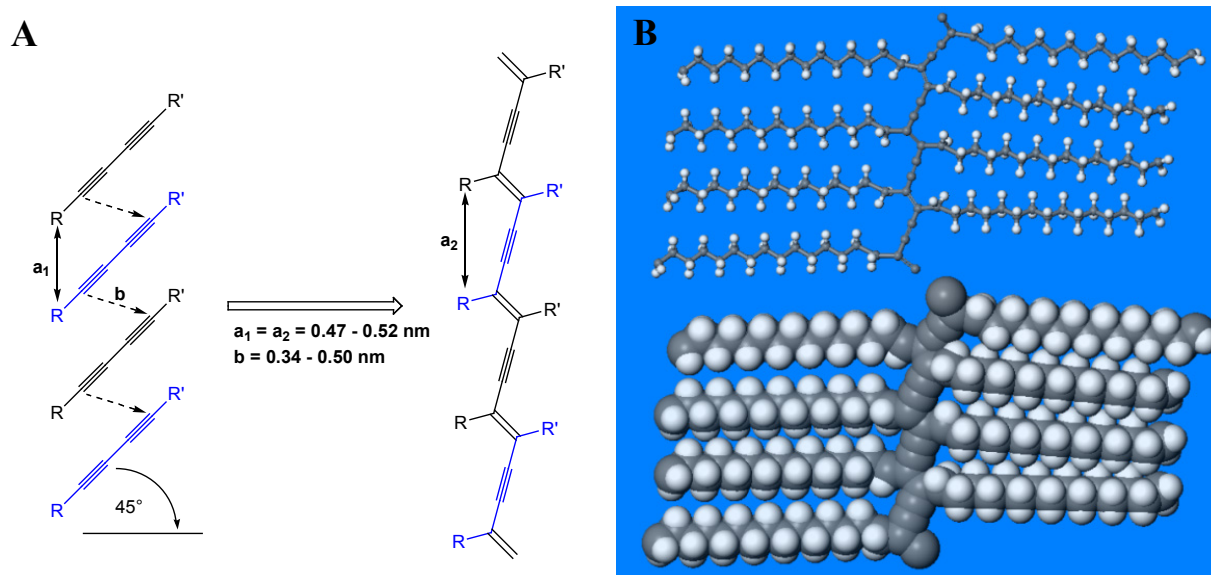


**Figure 3.60:** (A) Polymerization reaction of diacetylene molecules and (B) a ball and stick and CPK model of four polymerized C34diAc bolaamphiphile chains visualized with Materials Studio (Accelrys, Inc.).

The first polymerization experiments were carried out by M. Bastrop with PC-C32diAc-PC and Me<sub>2</sub>PE-C32diAc-Me<sub>2</sub>PE suspensions and were described in his PhD thesis.<sup>[49]</sup>

PC-C32diAc-PC suspensions ( $c = 5$  and  $10 \text{ mg ml}^{-1}$ ) turned blue upon UV irradiation indicating the formation of a blue polydiacetylene (PDA) “phase” when samples were irradiated at 0 °C or at room temperature, respectively. The “phases” formed by the bolaamphiphile suspensions are different from the PDA phases formed, e.g., by planar film, as they consist of polymerized fibers suspended in aqueous media and are not phases in the classical sense. When the polymerized sample was heated, the color of the suspension changed with temperature and turned from blue to purple to red upon heating from 10 to 30 to 40 °C. This thermochromism was reversible to some extent if the suspension was heated to 40 °C and subsequently cooled to 10 °C again. No reversibility was observed if the sample was heated above 50 °C. In contrast, Me<sub>2</sub>PE-C32diAc-Me<sub>2</sub>PE suspensions in acetate buffer at

pH 5 ( $c = 5 \text{ mg ml}^{-1}$ ) only turned yellow upon UV irradiation at  $5 \text{ }^\circ\text{C}$  and at room temperature.<sup>[49]</sup>

This behavior can be explained by the formation of an extended  $\pi$ -conjugated polymer backbone with enyne alternation of the C-C bond length (Figure 3.60). Absorption of light in the wavelength region of the visible light causes the observed coloring. A planar conformation of the polymer backbone and ordered side chains lead to the presence of a blue phase.<sup>[49, 103]</sup> The side groups of the diacetylene moieties of diacetylene containing molecules were proven to have a strong impact on the properties and the color of the PDAs. The side chains conformation can lead to a shift of the absorption maximum. With increasing temperature, higher flexibility of the side groups and thus induced rotation of the PDA backbone cause the formation of a red phase. This process also reduces the conjugation length of the polymer.<sup>[91]</sup> The purple phase was described as a transition state in the conversion of the blue into the red phase.<sup>[109]</sup> The formation of yellow phases was observed for PDAs in good solvents and may be ascribed to the presence of partially dissolved polymerized diacetylene bolaamphiphile fibers with a non-planar PDA backbone.<sup>[103, 105-106]</sup>

M. Bastrop explained the absence of blue or red “phases” for polymerized suspensions of  $\text{Me}_2\text{PE-C32diAc-Me}_2\text{PE}$  by the different structure of the aggregates due to the smaller size of the  $\text{Me}_2\text{PE}$  headgroup compared to the PC headgroup.<sup>[49]</sup> This results in a changed distance of the diacetylene groups and prevents the formation of extended polymerized groups, as this process is very sensitive to structural modifications like decreased distance between the diacetylene groups.<sup>[103]</sup>

The polymerization experiments described above were carried out in an isolated box, in which the bolaamphiphile suspension was thermostatted inside an ice water bath and irradiated with UV light. The samples were then placed into the UV/Vis spectrometer to record the spectra. New polymerization experiments with the diacetylene-modified bolaamphiphiles were made using a different spectrophotometer with a thermostatted cuvette holder, in which the samples could be irradiated directly with the UV lamp prior to the measurement of the absorption spectra. This improved the temperature stability during irradiation and measurement.

#### **3.4.2.1 Polymerization of Diacetylene-Modified Bolaamphiphiles with PC Headgroups**

Suspensions of PC-C32diAc-PC, PC-C34diAc-PC, and PC-C36diAc-PC were irradiated with UV light to achieve polymerization and to investigate the formation of colored “phases”.

### PC-C32diAc-PC

To test the reproducibility of the results described above, the experiments were repeated with newly synthesized PC-C32diAc-PC. The formation of a blue “phase” upon polymerization, however, could not be achieved again. Neither polymerization with the new experimental setup at 5 °C nor with the former setup at 0 °C resulted in a blue or even red coloring of the pPC-C32diAc-PC suspension. All suspensions turned slightly yellow.

Impurities remaining in the bolaamphiphile powder after synthesis might affect the polymerization reaction and the formation of a blue phase. For instance, it was reported that cadmium ions influence the structure and polymerizability of diacetylene systems as the formation of cadmium salts reduces the reactivity.<sup>[110]</sup> The influence of metal ions on the polymerizability of Langmuir-Blodgett films of 10,12-tricosadiynoic acid (TDA) through different coordination modes of metal ions to the carboxylate anion was also reported.<sup>[111]</sup> This suggests the possibility that residues of the synthetic procedure might have an effect on the behavior of the suspension.

### PC-C34diAc-PC

Polymerization of a PC-C34diAc-PC suspension at a concentration of  $c = 5 \text{ mg ml}^{-1}$  at 5 °C yields a red suspension that turns yellow upon heating to 20 °C (Figure 3.61).

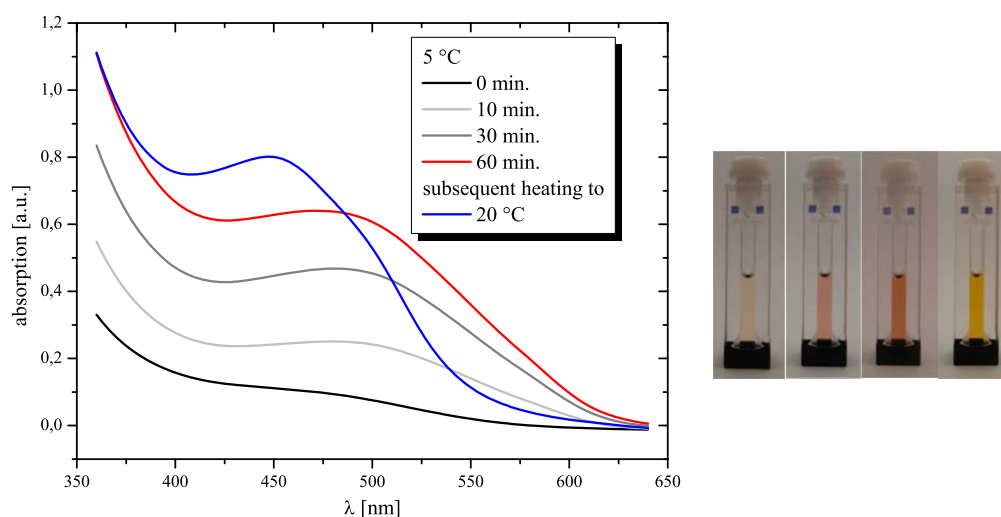


**Figure 3.61:** UV/Vis spectra of a PC-C34diAc-PC suspension ( $c = 5 \text{ mg ml}^{-1}$ ) after different irradiation intervals at 5 °C and after heating to 20 °C and photographs of the suspensions after 0, 10, and 60 minutes of UV irradiation at 5 °C and after heating to 20 °C.

Most suspensions of the diacetylene bolaamphiphiles were colorless prior to irradiation with UV light. However, this suspension already exhibited a light yellow color. This can be attributed to a small degree of polymerization of the bolaamphiphiles via stray UV light. The UV/Vis spectra in Figure 3.61 show an absorption maximum around 500 nm that shifts to

450 nm upon heating of the suspension. The intensity of the absorption increases with progressing irradiation time.

A suspension of PC-C34diAc-PC at the lower concentration  $c = 1 \text{ mg ml}^{-1}$  merely turns slightly yellow upon irradiation at  $5 \text{ }^\circ\text{C}$ . In addition, irradiation of a suspension with the concentration  $c = 5 \text{ mg ml}^{-1}$  at  $25 \text{ }^\circ\text{C}$ , which is above the fiber-micelle transition, also leads to the formation of a yellow colored sample.

### PC-C36diAc-PC

A PC-C36diAc-PC suspension ( $c = 1 \text{ mg ml}^{-1}$ ) was irradiated at  $5 \text{ }^\circ\text{C}$  resulting in a red color of the suspension after 30 minutes of irradiation. The UV/Vis spectrum shows a peak around 500 nm and a shoulder at 550 nm after 2 minutes of irradiation (Figure 3.62). The peak at higher wavelength diminishes with continuing irradiation until only the peak around 500 nm is visible after 30 minutes. Continued irradiation leads to a shift of the absorption maximum to 430 nm indicated by the orange to yellow color of the suspension.

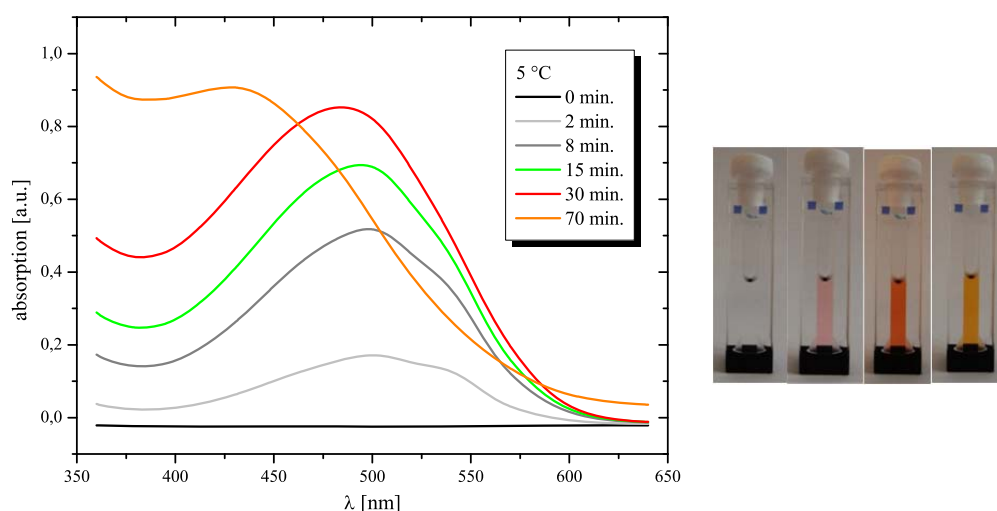


**Figure 3.62:** UV/Vis spectra of a PC-C36diAc-PC suspension ( $c = 1 \text{ mg ml}^{-1}$ ) after different irradiation intervals at  $5 \text{ }^\circ\text{C}$  and photographs of the suspensions after 0, 2, 30, and 70 minutes of irradiation.

Polymerization experiments with a PC-C36diAc-PC suspension at  $c = 5 \text{ mg ml}^{-1}$ , instead of  $1 \text{ mg ml}^{-1}$ , at  $5 \text{ }^\circ\text{C}$  essentially showed the same UV/Vis spectra but with increased intensity of the absorption. After 100 minutes of polymerization the suspension was still deep red in color with an absorption maximum at 500 nm. As more PC-C36diAc-PC molecules are present in the suspension it can be expected to take longer for all fibers to polymerize. In this case, the irreversible transition to the yellow “phase” was achieved by heating the suspension to  $30 \text{ }^\circ\text{C}$ .

Polymerization experiments with a PC-C36diAc-PC suspension at  $c = 5 \text{ mg ml}^{-1}$  but at  $25 \text{ }^\circ\text{C}$  yielded a light yellow suspension after 50 minutes of irradiation. However, after cooling of the suspension to  $5 \text{ }^\circ\text{C}$  further irradiation lead to the formation of a red “phase”. This indicates that not all of the PC-C36diAc-PC aggregates were polymerized after 50 minutes.

### DSC

DSC measurements of suspensions of pPC-C36diAc-PC at a concentration of  $1 \text{ mg ml}^{-1}$  after 30 and 70 minutes of irradiation are shown in Figure 3.63. The first sample, taken after 30 minutes of irradiation, was not heated above  $5 \text{ }^\circ\text{C}$  and was red prior to the DSC measurements. After the DSC measurement in the temperature range from  $2$  to  $95 \text{ }^\circ\text{C}$ , the color of the suspension was yellow. The second sample, taken after 70 minutes of irradiation, was yellow and did not change its color during the DSC measurement.

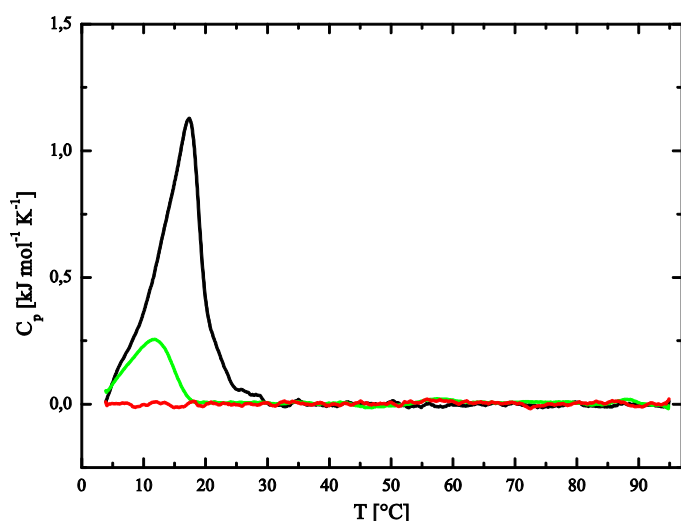


**Figure 3.63:** DSC heating scans for pPC-C36diAc-PC suspensions ( $c = 1 \text{ mg ml}^{-1}$ ) after polymerization at  $5 \text{ }^\circ\text{C}$  for 30 minutes (black: first scan, green: third scan) and 70 minutes (red). The heating rate was  $60 \text{ }^\circ\text{C h}^{-1}$ .

The first DSC heating scan of the red sample shows a broad peak at  $17 \text{ }^\circ\text{C}$  (black curve in Figure 3.63). All consecutive scans show only a smaller peak at  $11 \text{ }^\circ\text{C}$  (green curve in Figure 3.63). All scans of the yellow suspension show no transition at all (red curve in Figure 3.63).

After irradiation for 30 minutes, the red suspension probably contains a mixture of polymerized and unpolymerized fibers. In comparing the enthalpy of the first peak (black curve in Figure 3.63) of the DSC scans of the red suspension with the enthalpy of the following scans (green curve in Figure 3.63), it is obvious that the enthalpy decreases. The difference in the transition enthalpies might give an indication of the enthalpy of the irreversible red to yellow transition, which only occurs once in the first scan. This is supported by the temperature range of the peak that reaches up to  $30 \text{ }^\circ\text{C}$ , which is higher than for the unpolymerized PC-C36diAc-PC (Figure 3.52) but around the same temperature that the transition from red to yellow can be observed in the UV/Vis spectrometer. During the

transition, the side chains of the PDA backbone rearrange and become more disordered inducing the observed color change. This rearrangement is not reversible upon cooling of the suspension.

Similar findings have been reported before. In the case of polymerized sodium 10,12-pentacosadiynoate (PCDA-Na) a similar effect was observed for an irreversible red to orange transition at high temperature ( $> 130\text{ }^{\circ}\text{C}$ ).<sup>[112]</sup> At high temperature the alkyl side chains melt and are supposed to wobble and entangle to a degree that makes the recrystallization of the side chains impossible. During this process the conjugation length of the PDA backbone decreases resulting in the observed irreversible color change from red to orange. This transition is visible in the DSC scans only once in the first heating scan and also not in the cooling curves.

A similar behavior can be assumed for the PDA bolaamphiphiles, which have very long alkyl side chains attached to the PDA backbone. These chains can entangle easily because of the structure of the bolaamphiphile fibers making a re-formation of a more ordered structure impossible.

The DSC peak at  $11\text{ }^{\circ}\text{C}$  (green curve in Figure 3.63) can be expected to result from unpolymerized fibers of PC-C36diAc-PC although the temperature is  $7\text{ }^{\circ}\text{C}$  lower than the one determined for PC-C36diAc-PC without polymerization (Figure 3.52). This could result from the lower concentration of the unpolymerized PC-C36diAc-PC molecules in the irradiated suspension.

The DSC scan of the yellow suspension (red curve in Figure 3.63) shows no transition as no unpolymerized PC-C36diAc-PC molecules remain and all polymerized fibers are already in a disordered state. In addition, the DSC scans of the pPC-C36diAc-PC suspension in the yellow “phase” show that the transition from the red to the yellow “phase” is not reversible.

The two DSC measurements also show that the red to yellow transition can either be caused by increasing the temperature or by extended irradiation with UV light. As extended irradiation can cause local heating of the sample, too, both procedures induce an increased disorder of the alkyl side chains and the resulting color change.

### TEM

TEM images of the red and the yellow suspension are shown in Figure 3.64.

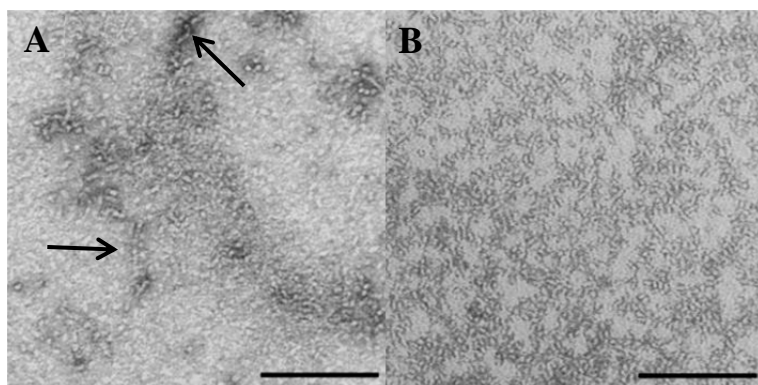


**Figure 3.64:** TEM images of (A) a red suspension of pPC-C36diAc-PC prepared at 5 °C prior to the DSC measurement and (B) a yellow suspension of pPC-C36diAc-PC prepared at 25 °C after the DSC measurement. The samples were stained with uranyl acetate. The bar corresponds to 100 nm.

Both images show no significant differences in the structure of the aggregates. Short fiber segments or elongated micelles that have a diameter of approximately 5 nm appear. This illustrates that the fiber structure shown to be formed by PC-C36diAc-PC at low temperature (see Chapter 3.4.1.1) cannot be

preserved completely upon polymerization of the diacetylene units. The TEM image of the red suspension prepared at 5 °C displays a few longer fiber segments (arrows in Figure 3.64) but mainly short segments.

### SANS

SANS measurements were carried out with a pPC-C36diAc-PC suspension after irradiation for 20 minutes at 5 °C to examine the structure of the polymerized aggregates more closely. The scattering data, IFT fits, and pair distance distribution functions (see Chapter 2.2.7) are provided in Figure 3.65.

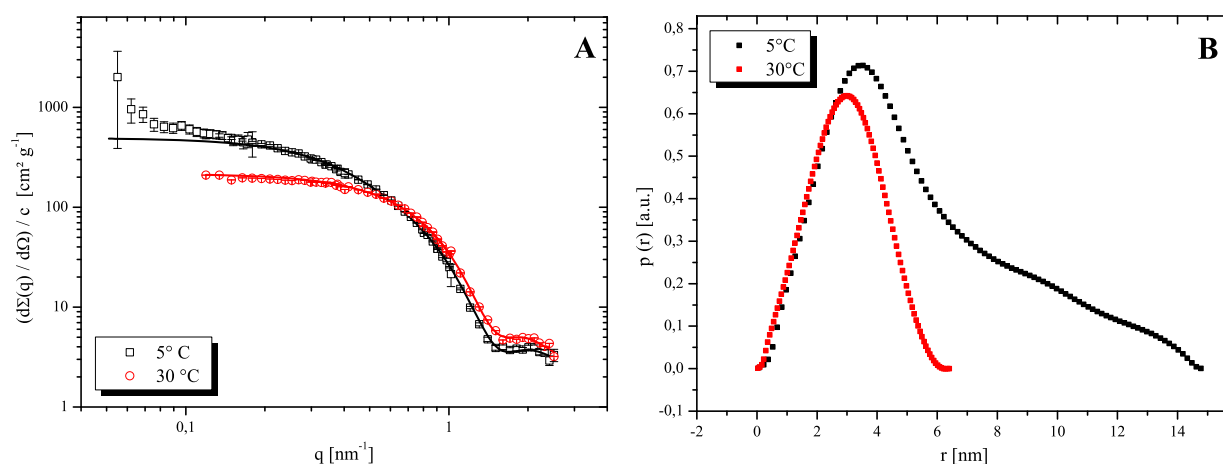


**Figure 3.65:** (A) SANS data with IFT fits and (B) pair distance distribution functions  $p(r)$  of a pPC-C36diAc-PC suspension ( $c = 1 \text{ mg ml}^{-1}$ ) at 5 and 30 °C after polymerization with UV light at 5 °C.

The slope of the scattering data at small and intermediate  $q$  values is smaller than expected for fibrous aggregates. The model of spheres was used for the IFT fits which are in good agreement with the experimental data. The results of the fits are provided in Table 3.7.

Aggregation numbers ( $N_{\text{agg}}$ ) cannot be calculated from the results of the fits as the molecular mass of the polymerized fibers could not be determined.

The analysis of the SANS measurements shows that the fiber structure is not preserved after polymerization of the diacetylene bolaamphiphile fibers supporting the interpretation of the TEM images (Figure 3.64). However, the pair distance distribution function  $p(r)$  at 5 °C shows an asymmetrical distribution indicating the additional presence of larger aggregates than at 30 °C as it can also be deduced from the higher scattering intensity at 5 °C. This was seen in the TEM images of the pPC-C36diAc-PC suspension at 5 °C (Figure 3.64) as well. The radius of the micelles obtained from the IFT fit at 5 °C is larger than the one usually determined for bolaamphiphile micelles.<sup>[27-28]</sup> This indicates that the aggregates are larger after polymerization than regular micelles.

**Table 3.7:** Results of IFT fits of the SANS measurements with pPC-C36diAc-PC suspended in heavy water at 5 and 30 °C.<sup>a</sup>

	T [°C]	aggregate shape	$D_{\text{max}}$ [nm]	$R_g$ [nm]	R [nm]
pPC-C36diAc-PC	5	micelles	15	$4.5 \pm 0.1$	$5.84 \pm 0.1$
	30	micelles	6.5	$2.27 \pm 0.1$	$2.93 \pm 0.1$

<sup>a</sup> $D_{\text{max}}$ : maximal size or cross-section of aggregate,  $R_g$ : radius of gyration, R: radius.

The SANS measurements reveal that most fiber aggregates of PC-C36diAc-PC break-up into very short segments upon polymerization. However, the presence of some longer segments shows that the procedure of polymerizing diacetylene containing bolaamphiphiles can be successful in general, e.g., with molecules containing longer chains or different headgroups like the Me<sub>2</sub>PE headgroup.

As described above, the distance and relative orientation of two adjacent diacetylene groups determine the reactivity of the diacetylene monomer.<sup>[103]</sup> The orientation of the single bolaamphiphile molecules inside the fiber structure apparently hinders the formation of colored polydiacetylene compounds and the absence of blue colored “phases” can be ascribed to this circumstance. However, the formation of red “phases” by the bolaamphiphile suspensions could be observed for the bolalipids with longer spacer chains indicating that the influence of the side chains on the orientation of the polymer backbone is a dominating effect.

Most transitions from the blue to the red phase, described in other systems, e.g., planar orientations of PDAs such as polymerized pentacosanoic acid, are irreversible.<sup>[91, 113]</sup> Functional moieties incorporated into the diacetylene compounds induced

some reversible phase transitions through additional stabilizing groups such as azobenzene units or hydrogen-bonding interactions inside the side chains.<sup>[91, 114-115]</sup>

Although the fiber structure of the single-chain bolaamphiphiles with PC headgroups could not be retained upon polymerization so far, the presented results prove that the formation of thermostable aggregates can be achieved. For this purpose, further changes to the structure of the diacetylene containing bolaamphiphile monomers have to be investigated, such as e.g., longer spacer chains or additional stabilizing moieties.

### 3.4.2.2 Polymerization of Diacetylene-Modified Bolaamphiphiles with Me<sub>2</sub>PE

#### Headgroups

Me<sub>2</sub>PE-C34diAc-Me<sub>2</sub>PE and Me<sub>2</sub>PE-C36diAc-Me<sub>2</sub>PE suspensions in acetate buffer at pH 5 were also irradiated with UV light to check polymerizability of the fibers and coloring of the suspensions.

#### Me<sub>2</sub>PE-C34diAc-Me<sub>2</sub>PE

A suspension of Me<sub>2</sub>PE-C34diAc-Me<sub>2</sub>PE in acetate buffer at pH 5 at the concentration  $c = 1 \text{ mg ml}^{-1}$  was polymerized with UV light at 5 °C. The colorless suspension turned red upon irradiation and yellow after heating of the system to 20 °C. The UV/Vis spectrum of the sample shows an absorption maximum around 500 nm after 40 minutes of irradiation. UV/Vis spectra after shorter polymerization periods exhibit a weaker absorption at 500 nm and a small shoulder at 550 nm (Figure 3.66).

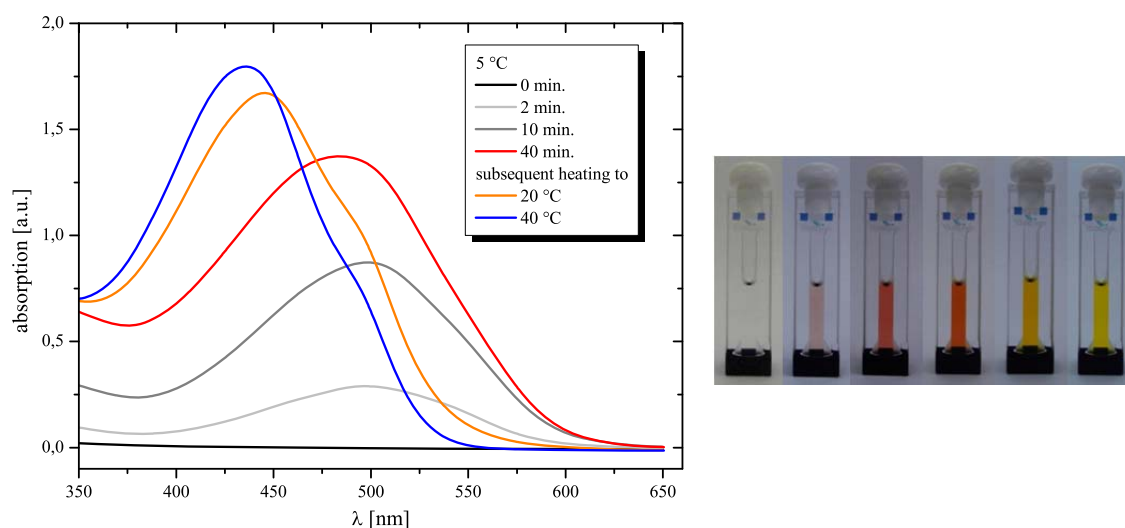


**Figure 3.66:** UV/Vis spectra of a Me<sub>2</sub>PE-C34diAc-Me<sub>2</sub>PE suspension in buffer at pH 5 ( $c = 1 \text{ mg ml}^{-1}$ ) after different irradiation intervals at 5 °C and subsequent heating to 20 and 40 °C and photographs of the suspension after 0, 2, 10, and 40 minutes of irradiation and subsequent heating of the suspension to 20 and 40 °C.

The yellow color of the suspensions after heating of the system to 20 and 40 °C is caused by the shift of the absorption maximum to 445 and 435 nm, respectively. Both spectra still have an additional smaller absorption band at 500 nm showing that the conversion of the “phases” is not complete. However, the transition from the red “phase” to the yellow “phase” is again irreversible.

Attempts to polymerize suspensions of Me<sub>2</sub>PE-C34diAc-Me<sub>2</sub>PE at a temperature above the DSC transition peak only resulted in the formation of yellow suspensions.

### Me<sub>2</sub>PE-C36diAc-Me<sub>2</sub>PE

The longer chain analogue Me<sub>2</sub>PE-C36diAc-Me<sub>2</sub>PE suspended in acetate buffer at pH 5 at the concentration  $c = 1 \text{ mg ml}^{-1}$  develops a wider spectrum of colors upon irradiation at 10 °C below the DSC transition. The UV/Vis absorption spectra first show a very broad absorption maximum from 530 to 580 nm, which results in a purple color of the suspension (Figure 3.67). With continued irradiation of the suspension, the absorption around 530 nm increases and an additional shoulder around 470 nm develops. After 45 minutes of polymerization the absorption is highest around 470 nm but absorption around 530 and 580 nm is still observed leading to a red color of the suspension. If the system is heated to 20 and 50 °C the color changes irreversibly to orange and yellow, respectively.

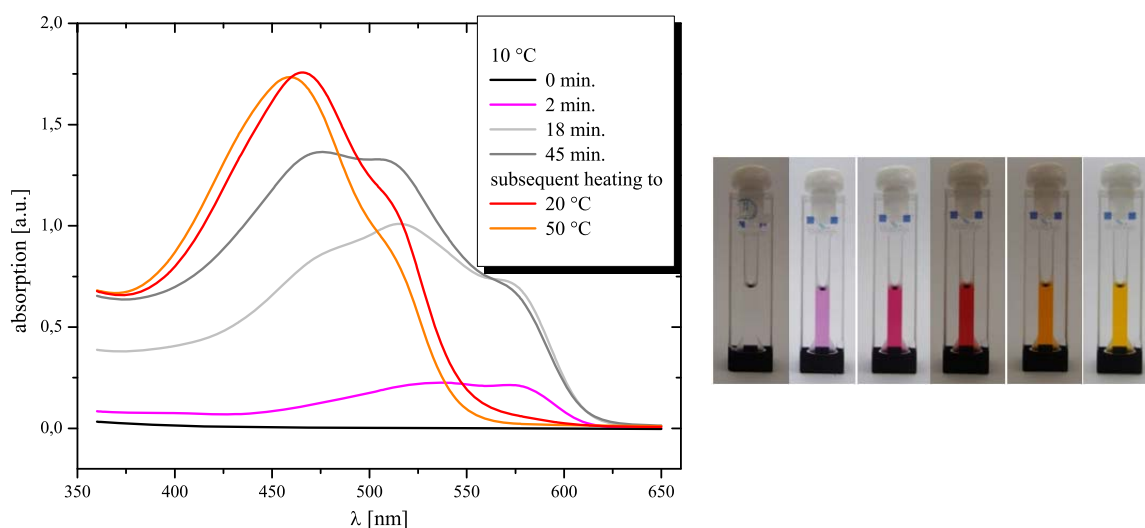


**Figure 3.67:** UV/Vis spectra of a Me<sub>2</sub>PE-C36diAc-Me<sub>2</sub>PE suspension in buffer at pH 5 ( $c = 1 \text{ mg ml}^{-1}$ ) after different irradiation intervals at 10 °C and subsequent heating to 20 and 50 °C and photographs of the suspension after 0, 2, 18, and 45 minutes of irradiation and subsequent heating of the suspension to 20 and 50 °C.

Polymerization of suspensions of Me<sub>2</sub>PE-C36diAc-Me<sub>2</sub>PE at a temperature above the DSC transition peak only resulted in the formation of yellow suspensions.

TEM

A TEM image, taken of the Me<sub>2</sub>PE-C36diAc-Me<sub>2</sub>PE suspension after polymerization at 10 °C for 45 minutes and heating up to 60 °C (see Figure 3.67), is displayed in Figure 3.68. Fiber segments with a diameter of 3 to 4 nm and a length of up to 100 nm are seen in this image. As the preparation temperature at 25 °C is already situated inside the range of the transition peak observed in the DSC scan of a non-irradiated sample (Figure 3.56), fibers are still visible. The TEM image also proves that polymerization does not destroy the fiber structure and that the fibers are stable to some extent at a temperature above the fiber-micelle transition of non-irradiated Me<sub>2</sub>PE-C36diAc-Me<sub>2</sub>PE.

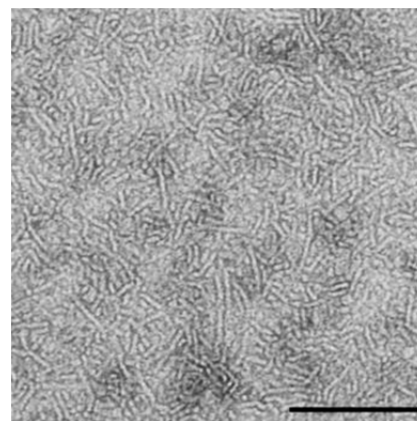


**Figure 3.68:** TEM image of a suspension of pMe<sub>2</sub>PE-C36diAc-Me<sub>2</sub>PE ( $c = 1 \text{ mg ml}^{-1}$ ) at 25 °C after polymerization at 10 °C and heating to 60 °C. The sample was stained with uranyl acetate. The bar corresponds to 100 nm.

SANS

SANS measurements of a suspension of pMe<sub>2</sub>PE-C36diAc-Me<sub>2</sub>PE in acetate buffer at pH 5 were carried out at 5 and 30 °C after irradiating the suspension for 20 minutes at 5 °C. A measurement at higher temperature was impossible due to limitations in measurement time. The scattering data with IFT fits (see Chapter 2.2.7) and the pair distance distribution functions  $p(r)$  are shown in Figure 3.69.

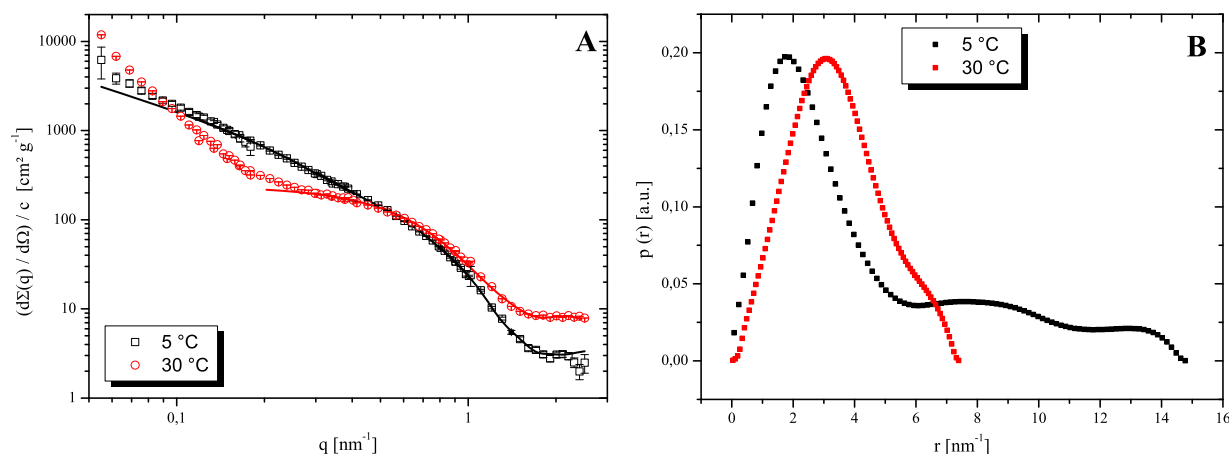


**Figure 3.69:** (A) Scattering data and IFT fits (solid lines) and (B) pair distance distribution functions  $p(r)$  of SANS measurements of a suspension ( $c = 1 \text{ mg ml}^{-1}$ ) of pMe<sub>2</sub>PE-C36diAc-Me<sub>2</sub>PE in acetate buffer at pH 5 after polymerization at 5 °C. IFT fit and pair distance distribution function  $p(r)$  of the measurement at 30 °C refer to the  $q$  region from  $q = 0.2 - 3 \text{ nm}^{-1}$ .

The scattering data of the measurement at 5 °C can be fitted well with the IFT method and the model of an infinitely long cylinder. However, the pair distance distribution function  $p(r)$  shows an asymmetrical profile again indicating a size distribution of the aggregates in suspension. This is the same effect already observed for the suspension of Me<sub>2</sub>PE-C36diAc-Me<sub>2</sub>PE prior to polymerization and can be explained by the formation of bundles of fibers (see Chapter 3.4.1.2). The scattering data of the measurement at 30 °C show two steps that suggest the presence of different aggregate structures in the suspension. At high  $q$  values ( $q = 0.2 - 3 \text{ nm}^{-1}$ ) the data can be fitted with the model of spherical micelles. The pair distance distribution function  $p(r)$  for this  $q$  region is symmetric (Figure 3.69B).

Results for the IFT fits are provided in Table 3.8. As the temperature of the measurement is situated inside the transition peak observed in the DSC scan of the non-irradiated suspension (Figure 3.56), it is reasonable to assume a transition of the fiber aggregates present at low temperature into smaller aggregates at higher temperature.

**Table 3.8:** Results of IFT fits of the SANS measurements with pMe<sub>2</sub>PE-C36diAc-Me<sub>2</sub>PE suspended in acetate buffer at 5 and 30 °C. The values for the measurement at 30 °C refer to the  $q$  region from 0.2 to 3 nm<sup>-1</sup>.<sup>a</sup>

	T [°C]	aggregate shape	D <sub>max</sub> [nm]	R <sub>g</sub> or R <sub>CS,g</sub> [nm]	R [nm]
pMe <sub>2</sub> PE-C36diAc- Me <sub>2</sub> PE	5	fibers	15	4.07 ± 0.05	5.76 ± 0.05
	30	fibers and micelles	7.5	2.65 ± 0.05	3.42 ± 0.05

<sup>a</sup>D<sub>max</sub>: maximal size or cross-section of aggregate, R<sub>g</sub>: radius of gyration, R<sub>CS,g</sub>: radius of gyration of cross-section  
R: radius.

Although the TEM images of the suspension of pMe<sub>2</sub>PE-C36diAc-Me<sub>2</sub>PE did show fibrous aggregates at 25 °C (Figure 3.68), they were shorter than the ones observed for Me<sub>2</sub>PE-C36diAc-Me<sub>2</sub>PE. Therefore, it is possible that the aggregates of the polymerized diacetylene bolaamphiphile are even smaller at higher temperature.

Compared to the results of the polymerization with the bolaamphiphiles with PC headgroups, a tendency for absorption maxima at higher wavelength can be observed for the bolaamphiphiles with Me<sub>2</sub>PE headgroups. This is particularly evident in the suspension of pMe<sub>2</sub>PE-C36diAc-Me<sub>2</sub>PE that exhibits an absorption maximum around 580 nm, which is characteristic for the presence of purple phases.<sup>[103]</sup>

Thermoreversible blue to red transitions and more stable PDAs were designed by incorporating other conjugated moieties into the side chains. This was shown for an azo chromophore-functionalized diacetylene molecule that forms micelles<sup>[115]</sup> and for 10,12-

pentacosadiynoic acid films by adding new functional groups enhancing the hydrogen-bonding interactions between the headgroups.<sup>[114]</sup> This might also be the reason for the absorption at higher wavelength in the case of the diacetylene bolaamphiphiles with Me<sub>2</sub>PE headgroups, as the Me<sub>2</sub>PE headgroup is able to form hydrogen bonds in its zwitterionic form at pH 5 and thus to stabilize the ordered structure of the PDA side chains.

The pH-dependence of the polymerizability and the color of the corresponding “phases” for diacetylene bolalipids were not examined so far. However, as the charge of the Me<sub>2</sub>PE headgroup was proven to influence the aggregation behavior (see Chapter 3.1), an influence of the headgroups protonation state on the polymerizability might be observed as well. pH-dependent coloring of PDA phases has also been described for other systems.<sup>[91, 116]</sup>

A positive effect on the stability and color of PDAs was found for the use of longer alkyl chains due to the high order the alkyl chains can induce.<sup>[117]</sup> This indicates that the use of diacetylene bolaamphiphiles with spacer chains longer than 36 carbon atoms might be an opportunity to improve the polymerizability of the aggregates. Further, as also determined by results of spacer chain length dependent DSC measurements,<sup>[28]</sup> this probably leads to an increased stability of the diacetylene-modified bolalipid fibers and to an improvement in the length of the fibers after polymerization.

### 3.4.3 Conclusions

The self-assembly of diacetylene containing bolaamphiphiles into fibrous aggregates is possible. However, the structural disturbance induced by the different bond angle of the diacetylene unit compared to the all-*trans* alkyl chain causes a pronounced shift of the fibers stability to a temperature below 20 °C. This effect can be counterbalanced by the use of overall longer spacer chains with longer alkyl chain units or by the use of headgroups that add to the stabilization, e.g., via hydrogen bonds. For the bolaamphiphiles with Me<sub>2</sub>PE headgroups, no fiber-fiber transition as for the non-modified analogues was observed.

Polymerization of the aggregates containing diacetylene-modified bolaamphiphiles is possible and can be traced by monitoring the development of colored products. Upon polymerization of bolaamphiphiles with PC headgroups most fibers break-down into micelle-like aggregates and only small numbers of longer segments are detectable. The use of Me<sub>2</sub>PE headgroups improves the polymerizability and the length of the polymerized fibers. TEM images of a pMe<sub>2</sub>PE-C36diAc-Me<sub>2</sub>PE suspension display fibers even after the suspension was heated to 60 °C. This shows that polymerizing the self-assembled fiber structure is a promising way to build thermostable fibers. Further efforts to increase the chain length of the

diacetylene containing bolaamphiphiles have to be made to improve the stability of the fibers during and after polymerization.

The formation of colored “phases” connected with the polymerization of diacetylenes via UV light is also apparent in systems of diacetylene bolaamphiphiles. Although the formation of a blue “phase” could not be reproduced in the case of pPC-C32diAc-PC, the development of yellow and red “phases” is observed for bolaamphiphiles with PC headgroups. Bolaamphiphiles with Me<sub>2</sub>PE headgroups additionally show the development of a purple “phase” with an absorption maximum shifted to higher wavelength. Extended irradiation or increase of the temperature cause an irreversible transition from red or purple “phases” to a yellow “phase”. The formation of yellow “phases” is due to a high degree of disorder in the PDA side chains as the single bolalipids are not as ordered in the nanofibers as PDAs in planar arrangements such as Langmuir-Blodgett films.

### 3.5 Interaction of Bolaamphiphiles with Gold Nanoparticles

The organization of gold nanoparticles (AuNPs) is the focus of many varying works as the specific properties of the AuNPs enable versatile applications in diagnostics, detection or electronics.<sup>[62, 118-120]</sup> AuNPs have been successfully aligned along DNA strands,<sup>[121]</sup> peptides,<sup>[122]</sup> polysaccharides,<sup>[123]</sup> polymers,<sup>[124]</sup> or wormlike micelles.<sup>[125]</sup> A stabilization of AuNPs using bolaamphiphiles has also been reported.<sup>[126]</sup>

The fibers formed by the bolalipid PC-C32-PC in aqueous suspension can also be used as a template for the one-dimensional orientation of AuNPs.<sup>[30]</sup> To improve the fixation of AuNPs achieved for this bolalipid, it is possible to vary the chemical structure of the spacer chain or the headgroup of the molecule to enable stronger interaction with the AuNPs.

For this purpose the alkyl spacer chain was modified to include sulfur atoms. The interaction between gold and sulfur is known to be very strong<sup>[62]</sup> and might be utilized to enhance the interaction between the bolaamphiphile fibers and the AuNPs as it was done for several other systems such as phosphocholine stabilized AuNPs,<sup>[127]</sup> or polymer stabilized AuNPs.<sup>[128]</sup>

Another approach is the adjustment of the hydrophilic bolaamphiphile headgroup. The use of bolaamphiphiles with lipoic acid included in the headgroup resulted in an improved fixation of AuNPs along the bolaamphiphile fibers.<sup>[30]</sup> The silicification of nanofibers formed by PC-C32-PC using thiol-modified tetraethyl orthosilicate (TEOS) also enabled the interaction with AuNPs. In this way, fixation of AuNPs along the fiber structure could be improved (unpublished results).

#### 3.5.1 Interaction of PC-C32SS-PC and Me<sub>2</sub>PE-C32SS-Me<sub>2</sub>PE Fibers with Gold Nanoparticles

The approach described here was to incorporate two thioether groups into the spacer chain of the bolalipids to increase the interaction between the hydrophobic chains and the hydrophobic AuNP surface.

#### TEM

To examine the interaction of the fibers of PC-C32SS-PC and Me<sub>2</sub>PE-C32SS-Me<sub>2</sub>PE with AuNPs (citrate stabilized AuNP, d = 5 nm) TEM images were taken at two different mixing ratios of bolalipid to AuNP (Figure 3.70).

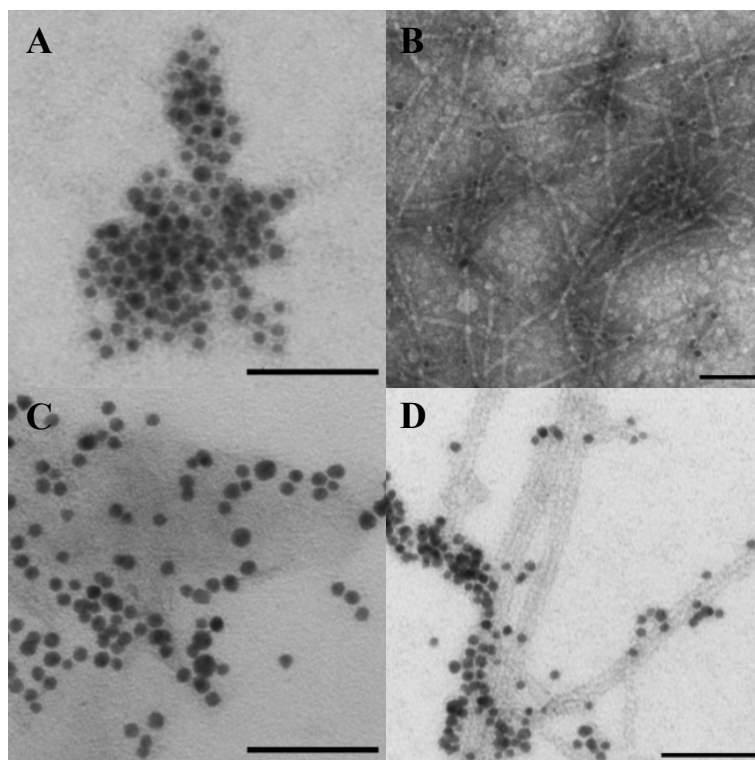


**Figure 3.70:** TEM images of (A, B) PC-C32SS-PC and (C, D) Me<sub>2</sub>PE-C32SS-Me<sub>2</sub>PE suspensions with AuNP ( $d = 5$  nm) at 5 °C in water and acetate buffer at pH 5, respectively. Mixing ratios are bolalipid : AuNP (A, C): 100:1 and (B, D): 1000:1. The samples were stained with uranyl acetate. The bar corresponds to 50 nm.

The images of PC-C32SS-PC show AuNPs surrounded by a layer of the bolalipid and accumulated into undefined aggregates at the ratio bolalipid to AuNP = 100:1 (Figure 3.70A). The fiber structure that is known to be formed by suspended PC-C32SS-PC at 5 °C is destroyed in the presence of the AuNPs. When the amount of AuNPs in the mixture is decreased (bolalipid to AuNP = 1000:1) fibers and fiber segments are visible in the TEM images. Single AuNPs are visible as well, but no direct contact or orientation of the AuNPs along these fibers is observable (Figure 3.70B). This is different in the case of the bolalipid with Me<sub>2</sub>PE headgroups (Figure 3.70D). At a mixing ratio 1000:1 single NPs are attached to the fibers or are clustered around them. However, at the lower ratio 100:1 the formation of fibers seems to be perturbed by the AuNPs again and an undefined aggregation of the bolalipid is observed (Figure 3.70C). The structure displayed at the ratio 100:1 might be composed of fiber segments oriented closely to each other which cannot be distinguished due to the low contrast and resolution of the image.

### ITC

A suitable method to determine the magnitude of the interaction between bolalipids in suspension and AuNPs is ITC.<sup>[129-130]</sup> The experiment can be performed in two ways with

either the NPs being titrated into a bolalipid suspension or vice versa. The concentration of the NP solution could not be changed, hence, the second method was chosen yielding molar ratios in the order of magnitude of the mixtures also used for the TEM images.

The interaction between PC-C32SS-PC micelles and AuNPs was investigated at 25 °C. The titration experiment is displayed in Figure 3.71.

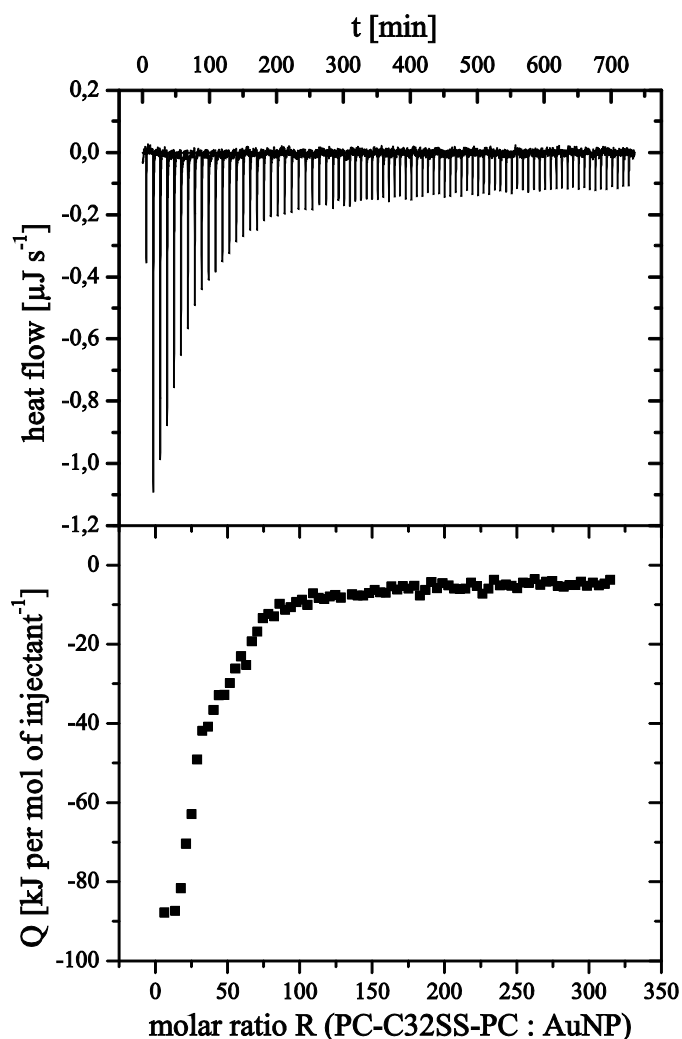


**Figure 3.71:** ITC binding experiment: titration of an aqueous PC-C32SS-PC suspension ( $c = 0.3 \text{ mM}$ ) into the AuNP solution ( $c = 8.3 \cdot 10^{-5} \text{ mM}$ ) with  $80 \times 1.5 \mu\text{l}$  at 25 °C. The heat of bolalipid dilution has been subtracted.

into fibers was examined and in the case of the PC-C32SS-PC suspension the interaction of AuNPs with micelles is determined. The binding heat  $Q$  for the binding of AuNPs to PC-C32SS-PC micelles is not only significantly higher, it also shows a steeper decrease with increasing amount of added injectant.

In the case of binding of AuNPs to PC-C32-PC fibers, the binding heat was attributed to hydrophobic interaction between the surface of the AuNPs and the hydrophobic part of the

From the course of the data in the upper part of Figure 3.71 it is evident that each injection causes an exothermic heat flow that decreases with increasing molar ratio. The corresponding binding heat  $Q$  is depicted in the lower part of Figure 3.71 as a function of the molar ratio. It shows a steep decrease and levels off at high molar ratios  $R$ .

Measurements with a PC-C32-PC suspension at 25 °C yielded a binding heat of PC-C32-PC to AuNPs of  $-15 \text{ kJ mol}^{-1}$ .<sup>[30]</sup> However, an important difference between this experiment and the ITC experiment with the PC-C32SS-PC suspension at 25 °C is the aggregation state of the bolalipids. In the case of the PC-C32-PC suspension the interaction of AuNPs with bolalipids aggregated

bolaamphiphiles exposed at the fiber surface.<sup>[30]</sup> The significantly higher binding heat for the binding of AuNPs to PC-C32SS-PC micelles is probably not caused by hydrophobic interactions but rather by interaction of the thioether groups with the AuNPs. The steep change of the reaction heat also indicates a stronger binding than for the binding of AuNPs to PC-C32-PC fibers.<sup>[30]</sup>

There are no calorimetric reference data available for the interaction between AuNPs and thioether groups but the free enthalpy of adsorption for a thiol-modified DNA group on gold surfaces has been found to be approximately  $-32 \text{ kJ mol}^{-1}$ .<sup>[131]</sup> The free energy of adsorption of dialkyl disulfides on gold surfaces was calculated to be approx.  $-100 \text{ kJ mol}^{-1}$ , or  $-50 \text{ kJ mol}^{-1}$  per  $\text{RS}^-$  group.<sup>[132]</sup>

The enthalpy of approximately  $-90 \text{ kJ mol}^{-1}$  determined in the ITC experiments for the binding of AuNPs to PC-C32SS-PC micelles still contains the contribution of the entropy and has higher negative values than the free enthalpy of this binding process would have. It is approximately twice as high as the above values of the free enthalpy of the binding of different sulfur moieties to gold. This indicates that probably two thioether groups interact with the AuNPs, although the different sulfur groups and their binding properties are not identical. Thiols bind to gold via the formation of thiolates whereas the bond of thioethers to gold is more coordinative.<sup>[133]</sup> Disulfide bonds can be cleaved to form two thiolate groups.<sup>[132]</sup> This makes a direct comparison difficult.

Although the binding heat of AuNPs to PC-C32SS-PC at a temperature inside the stability range of the fibers is not known, it can be assumed that the interaction between AuNPs and the thioether groups is still very strong. The interaction between the sulfur parts of the chain and the AuNPs is stronger than the hydrophobic interaction leading to aggregation into the fiber structure. Therefore the fibers break down and the AuNPs are surrounded by a layer of bolalipid as seen in the TEM images of these samples (Figure 3.70). At higher molar ratios the fiber structure remains intact and no significant interaction between fibers and AuNPs can be monitored as the AuNPs surface is already saturated with bolalipid and the excess molecules self-assemble into fibers.

### UV/Vis

Another way of detecting whether a fixation of AuNPs occurs in the presence of bolalipids is UV/Vis spectroscopy. UV/Vis spectra of PC-C32SS-PC and  $\text{Me}_2\text{PE-C32SS-Me}_2\text{PE}$  suspensions in mixtures with AuNPs at a temperature below the fiber-micelle transition are

shown, along with the spectra of the pure AuNP solution, in Figure 3.72. The maxima of the surface plasmon bands (see Chapter 2.2.5) of the pure AuNP solution are at 515 and 514 nm, respectively, corresponding to the AuNP concentration in the suspensions with the mixing ratios bolalipid to AuNP = 1000:1 and 100:1. The peaks of the spectra measured for the mixtures each exhibit a shift of 3 nm to 518 and 517 nm, respectively. A general difference between the spectra of the bolalipids or the concentrations in the mixtures cannot be discerned.

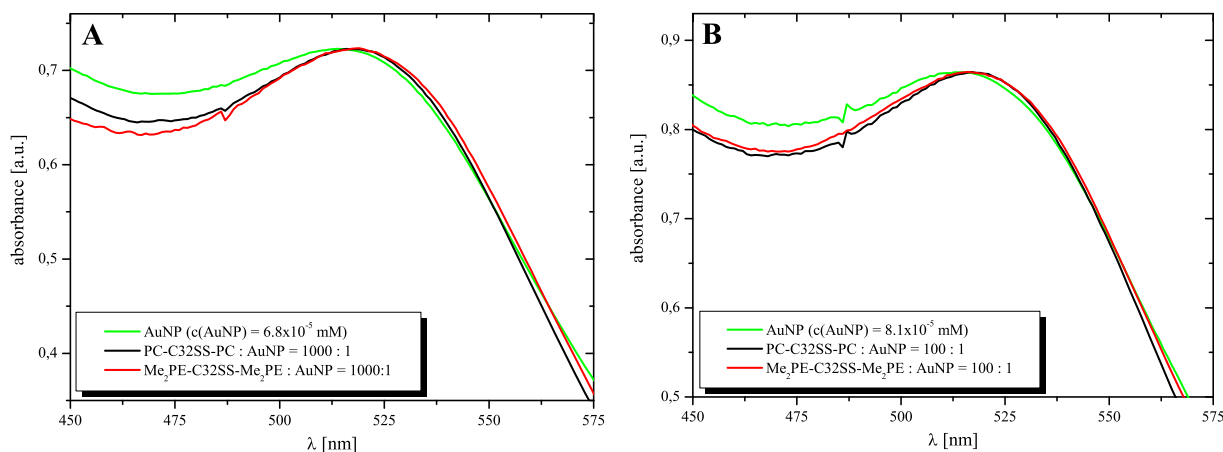


**Figure 3.72:** UV/Vis absorption spectra of PC-C32SS-PC and Me<sub>2</sub>PE-C32SS-Me<sub>2</sub>PE (acetate buffer at pH 5) suspensions with AuNPs (*d* = 5 nm) at 5 °C (PC headgroup) and 15 °C (Me<sub>2</sub>PE headgroup). Mixing ratios (A): 1000:1 and (B): 100:1. The pure AuNP solution at the same concentration is presented for comparison. AuNP spectra show no dependence on temperature.

The observed shift is probably not an effect of plasmon resonance but more likely due to an interaction of the bolalipids with the AuNPs as the shift is very small.<sup>[45, 128]</sup> This is also supported by the TEM images that show no close organization or even aggregation of the AuNPs. The size of the shift has the same magnitude found for AuNPs in mixtures with PC-C32-PC suspensions at 25 °C. However, the organization of the AuNPs along the PC-C32-PC fibers was significantly better.<sup>[30]</sup> The interaction between the sulfur atoms inside the bolaamphiphile chains and the AuNPs is too strong to enable a fixation alongside the fibers but leads to the break-up of the fiber structure if the amount of AuNPs present is too high as seen in the TEM images of these mixtures (Figure 3.70).

### Mixtures

Suspensions of mixtures of the bolalipids PC-C32-PC and Me<sub>2</sub>PE-C32-Me<sub>2</sub>PE with their corresponding sulfur analogues were also tested for their interaction with AuNPs. As the interaction between the sulfur atoms and the AuNPs turned out to be stronger than the hydrophobic interaction between the molecules preventing the orientation along the fibers, the

mixing with the bolalipids without sulfur might cause an improvement through dilution of the sulfur containing molecules inside the fibers. TEM images of some of the mixtures with the mixing ratios 1000:1 and 100:1 are shown in Figure 3.73.

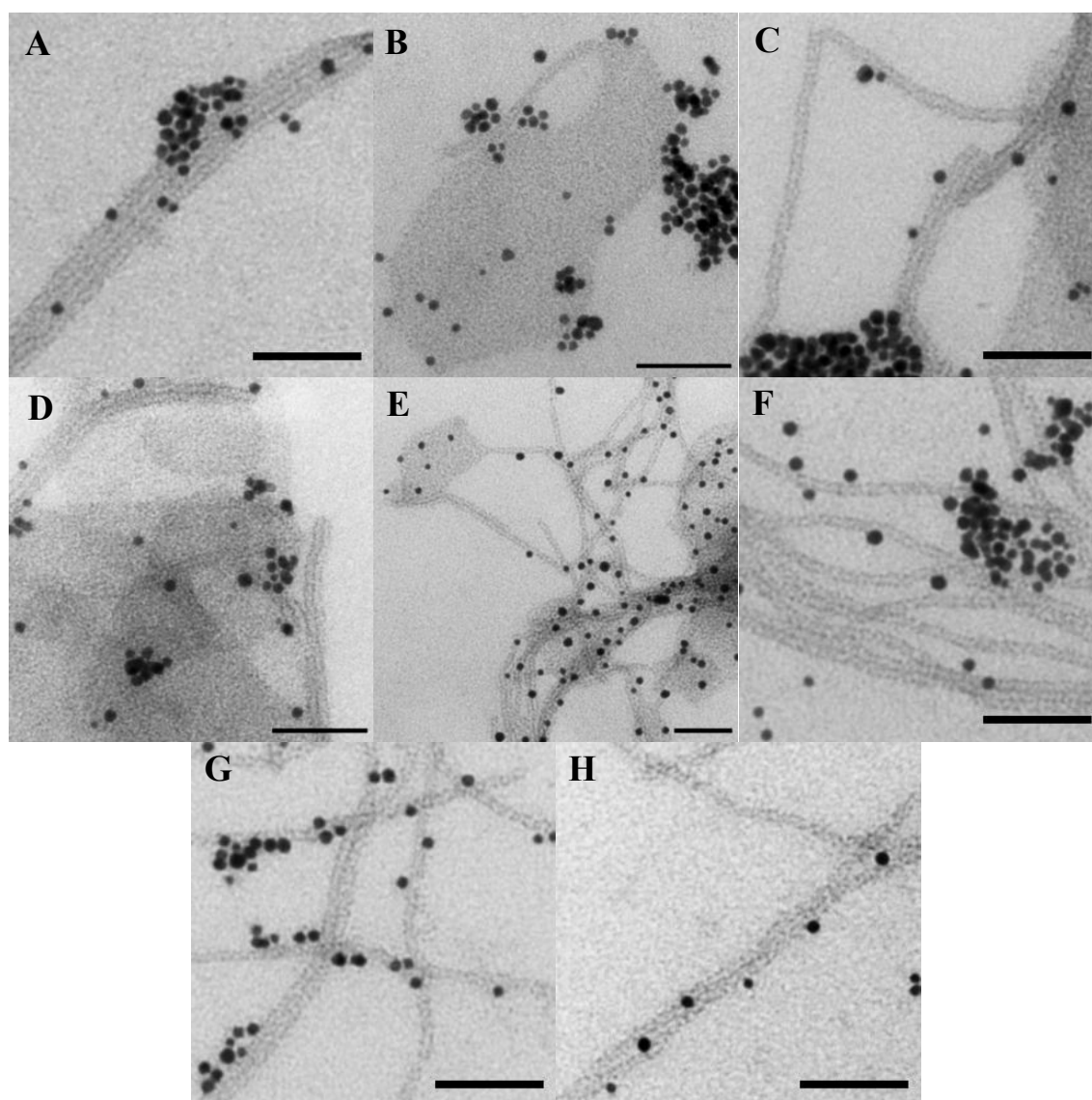


**Figure 3.73:** TEM images of mixtures of PC-C32SS-PC and PC-C32-PC with AuNP ( $d = 5$  nm) (**A-E**) and of mixtures of Me<sub>2</sub>PE-C32SS-Me<sub>2</sub>PE and Me<sub>2</sub>PE-C32-Me<sub>2</sub>PE (**F-H**) at 5 °C. The samples were stained with uranyl acetate. The bar corresponds to 50 nm.  $x$  is the molar ratio of PC-C32-PC or Me<sub>2</sub>PE-C32-Me<sub>2</sub>PE and the mixing ratio is bolalipid : AuNP. (**A,B**):  $x = 0.68$ , 100:1. (**C,D**):  $x = 0.68$ , 1000:1. (**E**):  $x = 0.51$ , 1000:1. (**F**):  $x = 0.65$ , 100:1. (**G**):  $x = 0.65$ , 1000:1. (**H**):  $x = 0.52$ , 100:1

The images of the mixtures with PC headgroups (Figure 3.73A-E) show that there is no increase in the fixation of AuNPs depending on different bolalipid composition or mixing ratio. In all cases, there seem to be lamellar aggregates present, which is very uncommon for these bolalipids. The aggregates might consist of short fiber segments oriented parallel to each other with very small distances making any distinction impossible at this resolution.

The images in Figure 3.73F-H do not show any lamellar aggregates for the mixtures with Me<sub>2</sub>PE headgroups. However, orientation of the AuNPs along the fibers cannot be observed either. Some AuNPs are attached to the fibers but the distances are quite large and irregular.

The use of mixtures of bolaamphiphiles with and without sulfur containing chains leads to no improvement in the organization and fixation of AuNPs in comparison to the unmixed sulfur containing bolalipids or the non-modified bolalipids with pure alkyl chains.

The variation of the headgroups as described with lipoic acid,<sup>[30]</sup> via silicification of the fiber structure (unpublished results) or with asymmetrical headgroups (see chapter 3.5.2) seems to be a more suitable way of improving the fixation of AuNPs.

### 3.5.2 Interaction of DMAPPC-C32-POH Fibers with Gold Nanoparticles

Since the asymmetrical bolalipid DMAPPC-C32-POH was shown to self-assemble in aqueous suspension into fibers as well, the change in the headgroup structure compared to PC-C32-PC fibers might influence the fixation of the AuNPs along the aggregates. In acetate buffer at pH 5, aggregation of the AuNPs was observed (see Chapter 3.5.1). Therefore, a suspension of DMAPPC-C32-POH in water was used for this purpose because of the sensitivity of the NPs to pH value and salts in the suspension.<sup>[62]</sup>

#### TEM

TEM images of DMAPPC-C32-POH suspensions with two different mixing ratios of bolalipid to AuNPs (100:1 and 1000:1) are shown in Figure 3.74.

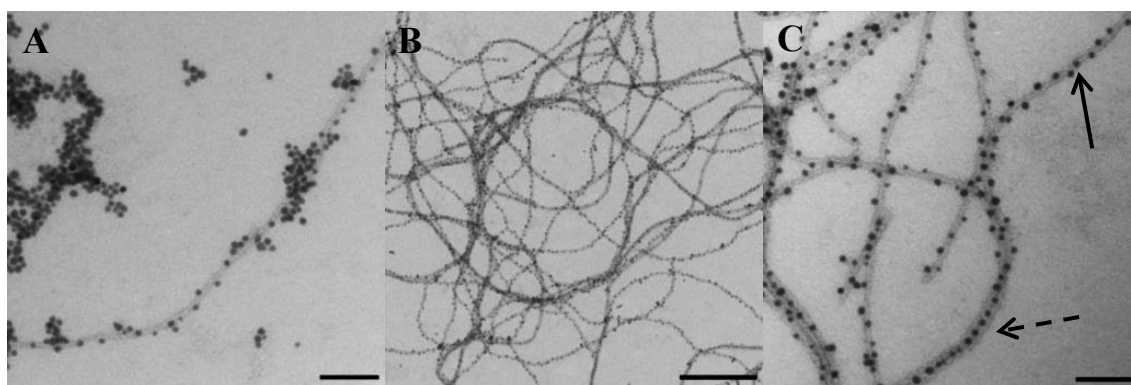


**Figure 3.74:** TEM images of a suspension of DMAPPC-C32-POH mixed with AuNPs ( $d = 5$  nm) in water at 25 °C. The samples were stained with uranyl acetate. The bar corresponds to (A,C): 50 nm and to (B): 250 nm. The mixing ratio bolalipid : AuNP is (A): 100:1 and (B,C): 1000:1.

At the mixing ratio bolalipid to AuNP 100:1 fibers can be observed with attached AuNPs. However, large clusters of aggregated AuNPs are also present. This suggests that the total amount of AuNPs is higher than the amount that can be fixated at the bolalipid fibers

(Figure 3.74A). At a ratio of bolalipid to AuNP of 1000:1, the AuNPs are oriented along the fibers very regularly (Figure 3.74B,C). In some parts, the AuNPs seem to follow the helical structure of the single bolaamphiphile fiber strands (solid arrow). In other parts, two fiber strands are oriented parallel to each other with AuNPs in between them (dashed arrow). Through this arrangement the AuNPs can interact with more DMAPPC-C32-POH fibers.<sup>[30]</sup>

Compared to the orientation of AuNPs along fibers of PC-C32-PC,<sup>[30]</sup> the images of the suspension with the mixing ratio DMAPPC-C32-POH to AuNP 1000:1 show an improved binding of AuNPs. Experiments with another headgroup modified bolaamphiphile that contains lipoic acid yielded similar amounts of fixated AuNPs.<sup>[30]</sup>

### UV-Vis

An additional method to study the binding of the AuNPs along the fibers is UV/Vis spectroscopy and the SPB of the AuNPs. The UV/Vis spectra of a mixture of DMAPPC-C32-POH, suspended in water, with AuNPs and the spectrum of the pure AuNPs at the same concentration are shown in Figure 3.75.

The maximum of the SPB is shifted from 518 nm for the pure AuNP solution to 525 nm in the mixture with DMAPPC-C32-POH. This increase is twice as high as the one observed for PC-C32-PC<sup>[30]</sup> or PC-C32SS-PC (see Chapter 3.5.1). The shift is probably caused by a change in the dielectric constant at the AuNP surface. The AuNPs seen in the TEM images of this mixture are too far apart from each other to exhibit coupling effects that would result in a large red shift of the peak maximum.<sup>[44]</sup>

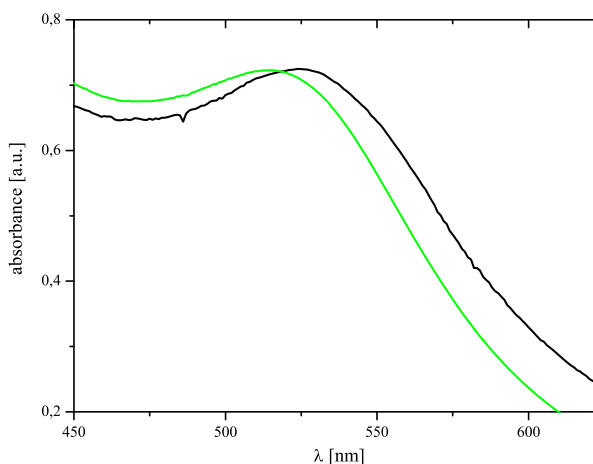


**Figure 3.75:** UV/Vis spectra of a mixture of DMAPPC-C32-POH with AuNPs (1000:1) (black) and of the pure AuNP solution at the corresponding concentration (green) at 25 °C. The AuNP concentration is  $c = 6.8 \cdot 10^{-5}$  mM.

The dominating interaction between AuNPs and the DMAPPC-C32-POH fibers is probably taking place at the POH headgroup. The citrate ligands are exchanged for the phosphate and the hydroxyl group of the POH headgroup. The observed shift of the SPB is probably generated by this strong interaction, which is stronger than in the case of

zwitterionic PC headgroups, which cannot replace citrate as ligand and where hydrophobic interaction between the alkyl chains of the bolalipids and the AuNPs surface determine the binding.

These results suggest that the interaction of the fibers with the AuNPs can not only take place via the hydrophobic chains but via the hydrophilic headgroups, too. This is also supported by experiments with a bolalipid that contains sulfur in the form of lipoic acid in the headgroup. The uniform organization of AuNPs could in this case be improved along with the amount of fixated AuNPs compared to experiments with non-modified PC-C32-PC fibers.<sup>[30]</sup> An additional indication is given by experiments with silicified nanofibers exhibiting a hydrophilic surface with hydroxyl groups or thiol groups (unpublished results). In these cases, TEM images also show an improved fixation and organization of AuNPs.

The interaction between the hydrophilic surface of ligand stabilized AuNPs and hydrophilic substrates has been described in other systems as well, e.g., as electrostatic interaction between positively charged didodecyldimethylammonium bromide (DDAB) stabilized AuNPs and negatively charged polymers<sup>[134]</sup> or as interaction via hydrogen bonds between mercaptoundecanoic acid stabilized AuNPs and poly(ethylene oxide).<sup>[135]</sup>

### 3.5.3 Conclusions

The interaction of the sulfur containing bolalipids PC-C32SS-PC and Me<sub>2</sub>PE-C32SS-Me<sub>2</sub>PE with AuNPs shows no improvement of the fixation of AuNPs compared to the results for PC-C32-PC.<sup>[30]</sup> On the contrary, TEM images and ITC measurements reveal that the fiber structure breaks down due to the strong interaction between the thioether groups and the AuNPs. Experiments with mixtures of bolaamphiphiles with and without sulfur in the spacer chain do not yield better results.

Orientation of AuNPs along the fibers of DMAPPC-C32-POH suspended in water shows an improvement compared to the orientation along fibers of PC-C32-PC. This is due to the interaction between the AuNPs and the hydroxyl group at the end of the POH headgroup.

This leads to the conclusion that the interaction of the bolaamphiphile fibers with AuNPs can also take place via hydrophilic interaction at the headgroups and not just via hydrophobic interaction between the AuNP surface and the alkyl spacer chain parts exposed at the fiber surface.

The best way to improve alignment of AuNPs is therefore the variation of the bolaamphiphile headgroup.

## 4 Conclusions

The aim of this work was to investigate how the aggregation behavior of symmetrical single-chain bolaamphiphiles such as PC-C32-PC and Me<sub>2</sub>PE-C32-Me<sub>2</sub>PE can be influenced and varied via slight changes of the chemical structure in the polar headgroup region or the alkyl chain or by changes of the aqueous medium by addition of salts. Additionally, possibilities to obtain functionality of the resulting aggregates for applications such as the alignment of bound gold nanoparticles or the formation of thermostable fibers were investigated.

### *1. Influence of pH value and salinity*

The headgroups of the bolaamphiphile **Me<sub>2</sub>PE-C32-Me<sub>2</sub>PE** are deprotonated at pH values above pH 10. Regardless of the negative charge positioned at the headgroups in this case, these molecules self-assemble into fibers in aqueous suspension. However, the stability range of the fibers is restricted to lower temperature. By addition of inorganic salts, it is possible to shield the electrostatic repulsion between the headgroups and induce an increased temperature stability of the nanofibers. Mono- and divalent salts were used at different concentrations. The strongest stabilizing effect was observed for calcium ions.

While a suspension of zwitterionic Me<sub>2</sub>PE-C32-Me<sub>2</sub>PE in acetate buffer at pH 5 exhibits the behavior of a viscoelastic gel, the suspension behaves like a viscous fluid at pH 11. The viscoelasticity can be regained through the addition of salts to the suspension at pH 11.

Rheological measurements reveal the absence of Maxwell-behavior, i.e., a finite relaxation time at low angular frequencies, in suspensions of Me<sub>2</sub>PE-C32-Me<sub>2</sub>PE at pH 5 and at pH 11 in the presence of salt. This is in contrast to the observation of Maxwell-behavior in most wormlike micellar systems.

### *2. Influence of two different headgroups*

The asymmetrical bolaamphiphile **DMAPPC-C32-POH** self-assembles into nanofibers in suspensions in water and also in acetate buffer at pH 5. The temperature dependence of the aggregates formed in these suspensions shows similarities to the suspensions of Me<sub>2</sub>PE-C32-Me<sub>2</sub>PE in acetate buffer at pH 5. The asymmetry does not induce the formation of new aggregate structures such as nanotubes or membranes but in buffer at pH 5 the fibers display a tendency to break more easily and to form irregular, circular structures.

This is also reflected by the rheological properties of the suspension that reveal decreased strain resistance at pH 5. This effect is not observed for the suspension in pure water. As the

protonation state of the DMAPPC headgroup is the same in both cases, the reason for the different behavior of the buffered suspension is the presence of buffer salts, which are able to interact with the charged headgroups.

In suspension, the asymmetrical bolaamphiphile **DMAPPC-C32-OH** self-assembles into a mixture of different aggregates without the formation of long fibers.

### *3. Influence of thioether groups in the spacer chain*

The thioether containing bolaamphiphiles **PC-C32SS-PC** and **Me<sub>2</sub>PE-C32SS-Me<sub>2</sub>PE** self-assemble into nanofibers as well. The fibers are less stable at higher temperature than those formed by the analogues with pure alkyl chains. In the case of **Me<sub>2</sub>PE-C32SS-Me<sub>2</sub>PE**, no fiber-fiber transition is observed.

The viscoelasticity of the **PC-C32SS-PC** suspension is significantly decreased compared to the gels formed by **PC-C32-PC**. In the case of **Me<sub>2</sub>PE-C32SS-Me<sub>2</sub>PE** this effect is less pronounced, which is due to the possibility of forming stabilizing hydrogen bonds between the headgroups.

The formation of fibers is observed for mixtures of the bolaamphiphiles with and without sulfur in the spacer chain as well. These mixtures show non-ideal miscibility of the components in schematic “phase diagrams” determined by DSC measurements.

### *4. Influence of diacetylene groups in the spacer chain*

The diacetylene containing bolaamphiphiles **PC-C34diAc-PC**, **PC-C36diAc-PC**, **Me<sub>2</sub>PE-C34diAc-Me<sub>2</sub>PE**, and **Me<sub>2</sub>PE-C36diAc-Me<sub>2</sub>PE** form fibers at low temperature. The temperature at which these fibers transform into micelles increases with increasing chain length.

Polymerization of the nanofibers can be achieved by using UV irradiation. Fibers of the bolaamphiphiles with PC headgroups are destroyed upon polymerization. Only a few longer segments of the fibers can be detected. In contrast, the fibers formed by the bolaamphiphiles with Me<sub>2</sub>PE headgroups are still stable after polymerization. This shows that the formation of thermostable fibers out of covalently linked bolaamphiphiles is possible and can be further improved by the use of longer spacer chains. The polymerization process can be monitored via the formation of colored polydiacetylene “phases”. The formation of a blue “phase”, described previously for **PC-C32diAc-PC**, could not be observed again. Nevertheless, polymerization of the suspensions below the transition temperature yielded red and purple

“phases” that irreversibly turned yellow upon extended irradiation or increase of the temperature.

#### 5. Interaction with Gold Nanoparticles

Orientation of AuNPs along the fibers of the bolaamphiphiles **PC-C32SS-PC** and **Me<sub>2</sub>PE-C32SS-Me<sub>2</sub>PE** with sulfur containing chains is impossible due to the strong interaction between the thioether groups and the AuNPs. The use of a mixture of bolalipids with and without sulfur containing spacer chains does not improve the fixation of AuNPs, either.

The fixation of AuNPs along the fibers of the asymmetric **DMAPPC-C32-POH** yields a very regular organization. This is caused by the strong interaction between the AuNPs and the POH headgroup.

This leads to the conclusion that the variation of the headgroup structure is the most suitable way to increase and control the fixation of AuNPs.

#### Concluding Remarks and Final Statements

The self-assembly of single-chain bolaamphiphiles into nanofibers is influenced by changes of the chemical structure that disturb the aggregation process such as different headgroups or disturbed bond angles inside the spacer chain compared to the non-modified bolaamphiphile PC-C32-PC. However, the influence of these changes is, in most cases, too small to inhibit the formation of nanofibers completely.

On the one hand, repulsive electrostatic interactions between the headgroups destabilize the fiber structure. On the other hand, charged or polarized headgroups can be utilized to stabilize the aggregates via attractive interactions such as hydrogen bonds or electrostatic interactions between adjacent headgroups. In this case, the attractive interaction between the headgroups increases the driving force, i.e., the hydrophobic interaction between the alkyl spacer chains, that leads to the self-assembly of the bolaamphiphiles into fibers.

Perturbation of the chain structure, conformation, and regular bond angle of the alkyl chain also cause destabilization of the fiber structure. Additionally, the use of heteroatoms inside the spacer chain causes changes of the polarity of the molecules. This destabilizing effect can be counterbalanced by the use of bolaamphiphiles with headgroups that add to the stability of the fibrous aggregates via attractive interactions between adjacent molecules. Another approach is the elongation of the spacer chain by addition of methylene units. This way, the hydrophobic interaction between the chains increases and compensates the

perturbation caused by heteroatoms or triple bonds. The formation of thermostable nanofibers could succeed utilizing this strategy by using spacer chains longer than 36 carbon atoms. This might then enable the development of viscoelastic bolaamphiphile gels that are independent of temperature.

Functionality of the bolaamphiphile nanofibers for the one-dimensional orientation of AuNPs can be gained via tailoring the properties of the headgroups for improving the interaction between headgroups and nanoparticles. This way, denser and more regular fixation of nanoparticles can be achieved allowing the formation of nanowires. A specific modification of the headgroups would also enable interaction with different nanoparticles, such as, e.g., CdSe NPs. One promising approach is the application of “click-chemistry” with alkyne functionalized bolaamphiphiles and azide containing stabilizing ligands for CdSe nanoparticles.

The results of the presented investigations enable and support the future exploration of these possibilities.

## 5 References

- [1] J.-H. Fuhrhop, T. Wang, *Chem. Rev.* **2004**, *104*, 2901-2937.
- [2] L. A. Estroff, A. D. Hamilton, *Chem. Rev.* **2004**, *104*, 1201-1218.
- [3] T. Benvegnu, M. Brard, D. Plusquellec, *Curr. Opin. Colloid Interface Sci.* **2004**, *8*, 469-479.
- [4] Y. Yan, T. Lu, J. Huang, *J. Colloid Interface Sci.* **2009**, *337*, 1-10.
- [5] D. L. Valentine, *Nat. Rev. Microbiol.* **2007**, *5*, 316-323.
- [6] J. L. Gabriel, P. Lee Gau Chong, *Chem. Phys. Lipids* **2000**, *105*, 193-200.
- [7] A. Gliozzi, A. Relini, P. L.-G. Chong, *J. Membr. Sci.* **2002**, *206*, 131-147.
- [8] P. L.-G. Chong, *Chem. Phys. Lipids* **2010**, *163*, 253-265.
- [9] G. Sprott, *J. Bioenerg. Biomembr.* **1992**, *24*, 555-566.
- [10] J. Israelachvili, *Intermolecular and Surface Forces*, 2. ed., Academic Press Limited, London, **1994**.
- [11] E. Soussan, A. Pasc-Banu, S. Consola, T. Labrot, E. Perez, M. Blanzat, R. Oda, C. Vidal, I. Rico-Lattes, *ChemPhysChem* **2005**, *6*, 2492-2494.
- [12] B. Vaidya, A. K. Goyal, K. Khatri, N. Mishra, R. Paliwal, S. Rai, S. Tiwari, S. P. Vyas, *Int. J. Biomed. Nanosci. Nanotechnol.* **2010**, *1*, 95-108.
- [13] T. Shimizu, *Bull. Chem. Soc. Jpn.* **2008**, *81*, 1554-1566.
- [14] T. Shimizu, *J. Polym. Sci., Part A: Polym. Chem.* **2006**, *44*, 5137-5152.
- [15] M. Masuda, T. Shimizu, *Langmuir* **2004**, *20*, 5969-5977.
- [16] D. T. Bong, T. D. Clark, J. R. Granja, M. R. Ghadiri, *Angew. Chem. Int. Ed.* **2001**, *40*, 988-1011.
- [17] P. Terech, R. G. Weiss, *Chem. Rev.* **1997**, *97*, 3133-3160.
- [18] S. R. Raghavan, *Langmuir* **2009**, *25*, 8382-8385.
- [19] R. Winter, F. Noll, *Methoden der Biophysikalischen Chemie*, 1. ed., Teubner Verlag, Stuttgart, **1998**.
- [20] I. Nakazawa, M. Masuda, Y. Okada, T. Hanada, K. Yase, M. Asai, T. Shimizu, *Langmuir* **1999**, *15*, 4757-4764.
- [21] R. Iwaura, K. Yoshida, M. Masuda, K. Yase, T. Shimizu, *Chem. Mater.* **2002**, *14*, 3047-3053.
- [22] J. Schneider, C. Messerschmidt, A. Schulz, M. Gnade, B. Schade, P. Luger, P. Bombicz, V. Hubert, J.-H. Fuhrhop, *Langmuir* **2000**, *16*, 8575-8584.
- [23] S. Franceschi, V. N. de, M. Riviere, A. Lattes, *New J. Chem.* **1999**, *23*, 447-452.
- [24] K. Koehler, G. Foerster, A. Hauser, B. Dobner, U. F. Heiser, F. Ziethe, W. Richter, F. Steiniger, M. Drechsler, H. Stettin, A. Blume, *Angew. Chem. Int. Ed.* **2003**, *43*, 245-247.
- [25] K. Koehler, G. Foerster, A. Hauser, B. Dobner, U. F. Heiser, F. Ziethe, W. Richter, F. Steiniger, M. Drechsler, H. Stettin, A. Blume, *J. Am. Chem. Soc.* **2004**, *126*, 16804-16813.
- [26] K. Koehler, A. Meister, G. Foerster, B. Dobner, S. Drescher, F. Ziethe, W. Richter, F. Steiniger, M. Drechsler, G. Hause, A. Blume, *Soft Matter* **2006**, *2*, 77-86.
- [27] A. Meister, M. Bastrop, S. Koschoreck, V. M. Garamus, T. Sinemus, G. Hempel, S. Drescher, B. Dobner, W. Richtering, K. Huber, A. Blume, *Langmuir* **2007**, *23*, 7715-7723.
- [28] A. Meister, S. Drescher, V. M. Garamus, G. Karlsson, G. Graf, B. Dobner, A. Blume, *Langmuir* **2008**, *24*, 6238-6246.
- [29] A. Meister, S. Drescher, G. Karlsson, G. Hause, U. Baumeister, G. Hempel, V. M. Garamus, B. Dobner, A. Blume, *Soft Matter* **2010**, *6*, 1317-1324.

- [30] A. Meister, S. Drescher, I. Mey, M. Wahab, G. Graf, V. M. Garamus, G. Hause, H. J. Mogel, A. Janshoff, B. Dobner, A. Blume, *J. Phys. Chem. B* **2008**, *112*, 4506-4511.
- [31] M. Wahab, P. Schiller, R. Schmidt, H. J. Mögel, *Langmuir* **2010**, *26*, 2979-2982.
- [32] M. Bastrop, A. Meister, H. Metz, S. Drescher, B. Dobner, K. Maeder, A. Blume, *J. Phys. Chem. B* **2009**, *113*, 574-582.
- [33] A. Meister, K. Koehler, S. Drescher, B. Dobner, G. Karlsson, K. Edwards, G. Hause, A. Blume, *Soft Matter* **2007**, *3*, 1025-1031.
- [34] S. Drescher, A. Meister, G. Graf, G. Hause, A. Blume, B. Dobner, *Chem. Eur. J.* **2008**, *14*, 6796-6804.
- [35] S. Drescher, K. Helmis, A. Langner, B. Dobner, *Monatsh. Chem.* **2010**, *141*, 339-349.
- [36] S. Drescher, G. Graf, G. Hause, B. Dobner, A. Meister, *Biophys. Chem.* **2010**, *150*, 136-143.
- [37] A. Blume, *Biochemistry* **1983**, *22*, 5436-5442.
- [38] M. W. Freyer, E. A. Lewis, *Methods Cell Biol.* **2008**, *84*, 79-113.
- [39] H. Günzler, H. M. Heise, *IR-Spektroskopie - Eine Einführung*, 3 ed., VCH, Weinheim, **1996**.
- [40] R. N. A. H. Lewis, R. N. McElhaney, *Fourier Transform Infrared Spectroscopy in the Study of Hydrated Lipids and Lipid Bilayer Membranes*, Wiley-Liss, Inc., New York, **1996**.
- [41] L. K. Tamm, S. A. Tatulian, *Q. Rev. Biophys.* **1997**, *30*, 365-429.
- [42] R. Mendelsohn, D. J. Moore, *Chem. Phys. Lipids* **1998**, *96*, 141-157.
- [43] M. Hesse, H. Meier, B. Zeeh, *Spektroskopische Methoden in der organischen Chemie*, 4. ed., Georg Thieme Verlag, Stuttgart, **1991**.
- [44] A. Moores, F. Goettmann, *New J. Chem.* **2006**, *30*, 1121-1132.
- [45] G. Mie, *Ann. Phys.* **1908**, *25*, 377-445.
- [46] P. Mulvaney, *Langmuir* **1996**, *12*, 788-800.
- [47] A. A. Lazarides, G. C. Schatz, *J. Phys. Chem. B* **2000**, *104*, 460-467.
- [48] A. J. Haes, R. P. Van Duyne, *Anal. Bioanal. Chem.* **2004**, *379*, 920-930.
- [49] M. Bastrop, Martin-Luther-University Halle-Wittenberg (Halle/Saale), **2010**.
- [50] R. Pecora, *J. Nanopart. Res.* **2000**, *2*, 123-131.
- [51] H. B. Stuhrmann, N. Burkhardt, G. Dietrich, R. Juenemann, W. Meerwinck, M. Schmitt, J. Wadzack, R. Willumeit, J. Zhao, et al., *Nucl. Instrum. Meth. A* **1995**, *356*, 124-132.
- [52] O. Glatter, *J. Appl. Crystallogr.* **1977**, *10*, 415-421.
- [53] J. S. Pedersen, *Adv. Colloid Interface Sci.* **1997**, *70*, 171-210.
- [54] S. Drescher, Martin-Luther-University Halle-Wittenberg (Halle/Saale), **2008**.
- [55] M. Almgren, K. Edwards, G. Karlsson, *Colloids Surf., A* **2000**, *174*, 3-21.
- [56] J. W. Goodwin, R. W. Hughes, *Rheology for Chemists - An Introduction*, The Royal Society of Chemistry, Cambridge, **2000**.
- [57] T. Mezger, *Das Rheologie-Handbuch: Für Anwender von Rotations- und Oszillations-Rheometern*, Vincentz Verlag, Hannover, **2000**.
- [58] R. G. Larson, *The Structure and Rheology of Complex Fluids*, Oxford University Press, New York, **1999**.
- [59] B. J. de Gans, N. J. Duin, D. van den Ende, J. Mellema, *J. Chem. Phys.* **2000**, *113*, 2032-2042.
- [60] M. T. Lopez-Lopez, L. Rodriguez-Arco, A. Zubarev, L. Iskakova, J. D. G. Duran, *J. Appl. Phys.* **2010**, *108*, 083503/083501-083503/083509.
- [61] M. Masuda, T. Shimizu, *Chem. Commun.* **2001**, 2442 - 2443.
- [62] M.-C. Daniel, D. Astruc, *Chem. Rev.* **2004**, *104*, 293-346.
- [63] M. A. Reppy, B. A. Pindzola, *Chem. Commun.* **2007**, 4317-4338.

- [64] N. M. Sangeetha, U. Maitra, *Chem. Soc. Rev.* **2005**, *34*, 821-836.
- [65] T. Wang, J. Jiang, Y. Liu, Z. Li, M. Liu, *Langmuir* **2010**, 18694-18700.
- [66] S.-H. Tung, Y.-E. Huang, S. R. Raghavan, *Soft Matter* **2008**, *4*, 1086-1093.
- [67] S.-H. Tung, Y.-E. Huang, S. R. Raghavan, *Langmuir* **2007**, *23*, 372-376.
- [68] C. A. Dreiss, *Soft Matter* **2007**, *3*, 956-970.
- [69] J. K. Candlish, G. R. Tristram, *Biochim. Biophys. Acta* **1964**, *88*, 553-563.
- [70] E. Miyoshi, T. Takaya, P. A. Williams, K. Nishinari, *Macromol. Symp.* **1997**, *120*, 271-280.
- [71] S. D. Shoemaker, T. K. Vanderlick, *J. Colloid Interface Sci.* **2003**, *266*, 314-321.
- [72] W.-R. Chen, P. D. Butler, L. J. Magid, *Langmuir* **2006**, *22*, 6539-6548.
- [73] P. Garidel, A. Blume, *Langmuir* **1999**, *15*, 5526-5534.
- [74] B. Seantier, B. Kasemo, *Langmuir* **2009**, *25*, 5767-5772.
- [75] Y. A. Ermakov, *Biochim. Biophys. Acta, Biomembr.* **1990**, *1023*, 91-97.
- [76] J. Marra, J. Israelachvili, *Biochemistry* **1985**, *24*, 4608-4618.
- [77] R. A. Böckmann, A. Hac, T. Heimburg, H. Grubmüller, *Biophys. J.* **2003**, *85*, 1647-1655.
- [78] S. A. Tatulian, *Eur. J. Biochem.* **1987**, *170*, 413-420.
- [79] R. Kumar, S. R. Raghavan, *Soft Matter* **2009**, *5*, 797-803.
- [80] J. F. Berret, in *Molecular Gels. Materials with Self-Assembled Fibrillar Networks* (Eds.: R. G. Weiss, R. Terech), Springer, Dordrecht, The Netherlands, **2006**, pp. 667-720.
- [81] R. Kumar, G. C. Kalur, L. Ziserman, D. Danino, S. R. Raghavan, *Langmuir* **2007**, *23*, 12849-12856.
- [82] C. Storm, J. J. Pastore, F. C. MacKintosh, T. C. Lubensky, P. A. Janmey, *Nature* **2005**, *435*, 191-194.
- [83] X. Huang, S. R. Raghavan, P. Terech, R. G. Weiss, *J. Am. Chem. Soc.* **2006**, *128*, 15341-15352.
- [84] J. H. Fuhrhop, D. Spiroski, C. Boettcher, *J. Am. Chem. Soc.* **1993**, *115*, 1600-1601.
- [85] M. Jackson, P. I. Haris, D. Chapman, *Biochim. Biophys. Acta* **1989**, *998*, 75-79.
- [86] P. Terech, D. Pasquier, V. Bordas, C. Rossat, *Langmuir* **2000**, *16*, 4485-4494.
- [87] C. W. Macosko, *Rheology - Principles, Measurements, and Applications*, VCH Publishers, Inc., New York, **1994**.
- [88] T. Markowski, Martin-Luther-University Halle-Wittenberg (Halle (Saale)), **2011**.
- [89] J. Guilbot, T. Benvegnu, N. Legros, D. Plusquellec, J.-C. Dedieu, A. Gulik, *Langmuir* **2001**, *17*, 613-618.
- [90] S. Mabrey, J. M. Sturtevant, *Proc. Natl. Acad. Sci. U. S. A.* **1976**, *73*, 3862-3866.
- [91] X. Sun, T. Chen, S. Huang, L. Li, H. Peng, *Chem. Soc. Rev.* **2010**, *39*, 4244-4257.
- [92] D. A. Jose, S. Stefan, K. Burkhard, *Chem. Eur. J.* **2009**, *15*, 7404-7412.
- [93] E.-K. Ji, D. J. Ahn, J.-M. Kim, *Bull. Korean Chem. Soc.* **2003**, *24*, 667-670.
- [94] J. Lee, H.-J. Kim, J. Kim, *J. Am. Chem. Soc.* **2008**, *130*, 5010-5011.
- [95] J. Song, Q. Cheng, S. Kopta, R. C. Stevens, *J. Am. Chem. Soc.* **2001**, *123*, 3205-3213.
- [96] D. S. Johnston, S. Sanghera, A. Manjon-Rubio, D. Chapman, *Biochim. Biophys. Acta, Biomembr.* **1980**, *602*, 213.
- [97] J. Song, Q. Cheng, R. C. Stevens, *Chem. Phys. Lipids* **2002**, *114*, 203-214.
- [98] J. Song, J. S. Cisar, C. R. Bertozzi, *J. Am. Chem. Soc.* **2004**, *126*, 8459-8465.
- [99] J. Song, R. C. Stevens, Q. Cheng, *ACS Symp. Ser.* **2005**, *888*, 96-109.
- [100] A. P. H. J. Schenning, E. W. Meijer, *Chem. Commun.* **2005**, 3245-3258.
- [101] Y. Okawa, M. Aono, *Nature* **2001**, *409*, 683-684.
- [102] W. Zhou, Y. Li, D. Zhu, *Chem. Asian J.* **2007**, *2*, 222-229.
- [103] M. Schott, *J. Phys. Chem. B* **2006**, *110*, 15864-15868.

- [104] X. Chen, S. Kang, Min J. Kim, J. Kim, Youn S. Kim, H. Kim, B. Chi, S.-J. Kim, Jin Y. Lee, J. Yoon, *Angew. Chem. Int. Ed.* **2010**, *49*, 1422-1425.
- [105] Y. Li, B. Chu, *Macromolecules* **1991**, *24*, 4115-4122.
- [106] G. N. Patel, J. D. Witt, Y. P. Khanna, *J. Polym. Sci., Polym. Phys. Ed.* **1980**, *18*, 1383-1391.
- [107] L. Hsu, G. L. Cvetanovich, S. I. Stupp, *J. Am. Chem. Soc.* **2008**, *130*, 3892-3899.
- [108] N. Fujita, Y. Sakamoto, M. Shirakawa, M. Ojima, A. Fujii, M. Ozaki, S. Shinkai, *J. Am. Chem. Soc.* **2007**, *129*, 4134-4135.
- [109] R. W. Carpick, D. Y. Sasaki, M. S. Marcus, M. A. Eriksson, A. R. Burns, *J. Phys.: Condens. Matter* **2004**, *16*, R679-R697.
- [110] B. Tieke, G. Lieser, *J. Colloid Interface Sci.* **1982**, *88*, 471-486.
- [111] X. Huang, S. Jiang, M. Liu, *J. Phys. Chem. B* **2004**, *109*, 114-119.
- [112] J. Pang, L. Yang, B. F. McCaughey, H. Peng, H. S. Ashbaugh, C. J. Brinker, Y. Lu, *J. Phys. Chem. B* **2006**, *110*, 7221-7225.
- [113] M. Wenzel, G. H. Atkinson, *J. Am. Chem. Soc.* **1989**, *111*, 6123-6127.
- [114] D. J. Ahn, E.-H. Chae, G. S. Lee, H.-Y. Shim, T.-E. Chang, K.-D. Ahn, J.-M. Kim, *J. Am. Chem. Soc.* **2003**, *125*, 8976-8977.
- [115] S. Wu, L. Niu, J. Shen, Q. Zhang, C. Bubeck, *Macromolecules* **2008**, *42*, 362-367.
- [116] S. J. Kew, E. A. H. Hall, *Anal. Chem.* **2006**, *78*, 2231-2238.
- [117] S. Dei, A. Matsumoto, *Chem. Lett.* **2007**, *36*, 784-785.
- [118] R. Wilson, *Chem. Soc. Rev.* **2008**, *37*, 2028-2045.
- [119] F. Westerlund, T. Bjørnholm, *Curr. Opin. Colloid Interface Sci.* **2009**, *14*, 126-134.
- [120] K. M. Mayer, J. H. Hafner, *Chem. Rev.* **2011**, *111*, 3828-3857.
- [121] M. Fischler, A. Sologubenko, J. Mayer, G. Clever, G. Burley, J. Gierlich, T. Carell, U. Simon, *Chem. Commun.* **2008**, 169-171.
- [122] C.-L. Chen, N. L. Rosi, *J. Am. Chem. Soc.* **2010**, *132*, 6902-6903.
- [123] A.-H. Bae, M. Numata, S. Yamada, S. Shinkai, *New J. Chem.* **2007**, *31*, 618-622.
- [124] Y. Ofir, B. Samanta, V. M. Rotello, *Chem. Soc. Rev.* **2008**, *37*, 1814-1825.
- [125] Y. Kondo, H. Fukuoka, S. Nakano, K. Hayashi, T. Tsukagoshi, M. Matsumoto, N. Yoshino, *Langmuir* **2007**, *23*, 5857-5860.
- [126] S. Sistach, K. Rahme, N. Perignon, J.-D. Marty, N. Lauth-de Viguerie, F. Gauffre, C. Mingotaud, *Chem. Mater.* **2008**, *20*, 1221-1223.
- [127] Q. Jin, J.-P. Xu, J. Ji, J.-C. Shen, *Chem. Commun.* **2008**, 3058-3060.
- [128] C. Mangeney, F. Ferrage, I. Aujard, V. Marchi-Artzner, L. Jullien, O. Ouari, E. D. Rékaï, A. Laschewsky, I. Vikholm, J. W. Sadowski, *J. Am. Chem. Soc.* **2002**, *124*, 5811-5821.
- [129] A. Gourishankar, S. Shukla, K. N. Ganesh, M. Sastry, *J. Am. Chem. Soc.* **2004**, *126*, 13186-13187.
- [130] H. Joshi, P. S. Shirude, V. Bansal, K. N. Ganesh, M. Sastry, *J. Phys. Chem. B* **2004**, *108*, 11535-11540.
- [131] R. Marie, H. Jensenius, J. Thaysen, C. B. Christensen, A. Boisen, *Ultramicroscopy* **2002**, *91*, 29-36.
- [132] A. Ulman, *Chem. Rev.* **1996**, *96*, 1533-1554.
- [133] M. W. J. Beulen, J. Bugler, B. Lammerink, F. A. J. Geurts, E. M. E. F. Biemond, L. K. G. C. Van, V. F. C. J. M. Van, J. F. J. Engbersen, D. N. Reinhoudt, *Langmuir* **1998**, *14*, 6424-6429.
- [134] L. Zhang, X. Sun, Y. Song, X. Jiang, S. Dong, E. Wang, *Langmuir* **2006**, *22*, 2838-2843.
- [135] R. R. Bhattacharjee, T. K. Mandal, *J. Colloid Interface Sci.* **2007**, *307*, 288-295.

---

## Acknowledgements

I want to thank everyone who supported me in working on this thesis.

Many thanks are directed to Prof. A. Blume for giving me the possibility to work on this fascinating topic and for his kind and helpful support.

I am grateful to A. Meister and S. Drescher for many suggestions, discussions, and the helpful answers to many questions concerning bolaamphiphiles.

S. Drescher and the group of Prof. B. Dobner I thank for the synthesis of the molecules and an (almost) never ending supply of new bolaamphiphiles.

I appreciate all my co-workers in the group of Prof. A. Blume, their helpfulness and the great working atmosphere, including coffee breaks, barbecues, Christmas parties and trips.

I thank S. Zimmermann for the work he did on the pH- and salt-dependent aggregation behavior of Me<sub>2</sub>PE-C32-ME<sub>2</sub>PE in his Bachelor's thesis.

For computer and technical support I thank A. Lonitz. I am thankful for B. Fölting's and I. Schaller's kind help with and conduction of DSC, ITC and FT-IR measurements.

I express my gratitude to G. Hause and A. Meister for taking numerous TEM images of the bolaamphiphiles.

I thank V. Garamus for the SANS measurements and the help with the analysis of the data.

Finally, I appreciate my family and friends for their unreserved help and support during my studies and the work on my thesis.

---

## List of Publications

### Publications

**G. Graf**, S. Drescher, A. Meister, B. Dobner, A. Blume, *J. Phys. Chem. B* **2011**, *115*, 10478-10487.

*Self-Assembled Bolaamphiphile Fibers Have Intermediate Properties between Crystalline Nanofibers and Wormlike Micelles: Formation of Viscoelastic Hydrogels Switchable by Changes in pH and Salinity*

S. Drescher, **G. Graf**, G. Hause, B. Dobner, A. Meister, *Biophys.Chem.* **2010**, *150*, 136-143.  
*Amino-functionalized single-chain bolalipids: Synthesis and aggregation behavior of new basic building blocks*

S. Drescher, A. Meister, **G. Graf**, G. Hause, A. Blume, B. Dobner, *Chem. Eur. J.* **2008**, *14*, 6796-6804.

*General Synthesis and Aggregation Behaviour of New Single-Chain Bolaphospholipids: Variations in Chain and Headgroup Structures*

A. Meister, S. Drescher, V. M. Garamus, G. Karlsson, **G. Graf**, B. Dobner, A. Blume, *Langmuir* **2008**, *24*, 6238-6246.

*Temperature-Dependent Self-Assembly and Mixing Behavior of Symmetrical Single-Chain Bolaamphiphiles*

A. Meister, S. Drescher, I. Mey, M. Wahab, **G. Graf**, V. M. Garamus, G. Hause, H. J. Mogel, A. Janshoff, B. Dobner, A. Blume, *J. Phys. Chem. B* **2008**, *112*, 4506-4511.

*Helical Nanofibers of Self-Assembled Bipolar Phospholipids as Template for Gold Nanoparticles*

### Oral Contributions

06/2011 European Student Colloid Conference, Falkenberg (Sweden)  
*pH- and salt-dependent aggregation behavior of symmetric single-chain bolaphospholipids*

03/2011 German Liquid Crystal Conference, Hamburg  
*pH- and salt-dependent aggregation behavior of symmetric single-chain bolaphospholipids*

06/2010 Meeting: (Glyco)lipids, structures, functions, and interactions, Hamburg  
*Self-assembly of single-chain bolaphospholipids in aqueous suspensions*

---

07/2009 European Student Colloid Conference, Almeria (Spain)  
*Self-assembly of asymmetric single-chain bolaphospholipids*

03/2009 Zsigmondy Colloquium, Bayreuth  
*Self-assembly of asymmetric single-chain bolaphospholipids*

### **Poster Contributions**

09/2010 Conference of the European Colloid and Interface Society, Prag (Czech Republic)  
*Polymerisation of self-assembled single-chain diacetylene-modified bolaphospholipids*

03/2010 Zsigmondy Colloquium, Chemnitz  
*Rheological properties of self-assembled symmetric single-chain bolaphospholipids*

09/2009 Meeting of the German Colloid Society, Hamburg  
*Rheological properties of self-assembled symmetric single-chain bolaphospholipids*

04/2008 Zsigmondy Colloquium, Essen  
*Self-assembly of sulphur containing symmetric bolaphospholipids and their interaction with gold nanoparticles*

10/2007 Meeting of the Colloid Society, Mainz  
*Self-assembly of a sulphur containing symmetric bolaphospholipid*

---

## Curriculum Vitae

### Personal Information

Name	Gesche Graf
Date of Birth	02. August 1982
Place of Birth	Kiel
Nationality	German

### Education and Research Experience

07/1993 - 06/2002	Friedrich-Schiller-Gymnasium, Preetz (Schleswig-Holstein) <i>Abitur</i>
10/2002 - 07/2007	Martin-Luther-University Halle-Wittenberg <i>Diplom</i>
2010/2011	Mentoring Program for female scientists (Mentoring Program MeCoSa)
08/2007 - 07/2011	Martin-Luther-University Halle-Wittenberg <i>PhD Student and Teaching Assistant</i>
08/2011 - 10/2011	Research Fellowship (Martin-Luther- University Halle-Wittenberg) <i>Project: "Investigations into Protein- Detergent Interactions at the water/air interface"</i>

---

## **Erklärung**

Hiermit erkläre ich, dass ich die vorliegende Dissertationsschrift selbstständig und nur unter Verwendung der angegebenen Quellen und Hilfsmittel angefertigt habe. Die den Werken wörtlich oder inhaltlich entnommenen Stellen habe ich als solche kenntlich gemacht.

Ich versichere, dass ich diese Arbeit bisher an keiner anderen Universität oder Hochschule im In- und Ausland vorgelegt habe.

Halle (Saale) im September 2011

Gesche Graf